

ISSN: 2153-036X Vol.1, No.1, May 2010



Scientific
Research

Journal of Biophysical Chemistry



ISSN 2153-036X



9 772153 036007

01

www.scirp.org/journal/jbpc

Journal Editorial Board

ISSN 2153-036X (Print) ISSN 2153-0378 (Online)

<http://www.scirp.org/journal/jbpc/>

Editor-in-Chief

Prof. Cornelis J. Van der Schyf Northeastern Ohio Universities Colleges of Medicine and Pharmacy, USA

Editorial Board (According to Alphabet)

| | |
|-------------------------------------|---|
| Prof. Bilian Chen | Fujian Normal University, China |
| Dr. Huizhong Chen | National Center for Toxicological Research, FDA, USA |
| Prof. I. Tuncer Degim | Gazi University, Turkey |
| Dr. Bouzid Menaa | Fluorotronics Inc., USA |
| Prof. Davood Nematollahi | Bu-Ali-Sina University, Iran |
| Prof. Kazuhisa Nishizawa | Teikyo University, Japan |
| Dr. Yoshiaki Ohashi | Human Metabolome Technologies, Inc., Japan |
| Dr. Marcela Pagano | Federal University of Ceará - UFC, Brazil |
| Prof. Ayyalusamy Ramamoorthy | University of Michigan, USA |
| Dr. Andrei P. Surguchov | VA Medical Center and Kansas University Medical Center, USA |
| Prof. Armen Trchounian | Yerevan State University, Armenia |
| Dr. Izabela Tworowska | RadioMedix, Inc., USA |
| Prof. Suresh C. Tyagi | University of Louisville, USA |
| Dr. Qihui Wu | La Trobe University, Australia |
| Prof. Ling Yang | Dalian Institute of Chemical Physics, CAS, China |
| Prof. Anyun Zhang | Zhejiang University, China |
| Prof. Hailiang Zhu | Nanjing University, China |
| Prof. Erik R.P. Zuiderweg | University of Michigan, USA |

Editorial Assistant

Thessaly Song Scientific Research Publishing Email:jbpc@scirp.org

Journal of Biophysical Chemistry

Journal Information

SUBSCRIPTIONS

Journal of Biophysical Chemistry (Online at Scientific Research Publishing, www.SciRP.org) is published monthly by Scientific Research Publishing, Inc., USA.

Subscription rates:

Print: \$50 per issue.

To subscribe, please contact Journals Subscriptions Department, E-mail: sub@scirp.org

SERVICES

Advertisements

Advertisement Sales Department, E-mail: service@scirp.org

Reprints (minimum quantity 100 copies)

Reprints Co-ordinator, Scientific Research Publishing, Inc., USA.

E-mail: sub@scirp.org

COPYRIGHT

Copyright©2010 Scientific Research Publishing, Inc.

All Rights Reserved. No part of this publication may be reproduced, stored in a retrieval system, or transmitted, in any form or by any means, electronic, mechanical, photocopying, recording, scanning or otherwise, except as described below, without the permission in writing of the Publisher.

Copying of articles is not permitted except for personal and internal use, to the extent permitted by national copyright law, or under the terms of a license issued by the national Reproduction Rights Organization.

Requests for permission for other kinds of copying, such as copying for general distribution, for advertising or promotional purposes, for creating new collective works or for resale, and other enquiries should be addressed to the Publisher.

Statements and opinions expressed in the articles and communications are those of the individual contributors and not the statements and opinion of Scientific Research Publishing, Inc. We assumes no responsibility or liability for any damage or injury to persons or property arising out of the use of any materials, instructions, methods or ideas contained herein. We expressly disclaim any implied warranties of merchantability or fitness for a particular purpose. If expert assistance is required, the services of a competent professional person should be sought.

PRODUCTION INFORMATION

For manuscripts that have been accepted for publication, please contact:

E-mail: jbpc@scirp.org

Water clusters in plants. Fast channel plant communications. Planet influence

Kristina Zubow¹, Anatolij Viktorovich Zubow², Viktor Anatolijevich Zubow^{1*}

¹“Aist Handels- und consulting GmbH”, R&D Department, Groß Gievitz, Germany; *Corresponding Author: aist@zubow.de

²Department of Computer Science, Humboldt University Berlin, Berlin, Germany; zubow@informatik.hu-berlin.de

Received 19 April, 2010; revised 30 April, 2010; accepted 7 May 2010.

ABSTRACT

In tubers of two potato cultivars and in one apple cultivar, water clusters, consisting of 11 ± 1 , 100 , 178 , 280 , 402 , 545 , 715 , 903 , 119 , 1351 , 1606 and 1889 molecules, were directly (in-vivo) analyzed by gravitation spectroscopy. The clusters' interactions with their surroundings during plant growth in summer 2006 in Germany were described where a model represents the states of water clusters in bio matrices. Furthermore, a comparison with clusters in irrigation water (river, rain) is given. To achieve a high and good quality yield it is necessary to choose the right irrigation water that has to correspond with the water cluster super structure in plants. The formation energy for the $(H_2O)_{280}$ cluster during plant growth is between 0.4 and 1.3 kJ/mol. Water clusters were found to communicate with surroundings by resonance field oscillations. The main cluster parameters which were investigated are intensities of oscillations, average molecular masses, rate of collapsed clusters, and total number of clusters in ensemble during potato (apple) growth. A correlation between the change of water cluster ensembles in plants with molecular masses of all clusters in isolated starch (in-vitro) during plant growth process is discussed. In particular for potato tubers' growth, there was observed a correlation between water cluster development and average molecular masses of amylopectin super coils. The communication of plants with each other and with surroundings proceeds by resonance field of oscillating water clusters. Planet gravitation was found to influence the water cluster structure in plants.

Keywords: Clusters; Field; Communication; Gravitation; Spectroscopy; Planets

1. INTRODUCTION

It is well known, that in the bulk water molecules form clusters [1]. Though clusters were discovered in biological matrices [2] until now there isn't still a method by which clusters in plants can be identified during growth in-vivo. By Okonchi Shoichi [3] it was suggested, that water molecules are in the form of clusters in living organisms. In **Figure 1** computer models of some water clusters are given. In our laboratory, we developed a gravitation spectrometer for water cluster identification in bio-matrices of plants [4-6]. Knowing the state of water clusters in plants could be helpful for understanding the relation between biochemical processes at nano-scale level during growth and qualitative yields.

The aim of the present work was to investigate water cluster ensembles in potato tubers and apples during their growth period in summer 2006 furthermore, to understand whether a communication of clusters with each other or with their surroundings is possible.

2. MATERIAL AND METHODS

Potato starch from different cultivars (“Agria-N” from Kartoffelzucht Böhm KG and “Kalena” from NORIKA Nordring-Kartoffelzucht-und Vermehrungs-GmbH, both of Germany) prepared by a standard method was chosen as investigation object. Pure amylopectin was provided by Bavaria State Research Center LfL. The mass spectra were measured with the gravitation spectrometer (GS) of the Aist Handels- und Consulting GmbH, Germany (www.zubow.de), where the energy (f) caused by the interaction of the clusters with a shock wave is a function of molecular masses of the oscillating clusters. Molecular masses of clusters were calculated by Zubow Equations [5]. The calibration of the device was carried out with the clusters $(H_2O)_{11-12}$ [7-9], $(H_2O)_{100}$ and $(H_2O)_{280}$ both by Chaplin [10] in bi-distilled water at 295 K [1]. The potato samples (tubers) were taken at the very same place (planted on 27.04.2006) whereas the apple

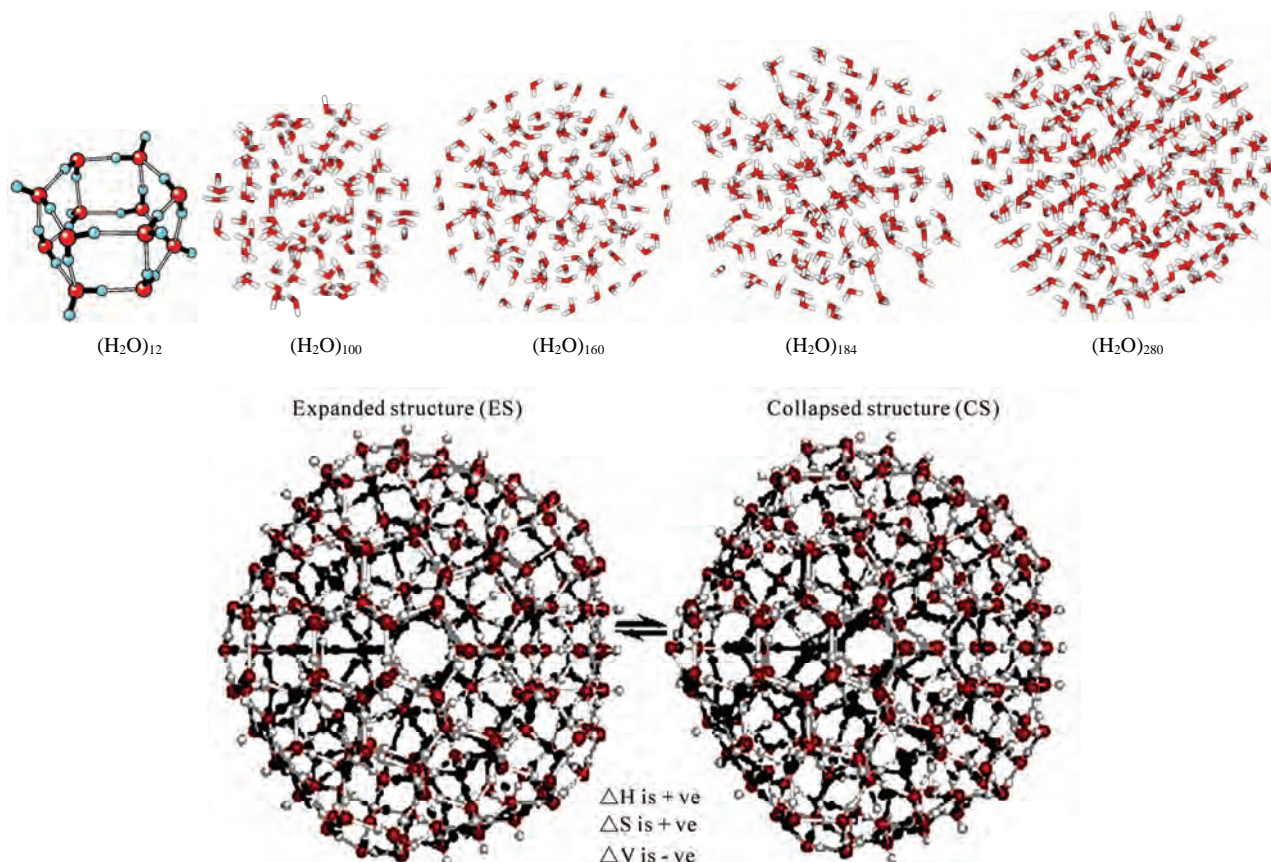


Figure 1. Calculated water cluster models (with kind permission of Prof. Chaplin [10] and Prof. Lenz A. [9]) hydrogen bonds were shown for $(H_2O)_{12}$ only.

sample of “alstar” cultivar was withdrawn at the very same tree and at the very same branch. Pure agarose of Aldrich ($T_{gel} = 315K$, $T_{fl} = 533K$) was used for preparing a model bio-matrix. Agarose hydrogels were prepared by dissolving agarose (0.3, 0.8 and 3 wt. %) in boiling distilled water ($15 \pm 5 \cdot 10^{-8}$, $\text{om}^{-1} \cdot \text{cm}^{-1}$) with following cooling until room temperature. Below the general Scheme 1 of the GS-measuring cell for the investigation of clusters in samples is shown [6]. The average day temperature (T_d , from 09.00 a.m. until 06.00 p.m.) between June 8th ($x_0 = 1987$) and September 1st ($x_i = 2070$) can be described with $T_d = 3E-05 \cdot x^3 - 0.1889 \cdot x^2 + 393.73 \cdot x - 273034$.

The GMS-method called in earlier works of authors as FNS-method is described in detail in [1,5], (algorithmus

see in **Figure 2**). The negative value of a signal in the

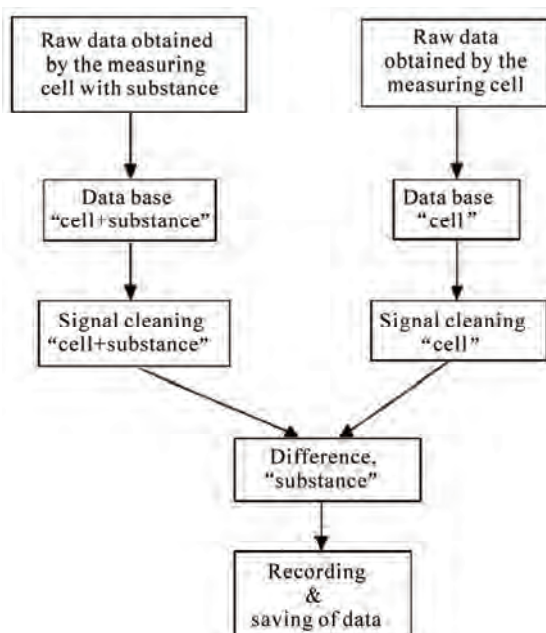
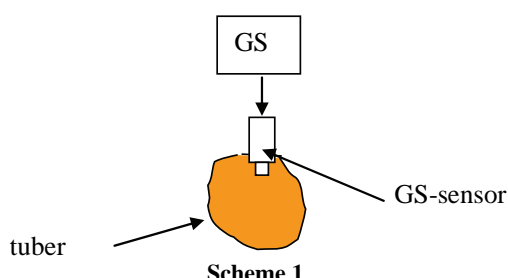


Figure 2. Secondary data extraction of GMS signals.



GS spectrum means energy absorption, which is necessary for melting of the collapsed cluster. On the other side, the positive signal is an energy release at the interaction of the shock wave with the expanded cluster, leading to its destruction. The signals of collapsed clusters were therefore described with minus and those of expanded one with plus. The Zayzev program Astronet, version ZET 9 (www.astrozet.net) was used to get information on the planet positions.

3. RESULTS AND DISCUSSION

Typical GS-spectra for rain and river water and water in potato tuber tissue are shown in **Figure 3**. As visible all clusters modeled in **Figure 1** are present here. Water clusters in materials were found to be in different forms (collapsed or expanded), which depends on the interaction of clusters with their surroundings [1]. In this study, we report the analysis data of water clusters (12, 100, 178, 280 and 1889) in potato tubers and apples during their growth in North Germany in 2006. The signal of clusters with 11 ± 1 water molecules is stable in all investigated samples and the expanded form (+f) of clusters is dominating over the collapsed one (-f). Remarkably, that the collapsed form is more enriched with energy than the expanded one.

The cluster of 100 water molecules in examined potatoes is in its collapsed form however in river water this cluster is expanded and in rainwater it is often missing. This means that the plants need energy to adapt the irrigation water cluster structure (river, lake, rain etc.) to

the water clusters in bio matrices. Irrigation water must have similar water cluster (long-range order) forms like those occurring in plants logically. It is therefore assumed that the irrigation water weakens the immune system of the plants and reduces indirectly their energy potential.

In **Figure 4**, the development of all clusters (water, bio molecules, solvated clusters of ion pairs [1,11] and bio polymers [2,12] in plants during growth in summer 2006 is shown. There are strong changes in the total number of clusters especially in the middle of summer and generally it trends toward decreasing. Differently from potatoes in apples, the total number of clusters is less strongly depending on growth time.

For a better understanding, we analyzed some water clusters in detail where we started with $(H_2O)_{12}$. In **Figure 5**, the degree of individuality or how this cluster interacts with its surroundings (f) in dependence on season time is given. In both potato cultivars, the $(H_2O)_{12}$ dynamics are nearly synchronous during growth. As visible, on 01.07.2006 the cluster lost almost completely its individuality to explain by a strong interaction with the bio-matrix of the potato tissue. After that the interaction weakens and the cluster individuality increases up to 12%. Beginning with 01.08.2006 there aren't any important changes. In apples, the cluster $(H_2O)_{12}$ possesses a much higher individuality than in potatoes that is visible as a maximum at 12.08.2006 (up to 15%). In potatoes this cluster interacts more strongly with surroundings in the bio-matrix than that one in apples. Possible cluster interaction with surroundings is shown in Scheme 2.

The interaction of the cluster consisting of 100 water molecules with its surroundings is given in **Figure 6**. This water cluster is in the collapsed form only during the indicated growth period. The interaction with surroundings is very weak ($|f| \gg 0$). The curves for both two potato cultivars have two peak areas where the cluster is active at the interaction with surroundings. The peak maxima are on July 15th and August 10th (arrows). Both peaks can be compared with those in **Figure 5**, but they are shifted for one month to a later time. For the $(H_2O)_{100}$ cluster in apples, there was found a broad peak between July 15th and August 10th. In this time range, the individuality reaches nearly zero indicating an unknown influence on the cluster formation on the part of the surroundings in the bio-matrix (see Scheme 2). Thus, similar processes involving cluster $(H_2O)_{100}$ proceed both in potatoes and in apples.

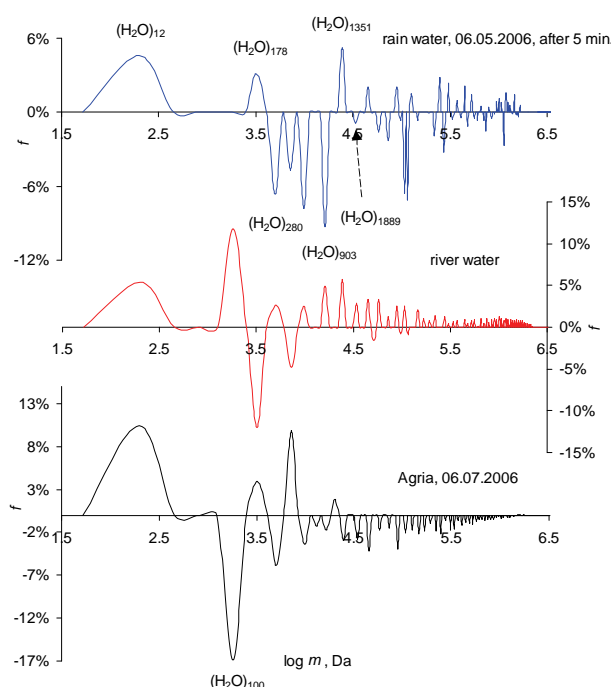
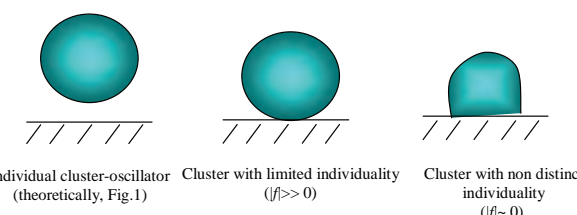


Figure 3. GM-spectra of water in different substances.



Scheme 2

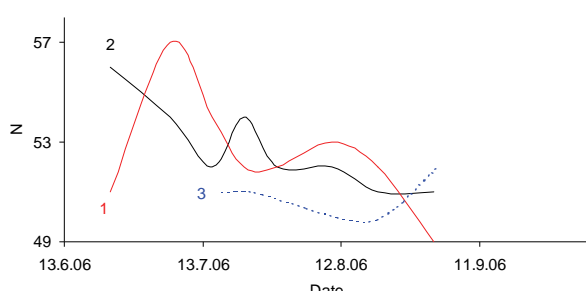


Figure 4. Number of cluster kinds in: 1 – tubers of Agria, 2 – tubers of Kalena, 3 – apple.

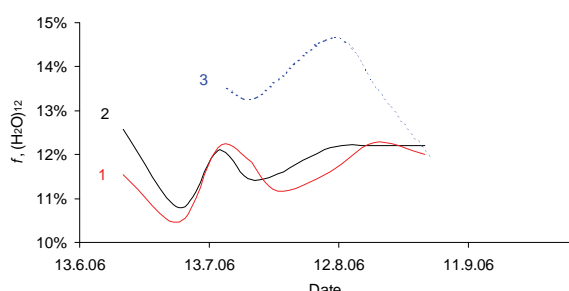


Figure 5. Relative rate of the water cluster $(\text{H}_2\text{O})_{12}$ in: 1 – tubers of Agria, 2 – tubers of Kalena, 3 – apple.

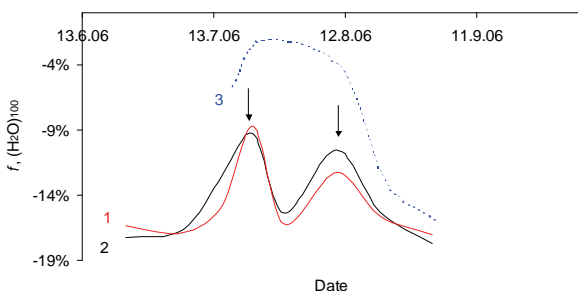


Figure 6. Relative rate of the water cluster $(\text{H}_2\text{O})_{100}$ in: 1 – tubers of Agria, 2 – tubers of Kalena, 3 – apple.

In the following these investigations were applied to the water cluster $(\text{H}_2\text{O})_{178}$ (**Figure 7**), that exists in the expanded form only. The curves are similarly with two maxima on July 15th and August 20th. Compared with the two potatoes cultivars the curve for apples shows higher f -values due to a stronger individuality of the clusters that means these clusters' interactions with the surroundings is lower. On the other side the behavior of all three curves is similarly and reflects a general biochemical processes in plants (marked by arrows), possibly. However, computer animation did not give this cluster, by Chaplin [10] the clusters consisting of 160 and 184 water molecules were computed only. To the authors the cluster $(\text{H}_2\text{O})_{178}$ is caused by bio-matrix influence. The mass analog of this cluster was found for

polysaccharides extracted from plants during the time from July 15th to August 20th too.

The next discussion concerns the water cluster of 280 molecules (**Figure 8**), that is present in the collapsed form only in all investigated plants. Independently on plant type for this cluster, we recognized clear individuality between July 15th and August 20th. Outside this time interval that means until July 15th and after August 15th all curves approaches to the zero line (x-axis). The cluster seems to react on changes in the bio matrices too. The influence of bio matrix leads to a dominating collapsed form. Later the August 15th ageing processes in potatoes and apples cause bio matrix compression. The biopolymers contract and press out included water molecules, comparably with the gel-xerogel transformation. The $(\text{H}_2\text{O})_{280}$ clusters shall be destroyed by densification of the bio matrix in ripe plants.

Figure 9 is shown how the formation energy of this cluster changes during the plant growth. E_{form} varies in the interval between 0.4 and 1.3 kJ/mol and achieves its highest value in the end of July. This result agrees satisfactorily with the formation energy for the cluster in fresh distilled water (0.4 kJ/mol) [1] and with the experimentally observed value of ~1 kJ/mol [10,13].

Finally, we shall study the water cluster $(\text{H}_2\text{O})_{1889}$, that was calculated by Chaplin [10] too (**Figure 10**). There are strong differences between the oscillations in the two potato cultivars on the one hand and in the apples on the other hand but generally, the f value changes were found

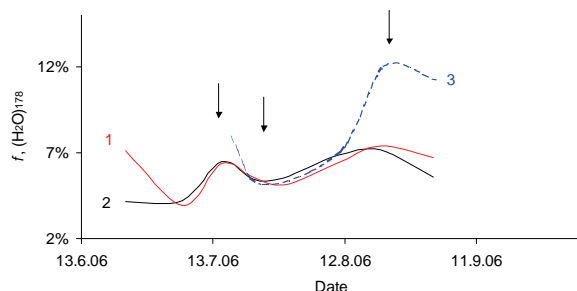


Figure 7. Relative rate of the water cluster $(\text{H}_2\text{O})_{178}$ in: 1 – tubers of Agria, 2 – tubers of Kalena, 3 – apple.

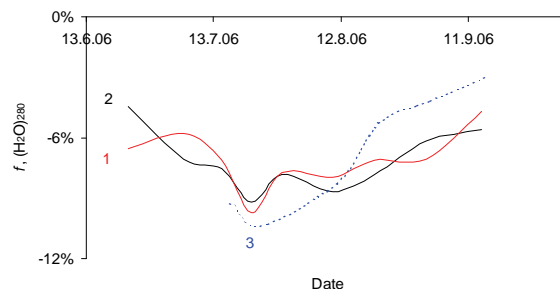


Figure 8. Relative rate of the water cluster $(\text{H}_2\text{O})_{280}$ in: 1 – tubers of Agria, 2 – tubers of Kalena, 3 – apple.

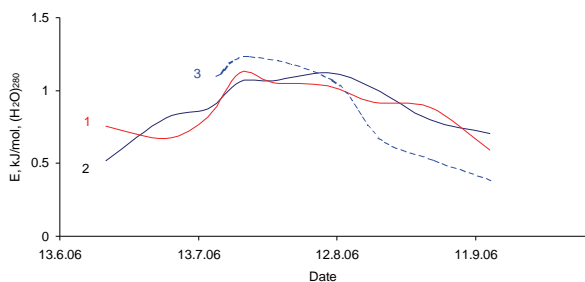


Figure 9. Changing formation energy of $(\text{H}_2\text{O})_{280}$ in plants during growth. 1 – tubers of Agria, 2 – tubers of Kalena, 3 – apple.

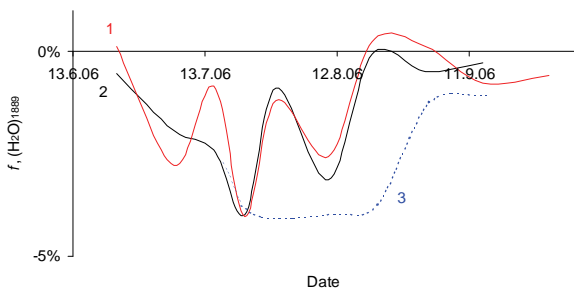


Figure 10. Relative rate of the water cluster $(\text{H}_2\text{O})_{1889}$ in: 1 – tubers of Agria, 2 – tubers of Kalena, 3 – apple.

to be lower than for the other smaller clusters (~ 4%). In potatoes, the interaction of this cluster with the surroundings during growth seems to be very sensitive and in September the signal disappeared completely, which applies for apples too.

The average molecular mass of all clusters in plants during growth is represented in **Figure 11**. By comparing it with **Figures 6** and **8** it can be concluded that the behavior of the average molecular mass of clusters in dependence on the time shows some similarities with signals of $(\text{H}_2\text{O})_{100}$ and $(\text{H}_2\text{O})_{280}$. Remarkably, that the absolute maxima for all curves are at the same time. It could be an indication for that similar biochemical processes on the level of super molecular structures proceed in the bio matrix of all investigated plants. Comparing the results of **Figures 6**, **7** and **11** at least 2 to 3 transformation processes in plants during growth can be concluded.

Based on the results discussed above the following model for water cluster forms in bio matrices of potato tubers has been suggested. In this model (**Figure 12**), the bio matrix is represented as line net and water clusters as balls. It is visible how the changing bio matrix influences the water cluster form. In young potato, $(\text{H}_2\text{O})_{100}$ and $(\text{H}_2\text{O})_{178}$ are in the collapsed form whereas $(\text{H}_2\text{O})_{280}$ and $(\text{H}_2\text{O})_{1889}$ are in the expanded one (dotted line). In the middle of summer the bio matrix grows very fast; which leads to large pores and the pressure on the part of the bio matrix on the water clusters becomes weaker. In

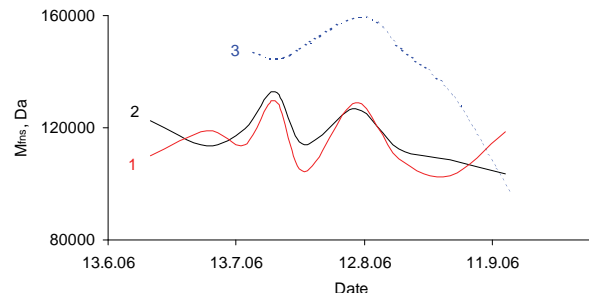


Figure 11. M_{fns} of all clusters in vivo versus the growth time: 1 – tubers of Agria, 2 – tubers of Kalena, 3 – apple.

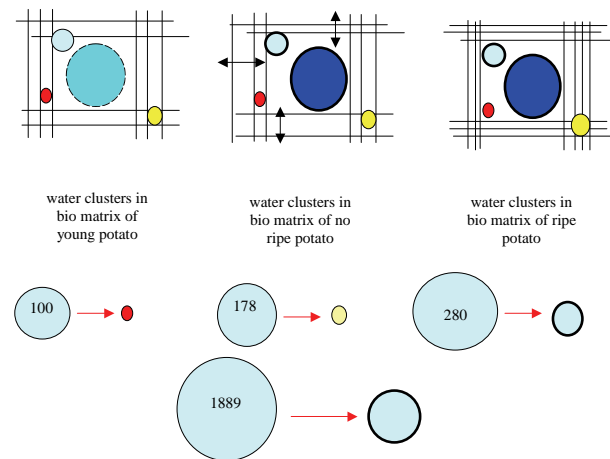


Figure 12. Model of water cluster interaction with bio matrix in dependence on growth time.

young plants, the individuality of clusters is more developed. With plant ripening, the bio matrix loses water due to, that all super molecular structures contract and release water in the plant tissue like gel xerogel transformation (syneresis).

For a better understanding of the bio matrix influence on the water clusters, amylopectin was extracted during the potato growth and the M_{fns} values were measured and compared with the M_{fns} values of all clusters in the potato tissue (**Figure 13**). The M_{fns} of amylopectin (grape-like clustering) is much higher than the corresponding value for all clusters in the potato tissue. Curve 1 as well as curve 2 has two maxima, though concerning their position there are some differences. The first maximum (marked with a star) in the curve 1 on July 6th corresponds with the minimum in the curve 2 on the other side, the second maximum of the curve 1 (August 10th) clearly correlates with the second maximum in the curve 2. The minimum (July 22nd) in curve 1 shall be explained with a debranching process of amylopectin at temperatures higher 298 K [14]. The similarities between both curves assume that the two events, which takes place in amylopectin (bio matrix) and water clusters in the potato tissue are interconnected.

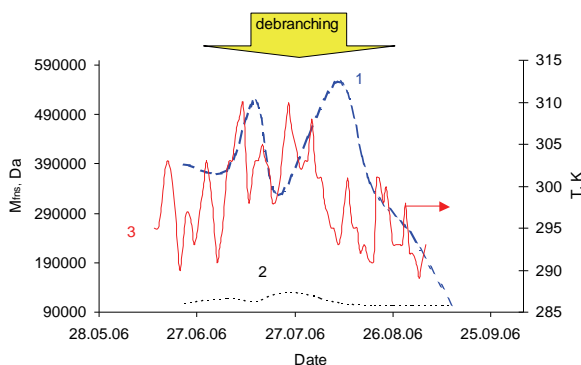


Figure 13. Average molecular masses (M_{fns}) of amylopectin super coils isolated from the potatoe cultivar Agria (1) and of all clusters in potatoe tuber tissue of Agria in vivo (2), the average day temperature line (3).

In the next, briefly some small water clusters shall be compared with M_{fns} of amylopectin (amorphous area) as a possible representative of the macromolecular structure in the bio matrix (**Figure 13**).

Both in young and ripe potatoes, the water cluster $(H_2O)_{100}$ is in a free undisturbed state (**Figure 6**) whereas during the growth (not ripe state, **Figure 12**) when the bio matrix changes a new interaction between this cluster and the bio matrix leads to a new cluster form. Both sides seem to influence each other (see the correlation between curves 1 and 2 in **Figure 6** and curve 1 in **Figure 13**). In contrary, $(H_2O)_{178}$ doesn't participate in active biochemical processes in the bio matrix (bad correlation between the curves 1 and 2 in **Figure 7** and curve 1 in **Figure 13**) due to that it is actively involved in the super molecular structure net of the bio matrix which retains this cluster.

Only on July 22nd shows the collapsed cluster $(H_2O)_{280}$ a strong individual behaviour in potatoes and apples (**Figure 8**), but in young and old plants the bio matrix destroys the cluster, the f -value approaches to zero (**Figure 12**).

Concerning the bio matrix influence on large clusters, the $(H_2O)_{1889}$ is the most sensitive one (**Figure 8**). During the growth it is permanently forced to change its form (**Figure 12**).

For the integral distribution of clusters in plants we found the following equation:

$$W_x = a \cdot \ln(m \cdot 10^{-5}) + b,$$

where W_x – the integral rate of cluster fractions, m – the mass of clusters in Dalton, the value of coefficients a and b change depending on the ripe degree. We describe these changes with the following equations for apple ("elstar", 83 ± 2 wt. % water in ripe state):

$$a = -5E-09 \cdot t^4 + 5E-05 \cdot t^3 - 0.1816 \cdot t^2 + 295.49 \cdot t - 180235,$$

$$b = 6E-09 \cdot t^4 - 6E-05 \cdot t^3 + 0.2311 \cdot t^2 - 378.76 \cdot t + 232739,$$

where, t – date of the test.

For potato tubers, the character of a and b changes cannot be described with these equations. The values a and b strongly depend on the ripe time and they reflect some changing processes in super molecular structures in tuber tissue during potato growth.

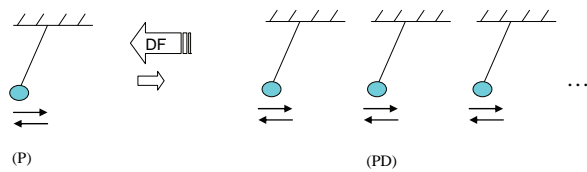
The signal frequencies (kHz) we detected directly for the water clusters in tubers of two potato cultivars and one apple cultivar consisting of 11 ± 1 , 100, 178, 280, 402, 545, 715, 903, 1119, 1351, 1606 and 1889 molecules were: 22.2, 7.3, 5.5, 4.4, 3.7, 3.1, 2.8, 2.4, 2.2, 2.0, 1.8 and 1.7.

3.1. Water Cluster Communication Field. A Channel of Plant Communications

Now we shall discuss a hypothetical oscillation model of one element being part of a multi element system (cluster like dimension). The oscillation of one molecule (P) can be envisaged as a pendulum and the oscillation of the dimension of P like a dimension of pendulums (PD), oscillating in one rhythm (minimization of the total energy and harmonisation of the model, Scheme 3).

In these systems, the pendulum oscillations depend both on the nature of the pendulum and its interaction with surroundings. The driving force (DF) of the association of some P in PD is the resonance that harmonizes the whole system leading to a higher stability and to a minimum of the total energy in the new ensemble. Furthermore, PD oscillations influence other oscillation systems in their surroundings by resonance, where stronger PD forces weak PD to oscillate in the rhythm of the strong PD. How strongly the surroundings shall be influenced by PD depends on the number of P in the ensemble. The information transfers from PD to P and backwards proceeds through the medium in which are pendulums.

It would be interesting to investigate the information transfer between clusters of water (PD) being in different vessels and of water in a model biological tissue (hydrogel). Agarose hydrogels are often used in biochemistry and microbiology where their chemical structure is well known and they can be considered as biological tissue [15,16]. If this information transfer channel exists really then it should be observed by analysing the influence of one PD_A (vessel A) on the other one (PD_B , vessel B). For that the water cluster ensembles in vessel A were stimulated by a forced stirring of water (destruction of long-range order) contemporaneously the water in vessel B at the distance x was in a calm state. The interaction of cluster ensembles belonging to water in different vessels was measured with help of the Zubow gravitation spec-



Scheme 3

trometer given in **Figures 14 and 15** [6].

Water clusters like oscillators or pendulum ensembles have to communicate with each other by a resonance field. Here, one dimension of a water cluster-pendulum in vessel A (**Figure 14**) interacts with another one of the same water cluster-pendulum in vessel B by the resonance between these pendulums (Scheme 2) where the resonance field is not homogenous, since it is influenced by a number of other surrounding resonators (water clusters of the neighboring river, water in floor, wood, clouds etc.). To check it, a simple experiment was carried out.

Before beginning the experiment and to achieve a thermal and mechanical balance the system was stored for 6 h excluding the influence of outer thermal flow, light and mechanical fields. At this time the characteristics of long-range order in water (**Figure 14**), agarose hydrogel and potato tissue (**Figure 15**) in which the GS-sensor was installed were measured three times. Then, water in vessel B was stirred for 1 min by a Teflon stirrer, the electrical engine was switched off and after 1 min the GS-spectra were taken in vessel A in an interval of 5 min. As visible in **Figure 14**, forced destruction of the long-range order in water in vessel B changes the long-range order in water of vessel A (strong increase of M_{fns}). This reaction supports the correctness of Scheme 2. According to Scheme 2 water clusters as oscillator ensembles interact each with other by resonance. We found that water clusters differently react on forced activation of their analogous in vessel B. Shortly after at 30 sec a maximum M_{fns} (250 kDa) was achieved, M_{fns} strongly decreased to 120 kDa and approximated then to a stable level.

The rare cluster (H_2O_{137}) is the most sensitive one to the resonance field influence of water that is placed in an other vessel, it appears and disappears. The vibration process lasts 5 minutes and is comparable with a decreasing oscillation.

Hence by the integral characteristics of the long-range order in liquids, e.g. M_{fns} , changes in the fine cluster structure cannot be analyzed for the observer the process was finished after 1 minute. At the level of individual clusters, to get an answer on the excitation from analogous in the other vessel can pass some minutes or even hours.

The question raised is whether water clusters, for instance in agarose hydrogel or in plant tissue (receiver), can communicate with cluster ensembles in stirred water (transmitter) that is at a distance of 18 cm and 31 cm. To give an answer on this question the next equipment was developed (**Figure 15**).

These communication signals (change of the average mass of the secondary activated water clusters in the receiver cell) are shown in **Figure 16**. In the first 10 minutes when the stirrer is switched off M_{fns} is nearly

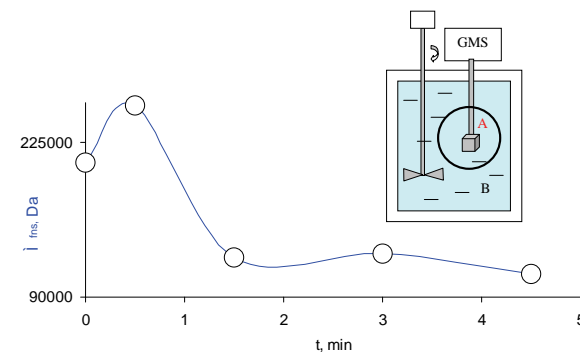


Figure 14. Change of M_{fns} in vessel A by stirring water in vessel B. Both vessels are filled with distilled water, 286 K. The stirring engine at GS-measuring was switched off. The equipment was isolated from light and mechanical vibrations.

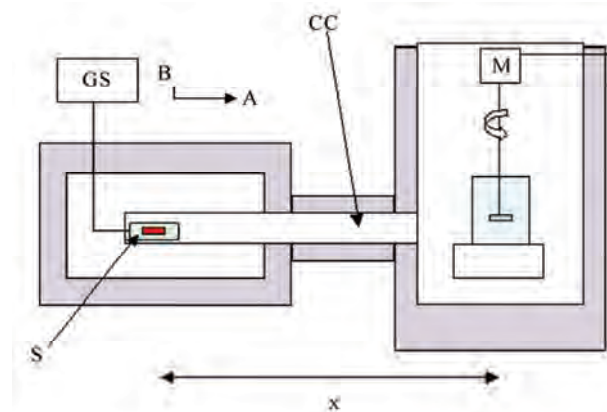


Figure 15. Scheme for the determination of the information field caused by the interaction of water clusters that are distant of each other. 286 K, $x = 18$ and 31 cm. GS-sensor and water-stirring equipment were placed in a sound isolated polystyrene foam containing box. Before each GS measurement (1 min) the stirring engine (M) was switched off. A - direct vessel communication by the communication channel (CC, pipe), B – contact-free variant (CC is directed to the line of the shortest interaction with an angle of 90°) S – sample (GS-sensor is in 3 wt. % agarose gel or directly in tuber tissue).

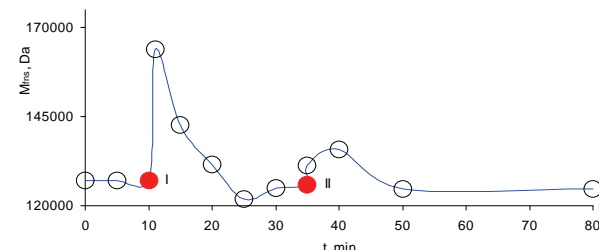


Figure 16. Effect of directed resonance interaction of water clusters in the measuring box with water clusters in the stirring vessel (**Figure 14**). I – measuring after 1 minute stirring and 1 minute break, directed position (**Figure 14** in the direction of A), II – measuring after 1 minute stirring and 1 minute break, non-directed position (**Figure 14** in the direction of B).

unchanged then, one minute stirring causes (transmitter) a strong increase of M_{fns} in the agarose hydrogel (receiver cell). This signal is unsymmetrical, while the increase is very steep the decrease proceeds more slowly. Based on this a wireless communication between these two systems, between transmitter (activated water) and receiver (water clusters in agarose hydrogel) was concluded. The same stirring procedure was repeated 10 minutes later and as visible the answer is similarly but of a lower intensity.

Analogous experiments were carried out with potato tubers in which the GS-sensor was installed (**Figure 15**). As for agarose hydrogel for the potato bio matrix (in-vivo) an answer reaction on the forced destruction of long-range order in water in a vessel that is at a distance of 18 cm was observed too (**Figure 17**). The test was made three times. The first peak is symmetrical though comparing with agarose hydrogel the decrease of M_{fns} is deeper. The second and third effects are similarly. The triple repeated experiments support clearly that there exists a communication channel between water clusters in tubers and water clusters of the surroundings.

Several water clusters in potato tubers differently react on impact of resonance field caused by the transmitter (forced stirred water in vessel), some clusters react fast within some seconds whereas other need more time (range of some minutes).

The strong increase of M_{fns} and then its fast falling down lower the M_{fns} level in a tuber without field influence indicate that this influence can be regarded as a shock wave, that consists of a falling and a reflective wave and that is comparable with low tide and high tide. The energy flow from activated clusters (see **Figure 18**) achieves the water clusters in the potato tuber after that the average cluster mass in the bio matrix increased. This process is characterized by condensation of small clusters and domination of large one.

In the following 15-20 min, after the energy impact and energy dissipation in the bio matrix thermodynamic balance has been recovered (**Figure 17**). The elasticity of this interaction can serve as characteristic for the stability of the bio matrix against the influence of fields caused by other molecular oscillators in the hydrosphere of the earth (natural and artificial irrigation, influence of large water masses, e.g. clouds).

The detail study of resonance processes of some clusters has shown that new clusters appear whereas old ones disappear finally, leading to changed surroundings by different clusters. The rare water cluster containing 226 molecules is formed at forced stirring of water [17]. In the potato tuber it is present too though the signal is of low intensity ($f = 0.1\%$) and it appears only after the third impact at 2750 seconds (**Figure 17**). Its oscillation intensity first increases eight times, then after 125 seconds (2875 s, **Figure 17**) it decreases 38-times, later

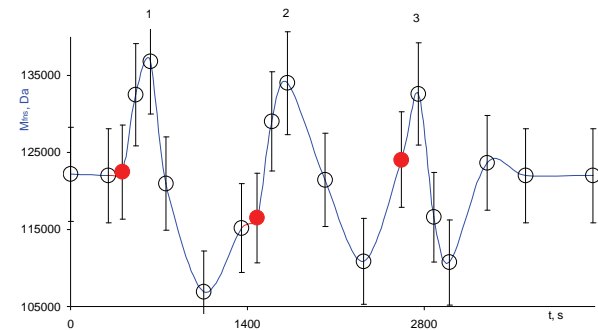


Figure 17. Change of the average molecular cluster mass in a potato tuber (in-vivo) under the resonance field influence of oscillating water clusters in a 2 L water vessel that is at a distance of 18 cm (**Figure 15**), 286 K. Communication medium – air. The black circle means the switching on of the stirrer for 1 minute. The spectra were taken when the engine was turned off.

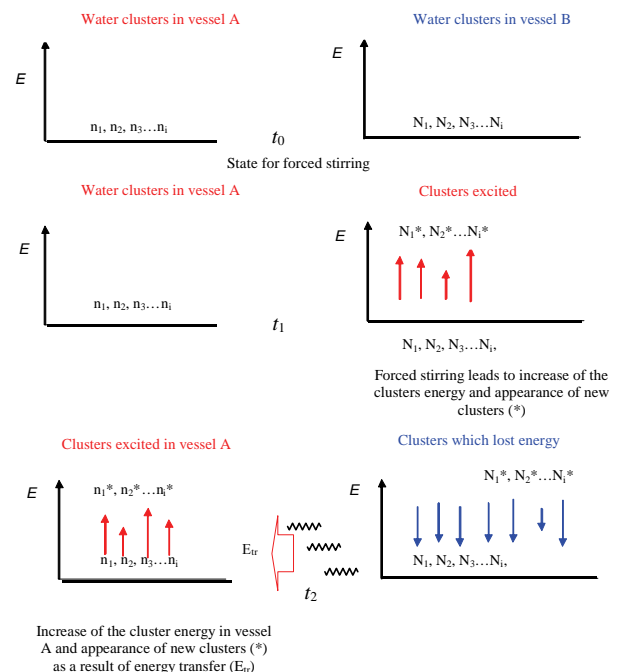


Figure 18. Scheme illustrating how the energy levels of water clusters in hydrogel were filled by energy transfer. Each oscillator is marked by $n_1, n_2, n_3\dots n_i$ (number of water cluster kinds in hydrogel) and by $N_1, N_2, N_3\dots N_i$ (number of water cluster kinds in forced stirred water). The energy levels of water clusters in hydrogel will be filled as soon as the energy (E_{tr}) is delivered from stirred water.

after 245 s (2995 s) it increases again 27-times and after 1385 s (4136 s) it calms down while the other clusters react five times weaker. Remarkably, this cluster is present in the communication net agarose hydrogel – water too (**Figure 15**), but it isn't in the water-water system (**Figure 14**). In the water-water system the most active role played an other cluster, namely $(H_2O)_{137}$. The acti-

vation of $(H_2O)_{226}$ seems to be caused by the presence of polysaccharides in the bio matrix. We assume that this cluster is integrated in the bio matrix pores of the tuber tissue and that it leaves these pores under the impact of shock waves where this process is reversible (Scheme 4).

The appearing of the new unstable state in the tuber bio matrix (Scheme 4, right part of equation) gives a signal to the plant, which can be interpreted as the beginning of the irrigation, the approaching of rain clouds or the rain beginning. As the consequence the plant switches on a preparation mechanism for irrigation. Analogous communication between plants and their surroundings at approaching of drought, frost and winds etc., is possible under participation of other cluster signals.

Additional studies showed there is a fast communication channel in the system tuber-tuber, namely a mechanically destroyed tuber influences its neighbouring tuber in which is a GS-sensor installed (Figure 15).

The information field of water clusters' interaction in tubers is sensitive to the water quality namely rain, river or distilled water (Figure 3) as well as to neighbours containing a large amount of water and possessing a cluster field like a dimension of resonators (Scheme 3). This information channel diversity permits to use it for plant communication. The amount of communication channels can be estimated for the first nine members of the cluster sequence by the next equation:

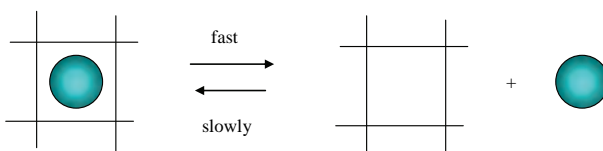
$$C = \sum_{i=1}^9 \binom{9}{i}$$

The equation gives 509 communication channels which can be multiplied by the number of kinds of super molecular structures (n) for instance water clusters surrounding uniform bio molecules in the bio matrix which appears like a unique oscillator block. The whole information field capacity is the following:

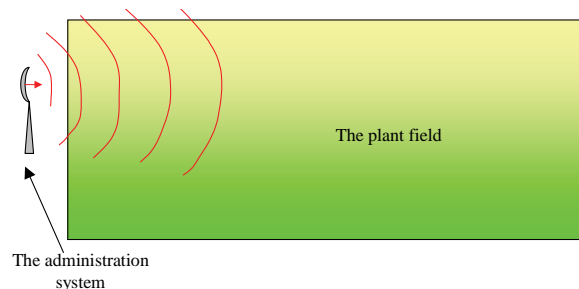
$$C_o = C \cdot n.$$

The transformation velocity is in the sound frequency area and depends on the traffic kind (cluster transmitter and cluster receiver) too, where the transformation quality can be influenced by external factors e.g. resonance fields of water clusters belonging to other systems.

For all clusters the oscillation frequencies are known therefore, it is possible to develop a program and equipment for an early warning system for plants about weather changes, parasite attacks additionally, for a system monitoring and stimulating the ripening process (Scheme 5).



Scheme 4



Scheme 5

In Figures 18 and 19, we shall represent the mechanism of a possible communication between biological systems realized by resonance fields of water clusters. We see two dimensions of equal oscillators (state t_0 , Figure 18), that are divided of each other by a molecular space, for instance air. The forced activation of oscillators of one dimension (in vessel B, Figure 18) by e.g. pumping with potential energy causes a new energy set of clusters (state t_1) which release this energy (E_u) after the forced energy pumping was finished and the system achieved the starting thermodynamic state (t_2). The released energy will be transferred as a gravitation energy wave to other dimension of oscillators where it causes an answer in the form of oscillation of the whole system as well as of some individual clusters of the same type. The Figure 18 can be applied for cluster communication in liquids as well as in bio matrices.

The influence of water clusters on the conformation of a bio molecule surrounded by different water clusters is shown in Figure 19 furthermore, it is shown how water clusters change the communication of the first bio molecule with a second one that is distant and that can belong to an other plant.

It was shown by [18] that water around a bio molecule change its conformation. Additionally, we found that at resonance interaction of water cluster ensembles with other analogous water cluster ensembles the weak ensembles adapt to the dominant ones. This adaptation process or harmonisations of water cluster oscillations force bio molecules in the receiver system to accept the conformation of dominating transmitter system. The consequence is that the receiver bio molecules have to participate in the same biochemical processes like the transmitter bio molecules. These processes change the biological and physiological behaviour of plants.

Practically, we observed this effect in summer 2006 for potatoes produced by "Clove" GmbH in North Germany. The influence of the water quality on the green plant part was visible for the potato cultivar Agria the irrigation with underground water led to colour loss followed by immunity weakening. On places of the same potato field where the irrigation machine didn't work the green plant part had a dark green colour. According to Figure 3 the cluster structure of water used for the irrigation isn't suitable to the water cluster structure in the

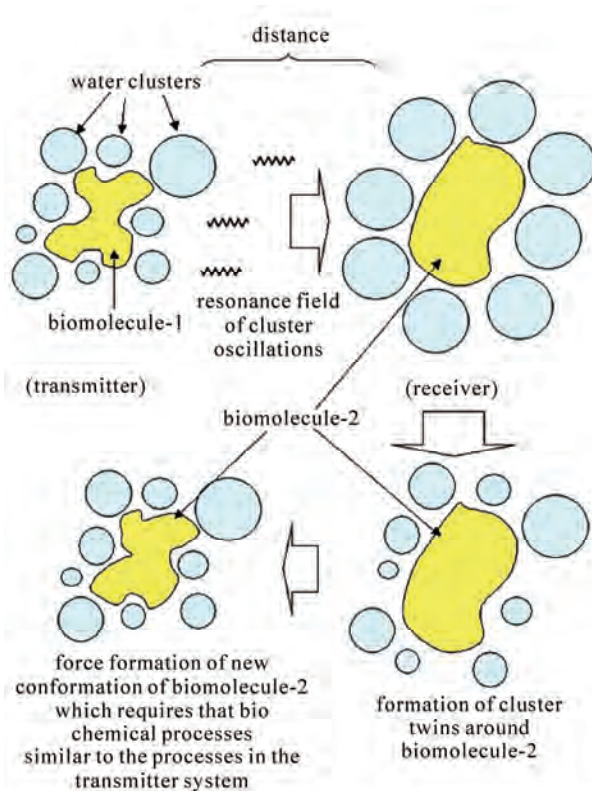


Figure 19. Model for information transfer from one biomolecule to an other one by forced change of the biomolecule conformation under the influence of water clusters.

plants. $(H_2O)_{12}$ (22.2 kHz), $(H_2O)_{178}$ (5.5 kHz), $(H_2O)_{280}$ (4.4 kHz) are similarly for the potato tissue and rainwater. In contrary, $(H_2O)_{100}$ (7.3 kHz), $(H_2O)_{178}$ and $(H_2O)_{280}$ in the river and underground water are differently and oscillate in a opposite form to water in potato. This means that the plants need more energy for the adaptation of the irrigation water to the own water clusters.

Based on the oscillator interaction (Scheme 3) and the experimental proof for water, agarose hydrogel and potato tissue it was concluded that this effect could be applied for other plants.

Therefore, water clusters play an important role as a cost factor at the water choice. On the other side this damage can be reduced by a corresponding preparation of irrigation water, for instance, by influencing the artificial water cluster communication field or with help of physical measures or better by a correct choice of irrigation water.

It is shown in **Figure 20** how the planets develop the relative molecular cluster energy in the interval C [6,12], in which masses and sizes of clusters are comparable with those of starch globular. In this once-only time, nearly all planets were together on one side to the sun. The surface of the 3D graphic is characterized by some regular maxima and minima, that correlate with planet influences (from left to right marked with red arrows):

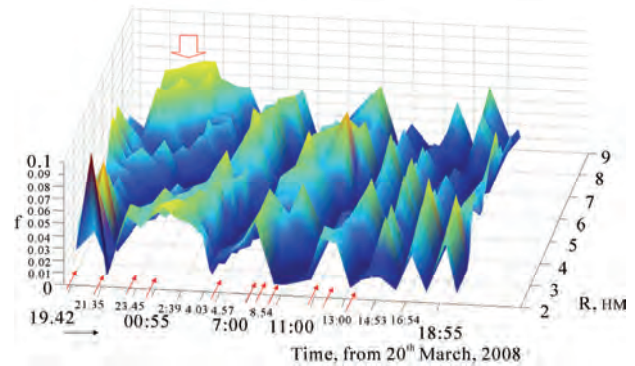


Figure 20. 3D graphic of GS spectra of potato bio matrix (interval C – for clusters of middle sizes) during full moon from March 20th 2008 (Berlin, summer time), f – energy rate of a cluster ensemble.

sunset at 19:19, Moon - Uranus opposition (180° at 21:28:25) and Mars - Pluto opposition (175°) in the slice plane of proton resonance [4,6]. All these events led to strong changes in the energy characteristics of all cluster ensembles in the potato bio matrix (marked with a broad arrow). Further, the other arrows shall be designated to the appearance in this slice plane of: Saturn at 23:38, Moon at 00:39, second gravitation focal point of Moon orbital at 04:53, center of our Galaxy at 07:00, sunrise at 07:17, Pluto at 07:18, Jupiter at 08:35, Neptune at 10:56 and nearly simultaneously Mercury and Venus at 12:03, Uranus at 12:31 und Sun at 13:17.

Then, the signal intensities were highly decreased though with preserving the regularity. In [4,6] we found out that planets influence the molecular matter by their gravitation radiation, that leads to a changed balance between proton dissolving in physical vacuum and proton condensation from physical vacuum. Thus, gravitation fields of planets were observed to impact strongly the cluster structure of molecules in bio matrices (long-range order) as well as consequently biochemical processes. These phenomena are signals for turning-on/off of biological cycles in the living matter.

4. CONCLUSIONS

Water in plants is present as clusters. These water clusters oscillate and communicate by oscillation with other water clusters of the surroundings. Water clusters and their distribution (collapsed or expanded) play an important role during plant growth. Their behavior in plants could be used as indicator for bio matrix development during plant growth. Plants communicate with each other and with surroundings by resonance field of oscillating water clusters. The right choice of irrigation water concerning the long-range order of water clusters could promote plant growth and reduce costs. Influence on plant communication by resonance field of water

cluster oscillation could be applied for early warning systems on weather changes (drought, rain, frost, sun radiation etc.) or for regulation of biochemical processes during ripe, storage (inhibition of gel-xerogel transformation) as well as for manufacturing processes. Water clusters in plants were found to be unique sensors for the gravitation influence of planets.

5. ACKNOWLEDGEMENTS

The financial support by the, Aist Handels- und Consulting "GmbH (FNS-project) is gratefully acknowledged. The authors thank Dr. M. Reichmann (Institut für Pflanzenbau und Pflanzenzüchtung, Bayerische Landesanstalt für Landwirtschaft, FRG) for the kind consulting and supply of pure potato amylopectin samples.

REFERENCES

- [1] Zubow, K.V., Zubow, A.V. and Zubow, V.A. (2005) Cluster structure of liquid alcohols, water and n-hexane. *Journal of Applied Spectroscopy*, **72(3)**, 321-328.
- [2] Zubow, A.V., Zubow, K.V. and Zubow, V.A. (2007) Investigation of the distribution of water clusters in vegetables, fruits and natural waters by flicker noise spectroscopy. *Biofizika*, in Russian, **52(4)**, 585-592.
- [3] Shoichi, O. (2004) Water structure in living organism. *Mizu no Tokusei to Atarashii Riyo Gijutsu*, 317-326.
- [4] Zubow, K.V., Zubow, A.V. and Zubow, V.A. (2010) Principle of gravitation spectroscopy. New form of molecular matter. Processes. Fields. Electronic book available via Aist H&C: <http://www.zubow.de/>
- [5] Zubow, K.V., Zubow, A.V. and Zubow V.A. (2009) Low frequency movement of cluster-12 in potato amylopectin during growth. Influence of white noises. *Journal Chemistry of Raw Plant Material*, in Russian, **2**, 81-88.
- [6] Zubov, K.V., Zubov, A.V. and Zubov, V.A. (2010) Ensemble of clusters – new form of molecular matter, risks and chances. Zubov equations. In: Columbus, F., Ed., *Chemical Industry Challenges - Issues and Prospects*. Nova Science Publishers, Inc., Commack. <http://www.novapublishers.com>
- [7] Bogdanov, E.V. and Manrova, G.M. (2000) Equiclusiter water model. *Biomedical Radioelectronics*, in Russian, **7**, 19-28.
- [8] Lee, H.M., Suh, S.B. and Kim, K.S. (2001) Structures, energies and vibrational spectra of water undecamer and dodecamer: An ab initio study. *Journal of Chemical Physics*, **114(24)**, 10749-10756.
- [9] Lenz, A. and Ojamäe, L. (2006) On the stability of dense versus cage-shaped water clusters: Quantum-chemical investigations of zero-point energies, free energies, basis-set effects and IR spectra of $(H_2O)_{12}$ and $(H_2O)_{20}$. *Chemical Physics Letters*, **418(4-6)**, 361-367.
- [10] Chaplin, M. (2009) Structural forms in the icosahedral water cluster. Available via South Bank University of London: <http://www.sbu.ac.uk/water/index.html>
- [11] Zubov, A.V., Zubov, K.V. and Zubov, V.A. (2007) Mechanism of sodium chloride diosolving in water and the process of the solution aging. *Russian Journal of Applied Chemistry*, **80(7)**, 1249-1255.
- [12] Zubow, K.V., Zubov, A.V. and Zubow, V.A. (2008) Use of flicker noise spectroscopy for undestroyed analysis of nano structures. *Diagnostics of Material*, in Russian, **74(9)**, 40-46.
- [13] Lee, H.M., Suh, S.B. and Kim, K.S. (2001) Erratum: Structures, energies and vibrational spectra of water undecamer and dodecamer: An ab initio study. [*Journal of Chemical Physics*, **114**, 10749 (2001)]. *Journal of Chemical Physics*, **115**, 7331-7334.
- [14] Batlle, N., Carbonell, J.V. and Sendra, J.M. (2000) Determination of depolymerization kinetics of amylose, amylopectin, and soluble starch by aspergillus oryzae – amylase using a fluorimetric 2-p-toluidinylnaphthalene-6-sulfonate/flow-injection analysis system. *Biotechnology and Bioengineering*, **70(5)**, 544-552.
- [15] Kadri, A., Lorber, B., Charron, C., Robert, M.C., Capelle, B., Damak, M., Jenner, G. and Giege, R. (2005) Crystal quality and differential crystal-growth behaviour of three proteins crystallized in gel at high hydrostatic pressure. *Acta Crystallographica, Section D: Biological Crystallography*, **D61(6)**, 784-788.
- [16] Zhang, J.L., Takayama, H., Matsuba, T., Jiang, R. and Tanaka, Y. (2003) Induction of apoptosis in macrophage cell line, J774, by the cell-free supernatant from *Pseudomonas aeruginosa*. *Microbiology and Immunology*, **47(3)**, 199-206.
- [17] Zubow, V.A., Zubow, K.V. and Zubow, A.V. (2006) The phenomenon of water clusters distribution in water and solvated clusters of ion pairs of NaCl in solution near the wall. The wall effect. *Journal of Chemical Industry*, in Russian, **83(6)**, 300-306.
- [18] Shirayev, A., Pagan, D.L., Gunton, J.D., Rhen, D.S., Saxena, A. and Lookman, T. (2005) Role of solvent for globular proteins in solution. *Journal of Chemical Physics*, **122(23)**, 234911.

Patterns of synuclein expression throughout lens development

Irina Surgucheva^{1,2}, Belinda MacMahon³, Andrei Surguchov^{1,2*}

¹Retinal Biology Research Laboratory, Veterans Administration Medical Center, Kansas City, USA; *Corresponding Author:
asurguchov@kumc.edu

²MO and Department of Neurology, Kansas University Medical Center, Kansas City, USA

³Washington University, St. Louis, USA

Received 20 December 2009; revised 4 February 2010; accepted 25 February 2010.

ABSTRACT

Synucleins belong to a family of small soluble proteins with chaperonic activity implicated in human diseases, but their normal function is not completely understood. Expression of α , β and γ -synucleins was analyzed in rat and human lens on different stages of development. No significant expression of α - and β -synucleins were found, whereas γ -synuclein was expressed in both species only on early stages of lens development. Examination of γ -synuclein upstream region demonstrated the similarity in its organization with promoter regions of crystallins and heat shock protein's genes. γ -Synuclein upstream region contains motives identical or similar to regulatory *cis*-elements in their promoters including binding sites for Pax6 and Sox. These results suggest that γ -synuclein plays a role in distinct temporal events in lens development, presumably acting as a specific chaperone.

Keywords: Lens; Crystallins; Synucleins; Promoter; Chaperones; Heat Shock Proteins

1. INTRODUCTION

The heat shock proteins (Hsps) are members of a gene family encoding molecular chaperones: the cytoplasmic mediators or protein folding. Chaperones in addition to their assistance in protein folding/unfolding fulfill multiple housekeeping functions, such as transport across membranes, participation in protein degradation [1] and modulation of the cytoskeleton [2].

Several reports demonstrated an important role of chaperones in embryonic development. For example, Hsp47 is a chaperone essential for early mammalian embryogenesis [3], members of the Hsp70 family control germ cell meiosis in mice [4] and Hsp70 is required for embryonic lens formation [5].

Synucleins are a family of small proteins with chaperonic properties [6,7] consisting of three members: α -, β -, and γ -synuclein (reviewed in [8]). Synucleins are abundant soluble proteins found primarily in nervous systems the functions of which are not completely understood. All synuclein members share a common structural design, with the first two thirds of the sequence organized within a series of amphipathic domains that may facilitate membrane binding. All three synucleins consist of a highly conserved N-terminal domain that includes a variable number of 11 amino acid repeats, and a less conserved C-terminal domain with a relatively high content of acidic amino acids. Synucleins are naturally unfolded proteins and they change their conformation dramatically upon lipid binding [9,10].

The functional role of all three synucleins in the development and maturation of neurons has been demonstrated by several groups. α -Synuclein has an important function in prenatal development and in the formation of the nervous system [11]. It is expressed in neurons very early in human gestation, starts disappearing in early childhood and reappear in the adult neurons [12]. γ -Synuclein has a distinct pattern of expression in the developing nervous system [13]. In eye tissues synucleins are expressed in neural retina and optic nerve [14], however, their presence in other ocular tissues was not thoroughly investigated.

We decided to examine whether members of the synuclein family are expressed in the course of lens development. The lens is an ocular tissue in which all cells are derived by the proliferation and differentiation of lens epithelial cells expressing numerous molecular chaperones. Several chaperones, for example, α -crystallins, are required for specific developmental events and are expressed during a short period of embryonic lens development [5,15-17]. We found significant developmental alterations in the expression of γ -synuclein in rat and human lens. The highest level of γ -synuclein expression in the lens was found in the embryonic steps, at early post natal steps its expression subsides and it is reduced considerably in the mature eye. The upstream region of

γ -synuclein gene contains nucleotide sequences similar to regulatory elements in crystallin genes and binding sites for Pax6 and other transcription factors controlling eye development.

2. EXPERIMENTAL PROCEDURES

2.1. Materials and Methods

Human fetal eyes were a generous gift of Dr. Rosario Hernandez (Department of Ophthalmology, Washington University School of Medicine, St. Louis, MO) received through the International Institute for the Advancement of Science (Exton, PA) and the Anatomical Gift Foundation (Laurel, MD). The samples with gestational age of 42 days, 44 days, 57 days and 20 weeks were used. The use of these samples was approved by Washington University Human Study commission. The eyes were fixed immediately after enucleation in 10% buffered formaldehyde for at least 6 hours.

Samples of rat's eyes were a kind gift of Dr. David Beebe (Department of Ophthalmology, Washington University School of Medicine, St. Louis, MO). Rats were cared for and handled in accordance with the ARVO Statement for the Use of Animals in Ophthalmic and Vision Research and were approved by the Washington University Animal Studies Committee.

Antibodies

Antibody against human γ -synuclein was raised in rabbit against the most unique portion of the protein and used as described earlier at dilution 1:2,500 [14]. For rat eye staining the dilution was 1:1,500. α - and β -synuclein antibody was purchased from Chemicon International Inc. (Temecula, CA) diluted 1:1,500 and 1:2,000, respectively. The specificity of antibodies was checked by Western blotting.

2.2. Immunohistochemical Staining

Eyes were fixed in paraformaldehyde/PBS, pH 7.4 at 40°C. From 8 to 12 sections were prepared and analyzed. After enucleation eyes were washed in PBS containing 0.1% glycine and processed for paraffin embedding. Slices of 5 μ m were cut and placed on silane-coated slides. Before immunostaining, slides were deparaffinized and incubated for 1 h in PBS/glycine at RT to reduce non-specific binding. Slides were preincubated with 5% milk for 30 min, rinsed and incubated with primary antibody for 30 min.

Biotinylated secondary antibody was placed on the sections and incubated for 30 min, washed with PBS, and reacted with streptavidin-peroxidase conjugate (Vector Laboratories) for 30 min. The bound antibody-peroxidase complexes on the sections were visualized using a 3,3'-diaminobenzidine tetrahydrochloride (DAB) substrate solution consisting of 1.5 mg of DAB and 50 μ l

of 30% hydrogen peroxide in 10 ml of 100 mM Tris-HCl, pH = 7.6. The sections were incubated in the darkness until brown staining appeared, washed in PBS, counterstained with hematoxylin, dehydrated, and coverslipped with Permount. Control sections were run in parallel, omitting the primary antibody. Other details of immunochemical staining are described previously [14].

2.3. Multiple Sequence Alignment

Multiple sequence alignment was performed using computer program Clustal W [18], pairwise alignment by Smith-Waterman full-length alignments between two sequences.

3. Results

To analyze the pattern of synuclein expression in lens tissues as a function of development, ocular tissues from rats from three age groups were used: day 18 embryos (E18), day 4 newborn animals (P4) and 10 month old rats (**Figure 1**). Human embryonic tissues at days 42, 44, 57 and 20 weeks were analyzed (**Figure 2**).

Results presented on **Figure 1**, demonstrate only slight aged-dependent variations in α -synuclein (a, d, g) and β -synuclein (b, e, h) expression in the rat's eye and significant developmental changes for γ -synuclein expression (c, f, i).

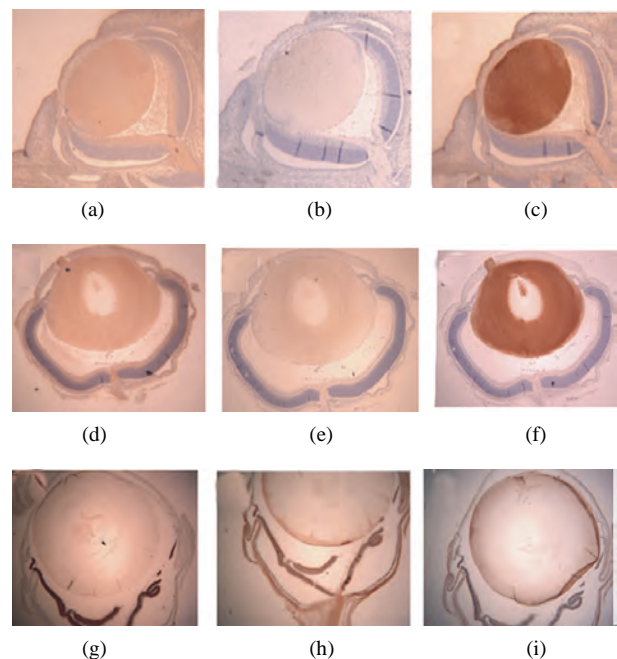


Figure 1. Immunohistochemical detection of synuclein reactivity in various parts of a rat eye on different steps of development. Top row (a-c) – 18 days embryos; middle row (d-f) – 4 day old rats; bottom row (g-i) – 10 months old rats. Left panel (a, d, g) – α -synuclein; middle panel (b, e, h) – β -synuclein; right panel (c, f, i) – γ -synuclein.

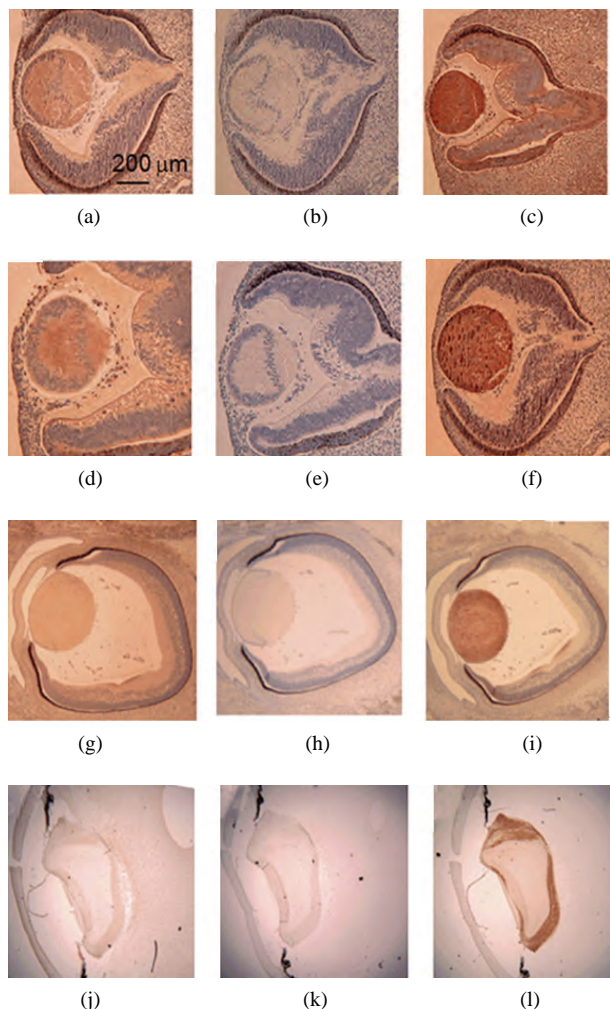


Figure 2. Immunohistochemical detection of synucleins in various parts of the human eye on different steps of development. Top row: 42 days, second row – 48 days, third row – 57 days, bottom row – 20 weeks. Left column - α -synuclein, middle column - β -synuclein, right column - γ -synuclein.

The highest level of γ -synuclein expression is in the E18 lens, at P4 the immunoreactivity becomes less intensive in the periphery of the lens and practically disappears in the central region. The lens from adult animal was not stained, except faintly in the periphery (**Figure 1(i)**).

In E18 rat evidence of γ -synuclein expression was detectable in the majority of both the lens epithelium and differentiating lens fibers (**Figure 1(c)**). In postnatal 4 days rats γ -synuclein nuclear level was decreased (**Figure 1(f)**) and in 10 month old rat's lens γ -synuclein is not detectable (**Figure 1(i)**).

Staining of human embryonic ocular tissues revealed basically the same temporarily alterations in the pattern of expression (**Figure 2**). Weak α -synuclein staining is present in the nuclear area of the lens at early stages of

development (42 and 44 days), reduced by day 57 and disappears by 20 weeks. β -Synuclein is not expressed in the lens at any developmental stage (**Figures 2(b), (e), (h)** and **(k)**). γ -Synuclein immunoreactivity is detectable in the whole lens on day 42 (**Figure 2(c)**), and disappears gradually first from the nuclear area of the lens and later from the whole lens (**Figures 2(f), (i)** and **(l)**).

Then we asked whether these temporary expression of γ -synuclein may be due to the transcriptional regulation of its gene in a similar way as the regulation of crystallin genes implicated in lens development. So we searched the upstream region of γ -synuclein gene for *cis*-regulatory elements similar to that controlling the developmental expression of crystallins and other lens proteins.

We found that γ -synuclein and crystallins have similar *cis*-acting regulatory elements in the upstream regions of their genes. For example, palindromic sequence -102 GGGAGATCCC -93 in γ -synuclein gene is similar to the regulatory elements downstream from -110 in the mouse and -109 in the chicken α A-crystallin gene (**Figure 3**) [19-21]. This palindrome has a key role in the activity of the α A-crystallin promoter and the regulated expression of this gene is indispensable for lens development. The importance of this palindromic element was also proven in experiments with cultured mouse lens cells [19]. Another sequence in γ -synuclein upstream region is decamer -220-AGGTGAGGCT-211 which is similar to α A-crystallin positive *cis*-regulatory element DE2B (-127/-118) contributing significantly to the lens expression of α A-crystallin [21].

γ -Synuclein promoter also contains nucleotide sequences similar to the regulatory elements in the promoter of another crystallin gene required for embryonic lens development- β B1-crystallin. The motif -290 GGGGCAG-284 in the upstream region of γ -synuclein gene is similar to a part of the PL1 regulatory element in mouse β B1-crystallin, whereas the motif -274-GCTGAGCCAGCA-263 is similar to a regulatory element PL2 in β B-crystallin gene (**Figure 3**) [22,23]. PL1 and PL2 sequences were identified as essential binding sites for Pax6, Maf and Prox1 transcription factors, which play a critical role in the lens development. These regulatory elements are evolutionarily conserved in the promoter regions of β B1-crystallin genes. Another motives in γ -synuclein promoter similar to Pax6 binding site [24,25] are the sequence -146 CTGGCCTCCGATCAAT-130 and the sequence -12-TGCACACCCACCATG including the initiating codon ATG (**Figure 3**).

One more feature of the γ -synuclein upstream region which makes it similar to Hsps promoters is the presence of multiple GAA/GAG or TTC/CTC motifs called heat shock elements (HSE) [26-28], for example, in the fol-

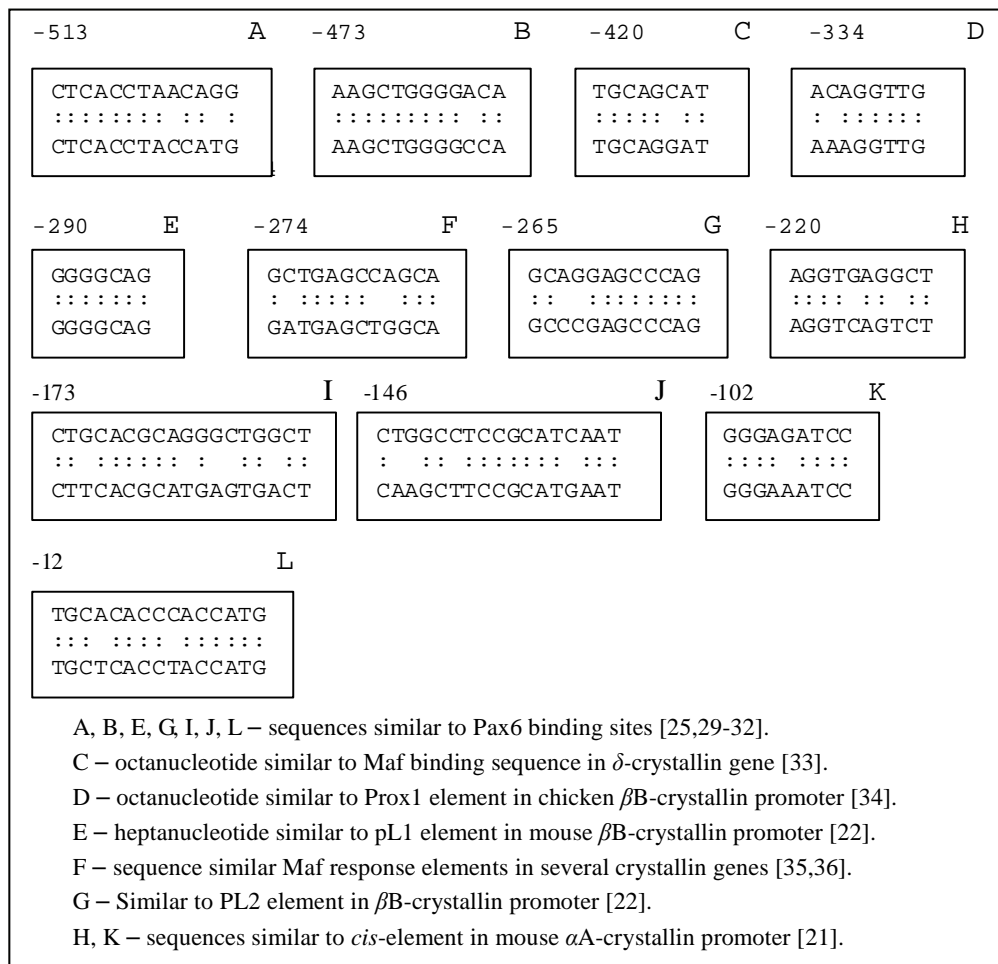


Figure 3. Comparison of the nucleotide sequences in the upstream region of γ -synuclein gene with regulatory elements of other genes implicated in the embryonic development.

lowing sequence -243CTCTGCCTTCCTATCCTGGAG GAAGGTGAGGCTGAACCTCCTCCCTCCCTCCCT CCCTC-183.

Finally, intron 1 of γ -synuclein gene which plays a critical role in transcriptional regulation [37] contains the heptanucleotide 121-TATCAAG-127 and the motif 286-CTGAGCCTGGACGCC-300 which are identical or very close to the binding sites for Sox and Pax6 transcription factors, respectively [38].

4. Discussion

Currently α -synuclein localization is studied most extensively in the brain and their expression in neurons and glial cells is described both in health and neurodegenerative diseases (see for review [8]). The role of γ -synuclein in breast cancer cells and its cellular localization is also well documented [39,40]. γ -Synuclein is also expressed in the retina and optic nerve [14]. Much less is known about localization of synucleins and their function in

health and diseases in other tissues. Here we present data on localization of synucleins in the lens at different steps of embryonic development.

Lens development occurs throughout the lifetime of the individual and involves the terminal differentiation of lens epithelial cells into lens fibre cells [41]. This process begins during embryogenesis and continues into adulthood and old age.

We have found that the expression pattern of γ -synuclein in developing rat and human lens is different from that of two other members of the family. While α -synuclein was detectable at a very low level and β -synuclein was not detectable at all, γ -synuclein was expressed on early steps of lens development, then its nuclear level is reduced during fiber cell differentiation and in mature lens γ -synuclein is not detectable.

Interestingly, previous study of three synuclein expression in embryonic and postnatal mouse development also showed that γ -synuclein has a different pattern of expression to that of two other synucleins [12,42]. In a search of

a possible explanation of γ -synuclein differential expression we compared its promoter region with the sequences involved in the regulation of transcription of other lens proteins. The majority of lens proteome consists of crystallins who possess chaperonic activity and some of them play important role in the lens development. For example, α A-crystallin is a highly expressed protein in the lens which is indispensable for lens development [19,43]. Crystallin gene expression in lens is regulated at the level of transcription by a sparse number of specific DNA-binding transcription factors which bind to *cis*-regulatory elements in the promoter regions of their genes. Interestingly, γ -synuclein upstream region contains motives identical or similar to *cis*-regulatory elements in promoter regions of α A- and β B-crystallins both of which are necessary for normal lens development.

The results presented here demonstrate that γ -synuclein is expressed during a short period of normal embryonic human and rat lens formation as part of the normal development program. This suggests that it plays a role during formation of vertebrate lens. We assume that chaperonic activity of γ -synuclein is required for some of the lens embryonic pathways. Another role of γ -synuclein may be connected with its involvement in apoptotic processes, since lens fiber differentiation involved component of classical apoptosis [44]. Finally, temporarily γ -synuclein expression in embryonic lens may be associated with its ability to participate in transcriptional regulation [45] and to affect distinct growth factor-induced signaling pathways that control normal lens development. It should be noted that since γ -synuclein expression is limited to relatively short period in lens development it can be found by gene arrays analysis only if RNA samples are taken at these particular steps of embryonic development.

Interestingly, the study of synuclein expression in the mammalian cochlea showed that developmentally, γ -synuclein can be seen in the region of the outer hair cells by E19, whereas α - and β -synuclein do not appear at embryonic step of development [46]. These results may indicate a special role of γ -synuclein in the developmental processes of both sensory systems. Thus, we can hypothesize that during lens development synucleins may fulfill one of specific functions, e.g. chaperonic activity or play a role in the regulation of apoptosis or transcription, however, they are eliminated from mature lens because they are prone to aggregate. Indeed, as was shown by Muchowski and coauthors [47], expression of recombinant α -synuclein in mature mouse lens leads to protein aggregation, opacification and cataract formation.

5. ACKNOWLEDGEMENTS

This study was supported by VA Merit Review grant and The Glau-

coma Foundation grant.

REFERENCES

- [1] Macario, A.J. and de Macario, E.C. (2007) Molecular chaperones: Multiple functions, pathologies, and potential applications. *Frontiers in Bioscience*, **12**, 2588-2600.
- [2] Quinlan, R. (2002) Cytoskeletal competence requires protein chaperones. *Progress in Molecular and Subcellular Biology*, **28**, 219-233.
- [3] Nagai, N., Hosokawa, M., Itohara, S., Adachi, E., Matsushita, T., Hosokawa, N., et al. (2000) Embryonic lethality of molecular chaperone Hsp47 knockout mice is associated with defects in collagen biosynthesis. *Journal of Cell Biology*, **150**(6), 1499-1506.
- [4] Dix, D.J., Allen, J.W., Collins, B.W., Mori, C., Nakamura, N., Poorman-Allen, P., et al. (1996) Targeted gene disruption of Hsp70-2 results in failed meiosis, germ cell apoptosis, and male infertility. *Proceedings of the National Academy of Sciences of the United States of America*, **93**(8), 3264-3268.
- [5] Evans, T.G., Yamamoto, Y., Jeffery, W.R. and Krone, P.H. (2005) Zebrafish Hsp70 is required for embryonic lens formation. *Cell Stress and Chaperones*, **10**(1), 66-78.
- [6] Souza, J.M., Giasson, B.I., Leeb, V.M. and Ischiropoulos, H. (2000) Chaperone-like activity of synucleins. *FEBS Letters*, **474**(1), 116-119.
- [7] Surgucheva, I., Ninkina, N., Buchman, V.L., Grasing, K. and Surguchov, A. (2005) Protein aggregation in retinal cells and approaches to cell protection. *Cellular and Molecular Neurobiology*, **25**(6), 1051-1066.
- [8] Surguchov, A. (2008) Molecular and cellular biology of synucleins. *International Review of Cell and Molecular Biology*, **270**, 225-317.
- [9] Perrin, R.J., Woods, W.S., Clayton, D.F. and George, J.M. (2002) Interaction of human alpha-Synuclein and Parkinson's disease variants with phospholipids. Structural analysis using site-directed mutagenesis. *Journal of Biological Chemistry*, **275**(44), 34393-34398.
- [10] Smith, D.P., Tew, D.J., Hill, A.F., Bottomley, S.P., Masters, C.L., Barnham, K.J., et al. (2008) Formation of a high affinity lipid-binding intermediate during the early aggregation phase of alpha-synuclein. *Biochemistry*, **47**(5), 1425-1434.
- [11] Ltic, S., Perovic, M., Mladenovic, A., Raicevic, N., Ruzdijic, S., Rakic, L., et al. (2004) Alpha-synuclein is expressed in different tissues during human fetal development. *Journal of Molecular Neuroscience*, **22**(3), 199-204.
- [12] Raghavan, R., Kruijff, L., Sterrenburg, M.D., Rogers, B.B., Hladik, C.L. and White, C.L. III (2004) Alpha-synuclein expression in the developing human brain. *Pediatric and Developmental Pathology*, **7**(5), 506-516.
- [13] Buchman, V.L., Hunter, H.J., Pinon, L.G., Thompson, J., Privalova, E.M., Ninkina, N.N., et al. (1998) Persyn, a member of the synuclein family, has a distinct pattern of expression in the developing nervous system. *Journal of Neuroscience*, **18**(22), 9335-9341.
- [14] Surguchov, A., McMahon, B., Masliah, E. and Surgucheva, I. (2001) Synucleins in ocular tissues. *Journal of Neuroscience Research*, **65**(1), 68-77.
- [15] Blechinger, S.R., Evans, T.G., Tang, P.T., Kuwada, J.Y.,

- Warren, J.T. Jr. and Krone, P.H. (2002) The heat-inducible zebrafish Hsp70 gene is expressed during normal lens development under non-stress conditions. *Mechanisms of Development*, **112(1-2)**, 213-215.
- [16] Boyle, D.L., Takemoto, L., Brady, J.P. and Wawrousek, E.F. (2003) Morphological characterization of the Alpha A- and Alpha B-crystallin double knockout mouse lens. *BMC Ophthalmology*, **3(3)**, 1-11.
- [17] Tallot, P., Grongnet, J.F. and David, J.C. (2003) Dual perinatal and developmental expression of the small heat shock proteins aB-crystallin and Hsp27 in different tissues of the developing piglet. *Biology of the Neonate*, **83(4)**, 281-288.
- [18] Chenna, R., Sugawara, H., Koike, T., Lopez, R., Gibson, T.J., Higgins, D.G., et al. (2003) Multiple sequence alignment with the Clustal series of programs. *Nucleic Acids Research*, **31(13)**, 3497-3500.
- [19] Nakamura, T., Donovan, D.M., Hamada, K., Sax, C.M., Norman, B., Flanagan, J.R., et al. (1990) Regulation of the mouse alpha A-crystallin gene: Isolation of a cDNA encoding a protein that binds to a cis sequence motif shared with the major histocompatibility complex class I gene and other genes. *Molecular and Cellular Biology*, **10(7)**, 3700-3708.
- [20] Jaworski, C.J., Chepelinsky, A.B. and Piatigorsky, J. (1991) The alpha A-crystallin gene: Conserved features of the 5'-flanking regions in human, mouse, and chicken. *Journal of Molecular Evolution*, **33(6)**, 495-505.
- [21] Klement, J.F., Cvekl, A. and Piatigorsky, J. (1993) Functional elements DE2A, DE2B, and DE1A and the TATA box are required for activity of the chicken alpha A-crystallin gene in transfected lens epithelial cells. *Journal of Biological Chemistry*, **268**, 6777-6784.
- [22] Mizuno, N., Ueda, Y. and Kondoh, H. (2005) Requirement for betaB1-crystallin promoter of *Xenopus laevis* in embryonic lens development and lens regeneration. *Development, Growth and Differentiation*, **47(3)**, 131-140.
- [23] Cui, W., Tomarev, S.I., Piatigorsky, J., Chepelinsky, A.B. and Duncan, M.K. (2004) Mafs, Prox1, and Pax6 can regulate chicken betaB1-crystallin gene expression. *Journal of Biological Chemistry*, **279(12)**, 11088-11095.
- [24] Epstein, J., Cai, J., Glaser, T., Jepeal, L. and Maas, R. (1994) Identification of a Pax paired domain recognition sequence and evidence for DNA-dependent conformational changes. *Journal of Biological Chemistry*, **269(11)**, 8355-8361.
- [25] Zhou, Y.H., Zheng, J.B., Gu, X., Saunders, G.F. and Yung, W.K. (2002) Novel Pax6 binding sites in the human genome and the role of repetitive elements in the evolution of gene regulation. *Genome Research*, **12(11)**, 1716-1722.
- [26] Amin, J., Ananthan, J. and Voellmy, R. (1988) Key features of heat shock regulatory elements. *Molecular and Cellular Biology*, **8(9)**, 3761-3769.
- [27] Perisic, O., Xiao, H. and Lis, J.T. (1989) Stable binding of Drosophila heat shock factor to head-to-head and tail-to-tail repeats of a conserved 5 bp recognition unit. *Cell*, **59(5)**, 797-806.
- [28] Yasuda, K., Ishihara, K., Nakashima, K. and Hatayama, T. (1999) Genomic cloning and promoter analysis of the mouse 105-kDa heat shock protein (HSP105) gene. *Biochemical and Biophysical Research Communications*, **256(1)**, 75-80.
- [29] Van Heyningen, V. and Williamson, K.A. (2002) Pax6 in sensory development. *Human Molecular Genetics*, **11(10)**, 1161-1167.
- [30] Kamachi, Y., Uchikawa, M., Tanouchi, A., Sekido, R. and Kondoh, H. (2001) Pax6 and SOX2 form a co-DNA-binding partner complex that regulates initiation of lens development. *Genes and Development*, **15(10)**, 272-286.
- [31] Lengler, J., Bittner, T., Münster, D., Gawad, A.-D. and Graw, J. (2005) Agonistic and antagonistic action of AP2, Msx2, Pax6, Prox1 AND Six3 in the regulation of Sox2 expression. *Ophthalmic Research*, **37(6)**, 301-309.
- [32] Yang, Y., Stopka, T., Golestaneh, N., Wang, Y., Wu, K., Li, A., et al. (2006) Regulation of alphaA-crystallin via Pax6, c-Maf, CREB and a broad domain of lens-specific chromatin. *EMBO Journal*, **25(10)**, 2107-2118.
- [33] Muta, M., Kamachi, Y., Yoshimoto, A., Higashi, Y. and Kondoh, H. (2002) Distinct roles of SOX2, Pax6 and Maf transcription factors in the regulation of lens-specific delta1-crystallin enhancer. *Genes to Cells*, **7(8)**, 791-805.
- [34] Chen, X., Taube, J.R., Simirskii, V.I., Patel, T.P. and Duncan, M.K. (2008) Dual roles for Prox1 in the regulation of the chicken betaB1-crystallin promoter. *Investigative Ophthalmology & Visual Science*, **49(4)**, 1542-1552.
- [35] Kerppola, T.K. and Curran, T. (1994) Maf and Nrl can bind to AP-1 sites and form heterodimers with Fos and Jun. *Oncogene*, **9(3)**, 675-684.
- [36] Mahoney, K.M., Petrovic, N., Schacke, W. and Shapiro, L.H. (2007) CD13/APN transcription is regulated by the proto-oncogene c-Maf via an atypical response element. *Gene*, **403(1-2)**, 178-187.
- [37] Lu, A., Gupta, A., Li, C., Ahlborn, T.E., Ma, Y., Shi, E.Y., et al. (2001) Molecular mechanisms for aberrant expression of the human breast cancer specific gene 1 in breast cancer cells: control of transcription by DNA methylation and intronic sequences. *Oncogene*, **20(37)**, 5173-5185.
- [38] Grinchuk, O., Kozmik, Z., Wu, X. and Tomarev, S. (2005) The Optimedin gene is a downstream target of Pax6. *Journal of Biological Chemistry*, **280(10)**, 35228-35237.
- [39] Jia, T., Liu, Y.E., Liu, J. and Shi, Y.E. (1999) Stimulation of breast cancer invasion and metastasis by synuclein gamma. *Cancer Research*, **59(3)**, 742-747.
- [40] Gupta, A., Inaba, S., Wong, O.K., Fang, G. and Liu, J. (2003) Breast cancer-specific gene 1 interacts with the mitotic checkpoint kinase BubR1. *Oncogene*, **22(48)**, 7593-7599.
- [41] Wrude, M.A. (1996) Cellular and molecular features of lens differentiation: a review of recent advances. *Differentiation*, **61(2)**, 77-93.
- [42] Ninkina, N.N., Privalova, E.M., Pinon, L.G., Davies, A.M. and Buchman, V.L. (1999) Developmentally regulated expression of persyn, a member of the synuclein family, in skin. *Experimental Cell Research*, **246(2)**, 308-311.
- [43] Brady, J.P., Garland, D.L., Green, D.E., Tamm, E.R., Giblin, F.J. and Wawrousek, E.F. (2001) AlphaB-crystallin in lens development and muscle integrity: A gene knockout approach. *Investigative Ophthalmology & Visual Science*, **42(12)**, 2924-2934.
- [44] Wrude, M.A. (2000) Minireview: Apoptosis as seen through a lens. *Apoptosis*, **5(3)**, 203-209.
- [45] Surgucheva, I. and Surguchov, A. (2008) γ -synuclein: Cell-type-specific promoter activity and binding to tran-

- scription factors. *Journal of Molecular Neuroscience*, **35(3)**, 267-271.
- [46] Akil, O., Weber, C.M., Park, S.N., Ninkina, N.N., Buchman, V.L. and Lustig, L.R. (2008) Localization of synucleins in the mammalian cochlea. *Journal of the Association for Research in Otolaryngology*, **9(4)**, 452-463.
- [47] Muchowski, P.J., Ramsden, R., Nguyen, Q., Arnett, E.E., Greiling, T.M., Anderson, S.K., *et al.* (2008) Noninvasive measurement of protein aggregation by mutant huntingtin fragments or alpha-synuclein in the lens. *Journal of Biological Chemistry*, **283(10)**, 6330-6336.

Molecular dynamics simulation analyses of viral fusion peptides in membranes prone to phase transition: effects on membrane curvature, phase behavior and lipid-water interface destabilization

Manami Nishizawa, Kazuhisa Nishizawa*

Department of Laboratory Medicine, School of Medical Technology, Teikyo University, Tokyo, Japan; *Corresponding Author:
kazunet@med.teikyo-u.ac.jp

Received 8 January 2010; revised 3 February 2010; accepted 18 February 2010.

ABSTRACT

To gain insight into the atomistic details of membrane fusion induced by fusogenic peptides, molecular dynamic simulations of synthetic peptides, derived from viral fusion proteins, contained in lipid bilayers were performed. A 20 amino acid peptide from the N-terminus of the influenza HA fusion peptide (WT20) assumed the oblique orientation at the interface between water and the membrane made up of dipalmitoylphosphatidylcholine (DPPC)/palmitic acid (PA), as reported previously for different membranes. Simulations of WT20 embedded in bilayer membranes made up of dioleoylphosphatidylethanolamine (DOPE) and DPPC/PA showed a positive curvature-inducing effect, whereas WT20 showed a negative curvature-inducing effect on a DPPC bilayer. In phase reconstitution analyses starting from a random mixture of DPPC, PA and water molecules, WT20 weakly stabilized an inverted hexagonal phase. In the latter analyses WT20 preferentially assumed a transmembrane orientation as opposed to the interfacial orientation, regardless of the phase to which the system settled (lamellar vs. inverted hexagonal). In another set of analyses using systems containing a water layer between the apposed DPPC/PA (and DOPE) monolayers, the behavior of WT20 during the formation of an intermembrane connection (or stalk) was examined. Comparison among the mutants supports a view that the oblique orientation of WT20 facilitates the perturbation of the lipid-water interface and the stalk formation. Taken together, these results imply that the influenza HA fusion peptide can have substantial effects on the membrane curvature and can assume a wide range of orientation/position in

membranes depending on the local environment of the lipid/water system. Its movability and oblique orientation appear to be associated with its ability to perturb membrane/water interfaces.

Keywords: Molecular Simulation; Fusion Peptide; Stalk Formation; Lipid Mixing; Hemifusion

1. INTRODUCTION

Fusion of viral and plasma or endosomal membranes is mediated by envelope glycoproteins, known as fusion proteins. For many viruses, fusion requires major structural modification of the fusion protein. Such modification has been established, for example, for influenza virus hemagglutinin (HA) and HIV gp41 proteins [1-6]. The ectodomain of HA has been shown to consist of six polypeptides forming a trimer of HA1-HA2 complexes. The N-terminus of HA2, critical for HA fusion activity, has a highly conserved, hydrophobic sequence, referred to as the fusion domain or fusion peptide (FP) [7,8]. In response to low pH in the endosome, HA changes conformation and projects its fusion peptide towards the target cell membrane [2,9].

Sequence and mutational analyses have identified and characterized FPs of fusion proteins for a number of viruses. Many findings support the direct involvement of FP, which is typically located at the N-terminus, in fusion between viral and cellular membranes (e.g. [7,10-15]). Studies of the full-length fusion protein and in vitro assay of fusion peptide activities provided important clues on protein-induced membrane fusion events. In addition, synthetic FPs have been shown to exhibit membrane fusion and lytic activities [16-26].

The FP of the Newcastle Disease Virus was shown to adopt an oblique angle in a DPPC monolayer [27]. Since then, the tilted orientation has been reported for FPs of

several fusion proteins involving SIV gp32 [28], HIV-1 gp41 [29] and HA2 [30]. More recently, Tamm and co-workers, using NMR and EPR, showed that the FP of HA (or HAFP) forms a shallow-angle inverted V structure [31,32]. Their subsequent studies of the mutants G1V and W14A support the view that the inverted V shape and/or oblique orientation plays an important role in the fusogenicity of the peptide [33,34]. The N-terminus FP and membrane proximal external region (MPER) of HIV-1 gp41 also exhibit lipid destabilizing and fusion activity against liposomes [25,26,28,35,36]. Several other peptides from proteins involved in lipid metabolism or from neurotoxic proteins have also been shown to adopt a tilted orientation (for review see [27,37]). Charlotteaux *et al.* [37] have proposed that the tilted orientation may be responsible for the lipid destabilizing activity of FPs. For HAFP, although experimental findings vary in several aspects, there is general consensus that the significant α -helical content and oblique orientation of HAFP in the membrane are important for fusogenicity [30,38,39].

Recent computational molecular simulations have been extended to studies of phase transitions of lipids, providing opportunities to study how the formation of nonlamellar phases is affected by lipid composition and peptides [40]. Marrink and Tieleman carried out atomistic molecular dynamics (MD) simulations of monoolein in an inverted cubic phase of the diamond type [41]. Importantly, a dipalmitoylphosphatidylcholine (DPPC)/palmitic acid (PA)/water 1:2:20 system exhibits membrane fusion and transformation from a lamellar to the inverted hexagonal phase in a manner similar to experimental systems [42]. Coarse-grained (CG) simulations of DOPE and DOPE/DOPC (dioleoylphosphatidylcholine) bilayers showed that spontaneous formation of stalks between the lamellar bilayers is triggered either by increasing the temperature or by reducing the hydration level [43]. It has also been shown that a transmembrane peptide induces lipid sorting as well as the lamellar to inverted phase transition in CG simulations [44].

Given the progress in molecular dynamics simulations, one may ask whether membrane fusion induced by FPs can be studied with MD simulations. Several simulation studies of FPs with explicit treatment of the water/lipid membrane have been carried out [45-48]. They showed that the oblique and kinked structure of FPs is stable for at least 5-18 ns in DMPC (dimyristoyl-phosphatidylcholine) bilayer [47] and in POPC (palmitoyloleoyl-phosphatidylcholine) bilayers [46,48]. A recent study on oligomerization of HAFP, which utilized an implicit treatment of water, has shown that many different configurations (peptide/peptide and peptide/membrane) have similar energy levels [49]. How such structural features of FPs are associated with its fusogenicity is important. However, MD simulation analysis of mem-

brane fusion is generally in its infancy. Hence, using the DPPC/PA and DOPE systems that have been shown to reproduce the phase behavior reported for the corresponding experimental system [42,50,51], we performed the following sets of simulations (~3 μ s in total) to examine dynamics of HAFP and other peptides.

First, the equilibrium position/orientation in the bilayer membranes of HAFP was analyzed (in the ‘equilibrium analysis’ section). Second, using relatively large patches of membranes, the effect of HAFP on the membrane curvature was examined (‘curvature analysis’). Third, using the phase reconstitution system made up of DPPC/PA/water, the effect of HAFP on the phase behavior was analyzed (‘phase analyses’). Finally, in the Discussion section, we show some non-equilibrium MD simulation results to examine the behavior of HAFP and MPER during the formation of an intermembrane connection (‘stalk propensity analyses’). Overall results are consistent with recent experimental and theoretical findings, suggesting the potential usefulness of the atomistic simulation approach for studying peptide-induced fusion. However, given the previous simulation studies of HAFP with the DMPC and POPC membranes [46-48], we here attempted to examine the peptide dynamics in lipid structures involving non-lamellar ones. Therefore, the simulation conditions are not physiological and corresponding experiments involving the peptides have not been done. Since this approach cannot stand alone, experimental and structural studies that solidify the hypothesis are necessary.

2. SIMULATION DETAILS

The GROMACS 3.3.1 program was used for MD simulations [52]. For DPPC, the parameters by Berger were used [53]. For palmitic acid (PA), the protonated state was used as in Knecht *et al.* [42]. The PA carboxyl group was parameterized based on the glutamic acid from the GROMOS-87, whereas for the remaining acyl chain, the Berger parameter was used [53]. For DOPE, the parameter by Berger *et al.* [53] with modification by de Vries [50] was used. For the HAFP, X31 sequence, referred to as WT20, was used as in [32]. For the MPER of HIV-1, the segment of amino acids 662-683 was used based on Sun *et al.* [54]. The sequence of the peptides analyzed are:

WT20: GLFGAIAGFIENGWEGMIDG

W14A: GLFGAIAGFIENGAEGLGMIDG

G1V: VLFGAIAGFIENGWEGMIDG

WT13: GLFGAIAGFIENG

WT8: GLFGAIAG

MPER: ELDKWASLWNWFNITNWYIK,

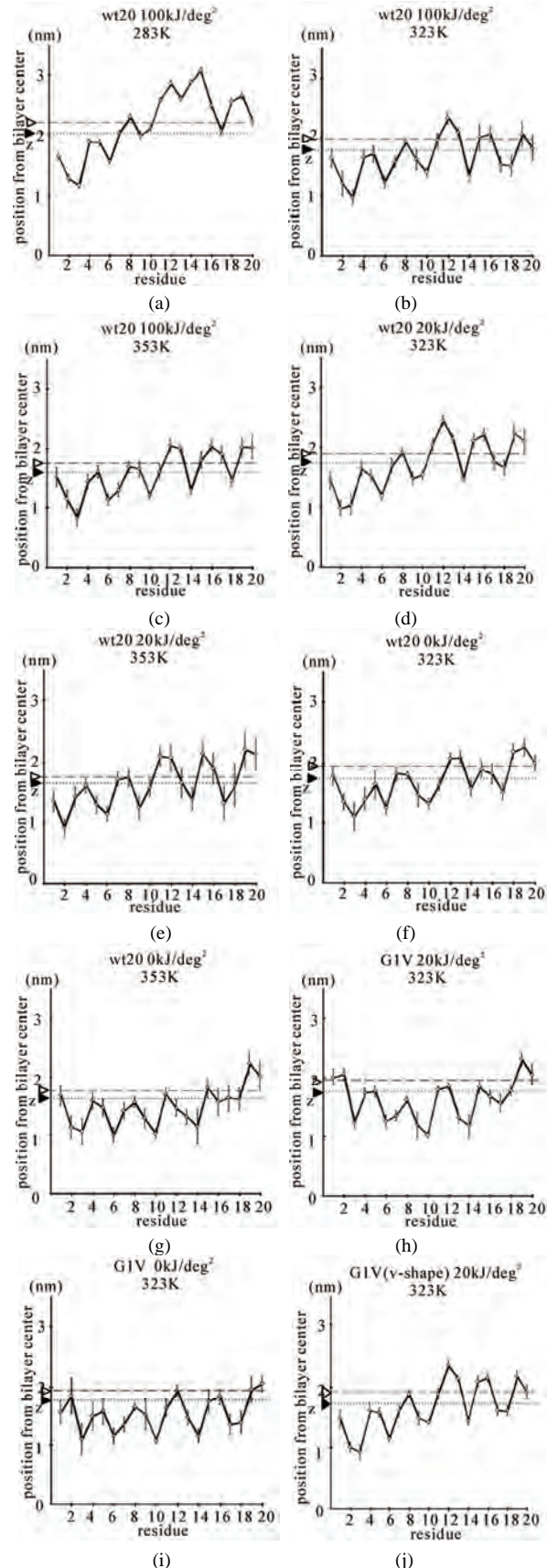
Note that W14A and G1V are identical with WT20 except for the altered residue shown with an underline. For the peptides and their mutants, the GROMOS-96

parameter set was used. For water, the simple-point charge (SPC) model [55] was used as in Knecht *et al.* [42]. For all simulations, the bond lengths of lipids and water molecules were restrained using the LINCS and SETTLE respectively [56,57]. To account for the long-range electrostatic interactions, the particle-mesh Ewald (PME) algorithm [58] was used with the real-space cutoff at 9 Å and the maximal grid size of 0.12 Å. Berendsen coupling was used for temperature control [59]. The pressure was controlled by the Berendsen barostat at 1 atm coupling all directions of the box to 1 bar allowing the box to deform.

As stated in the Introduction, this study consists of the equilibrium analysis, the curvature analysis, the phase analysis and the stalk propensity analysis. For all DPPC/PA membranes, the initial coordinates were created by randomly placing the DPPC and PA in a manner shown in [42]. The DOPE bilayer was prepared as described in [50]. Our preliminary analyses reproduced the phase behavior of the DPPC/PA/water system reported in [42]. 1:20 DOPE/water did not show a H_{II} transition at 353 K within 10 ns. For peptides, coordinates for the initial structures were based on NMR analyses [31,33,34,54]. For WT20, G1V and W14A, model 8 (of PDB code 1IBN), model 2 (of 1XOP) and model 17 (of 2DCI) were used respectively, based on the root mean square deviation (RMSD) of the backbone heavy atoms from the other models. Likewise, for the MPER the model 3 of 2PV6 was used [54]. For the HAFP, the N-terminus of the peptides was protonated as in Zhou *et al.* [60], whereas the C-terminus was capped with NH_2 . The N- and C-termini of MPER were acetylated and amidated, respectively. The sidechains of Glu11 and Glu15 of the HAFP were protonated except for set 16 based on the study by Zhou *et al.* [60]. For ionizable residues of the MPER, the standard protonation state at pH 7 was used.

For the equilibrium analysis (**Figure 1**), a membrane composed of DPPC/PA/water 1:2:40 was pre-equilibrated, then the peptides were embedded in a position/orientation similar to those in [31,33,34,54]. A 100 ps run was carried out with positional restraints on all peptide atoms, followed by a 10 ns run at 323 K with restraints only on the dihedral angles (**Figure 1** and see below).

For the curvature analysis (**Figure 3**), three different bilayers were used: 1) 192 DPPC, 384 PA and 15909 water molecules, 2) 270 DOPE and 10324 water molecules, and 3) 240 DPPC and 11065 water molecules. The approximate size of the simulation box (in x, y, z dimensions) was for: 1) $4.5 \times 23.3 \times 9.4 \text{ nm}^3$, 2) $4.5 \times 18 \times 8.5 \text{ nm}^3$, and 3) $4.5 \times 20 \times 8.0 \text{ nm}^3$. Three WT20 peptides were placed at the lipid/water interface and 20 ns simulations were carried out. The curvature was measured using the distance d , which is the distance between the



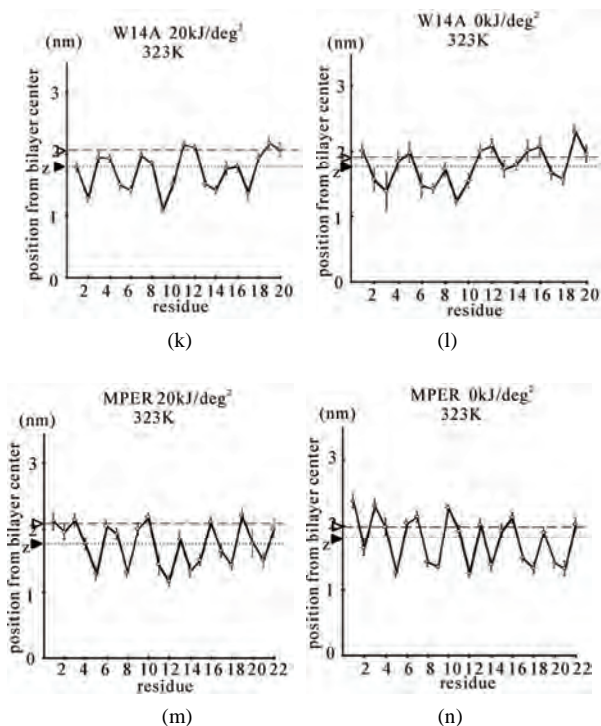


Figure 1. The average z-positions of peptide sidechains in the equilibrium analysis. Shown are the COMs (the center of mass) of side chains and standard deviation (error bars) obtained from the period between $t = 5$ and 10 ns. (a-c) DPPC/PA/water/WT20 1:2:40:1 system with the dihedral restraints $100 \text{ kJ}/(\text{deg})^2$ at 283 K (a), 323 K (b) and 353 K (c). (d, e) Results of the same system as in (a-c) but with using $20 \text{ kJ}/(\text{deg})^2$ restraints at 323 K (d) and 353 K (e). (f, g) Results of the same system as (a-c) but without dihedral restraints at 323 K (f) and 353 K (g). The average positions of the phosphorus atoms in lipid molecules are shown by arrowheads. (h) G1V data at 323 K with $20 \text{ kJ}/(\text{deg})^2$ restraints. (i) G1V data at 323 K without restraints. (j) G1V data at 323 K restrained to the 1IBN (pH 5 NMR-structure of WT20) with $20 \text{ kJ}/(\text{deg})^2$ dihedral restraints. (k) W14A at 323 K with $20 \text{ kJ}/(\text{deg})^2$ restraints. (l) W14A at 323 K without restraints. (m) DPPC/PA/water/MPER 1:2:40:1 system with the $20 \text{ kJ}/(\text{deg})^2$ restraints, at 323 K. (n) Same as (m), but without the restraints. In each figure, an open triangle represents the average position of the COM of phosphorus atoms of DPPC, whereas a closed triangle represents that of carbonyl oxygen atoms of DPPC.

bilayer midplane and the COM of the group of the lipid molecules whose x-coordinate of the COM is located within the range covered by the three peptides as shown by the cartoon in the **Figure 3**.

For the phase analysis (**Figure 4**), the procedure was based on [42]. A system composed of 32 DPPC, 64 PA, 640 SPC water molecules with or without WT20 was used. 30 ns simulations were performed starting from the initial structures generated randomly using the Genbox module of the Gromacs suite.

For the stalk propensity analysis (**Figure 5**), the initial coordinates of lipids and peptides were sampled from the

last 0.5 ns of the equilibrium analysis runs (at 323 K), whereas the hydration level was reduced to e.g., DPPC/PA/water 1:2:20. (The structure at 353 K was not used because the reduction of the hydration level from 1:2:40, if carried out at 353 K, appears to be too strong a perturbation.) The amount of water between the monolayers was adjusted without moving the peptide or lipid. To reduce the bias further, we sampled different frames from the equilibrium analysis. Care was taken to vary the coordinates and initial velocities among the runs. In this study, a stalk was defined as follows. First, a connection of lipid molecules between the lipid monolayers was found which existed for > 1 ns. Second, this connection was judged to be a stalk when it could be regarded as a cylinder that contained some of the atoms of three or more lipid molecules and 10 or less water molecules, within any 3\AA segment of the cylinder. For the two-peptide stalk propensity analysis, the lipid/peptide coordinates at 323 K were aligned such that the peptides contained in the proximal monolayers apposed to each other and oriented in three different relative configurations (parallel, cross and anti-parallel). For example, for the cross configuration, two peptides form a ‘cross’ when viewed from the top, whereas, for the anti-parallel configuration, the N-terminus of one peptide and the C-terminus of the other overlap when viewed from top. For all the configurations, the x- and y-coordinates of the center of mass of the two peptides were identical.

One feature of this study is that many simulations utilized restraints on the ϕ and ψ dihedral angles of the peptide backbone, using the initial structures (*i.e.*, the models from 1IBN and 2PV6) as the reference structures. For the restraints, a coefficient of $100 \text{ kJ}/(\text{deg})^2$ (strong restraint) and $20 \text{ kJ}/(\text{deg})^2$ (weak restraint) were tried. With the weak restraints at the high temperature (353 K), the helicity of WT20 was preserved, but the kink-like structure was less prominent (**Figure 1** and data not shown). However, to minimize the effect of the artificial restraints, we utilized the weak restraints in many of the simulations. As the Results section shows, when the dihedral restraints were removed, structural variation was large in the pre-runs and in our preliminary analyses; the stalk-forming ability of the peptide was low compared to the peptide with the restraints. This led us to apply restraints in many of the simulations. The effects of the restraints must be critically assessed in future studies.

In this study, the z-axis is perpendicular to bilayer. For the secondary structure analysis, the DSSP program (<http://www.cmbi.kun.nl/gv/dssp>) was used based on [61]. Calculations were carried out on 15 AMD 2.2-GHz processors. All molecular images were made with VMD [62].

3. RESULTS

3.1. Equilibrium Analysis

First, the equilibrium position and structure of the pep-

tides were analyzed. The positions of the COM of the amino acid sidechains in DPPC/PA/water/WT20 1:2:40:1 simulations were analyzed (**Figures 1(a)-1(g)**). The composition was chosen because the phase behavior (*i.e.*, lamellar vs. inverted hexagonal) has been studied by both experiments [51] and simulations [42] under similar conditions. The temperature was varied widely (from 283 K to 353 K) because of the potential usefulness of the system for peptide dynamics analyses with lipids in a non-lamellar phase. For Gly residues the position of the C_α atom is shown in **Figure 1**. Under this water-rich condition, no intermembrane connection was formed during 10 ns. Note that for **Figures 1(a)-1(c)**, the 100 kJ/(deg)² restraints on the peptide backbone dihedral angles were used (see Simulation Details). At 323 K, WT20 resided in a slightly deeper part of the membrane than at 283 K, most likely because the area per lipid molecule increased and the headgroup layer was able to accommodate the peptide better at 323 K (**Figures 1(a)** and **1(b)**). (In the pilot analyses, the area of the membrane

(128 DPPC and 256 PA molecules) was 52.3, 67.3 and 78.4 nm² at 283, 323 and 353 K respectively). At 323 K, the position and orientation of WT20 were largely similar to those of previous simulations [46-48]. At 353 K, the structure was similar to that at 323 K, with the exception that the lipid acyl chains were opened wider, making the bilayer thinner than at 323 K (**Figure 1(c)**).

As previous simulation studies have described [46-48], the overall structure was V-like in shape, but the angle of V was larger than the pH 5 NMR-structure (PDB code 1IBN) by Han *et al.* [31].

When the restraints were weakened to 20 kJ/(deg)², the general orientations were similar to those found with 100 kJ/(deg)² restraints (**Figures 1(d), 1(e)**). The α -helix content was also similar to that with 100 kJ/(deg)² restraints (**Figures 2(a), 2(b)**). At 353 K, α -helical content was $63.5 \pm 10.3\%$ for 100 kJ/(deg)² and $68.1 \pm 8.1\%$ for 20 kJ/(deg)² for the last 5 ns (**Figures 2(a), 2(b)**), similar to ~66.8% for the pH 5 structure (1IBN). However, when

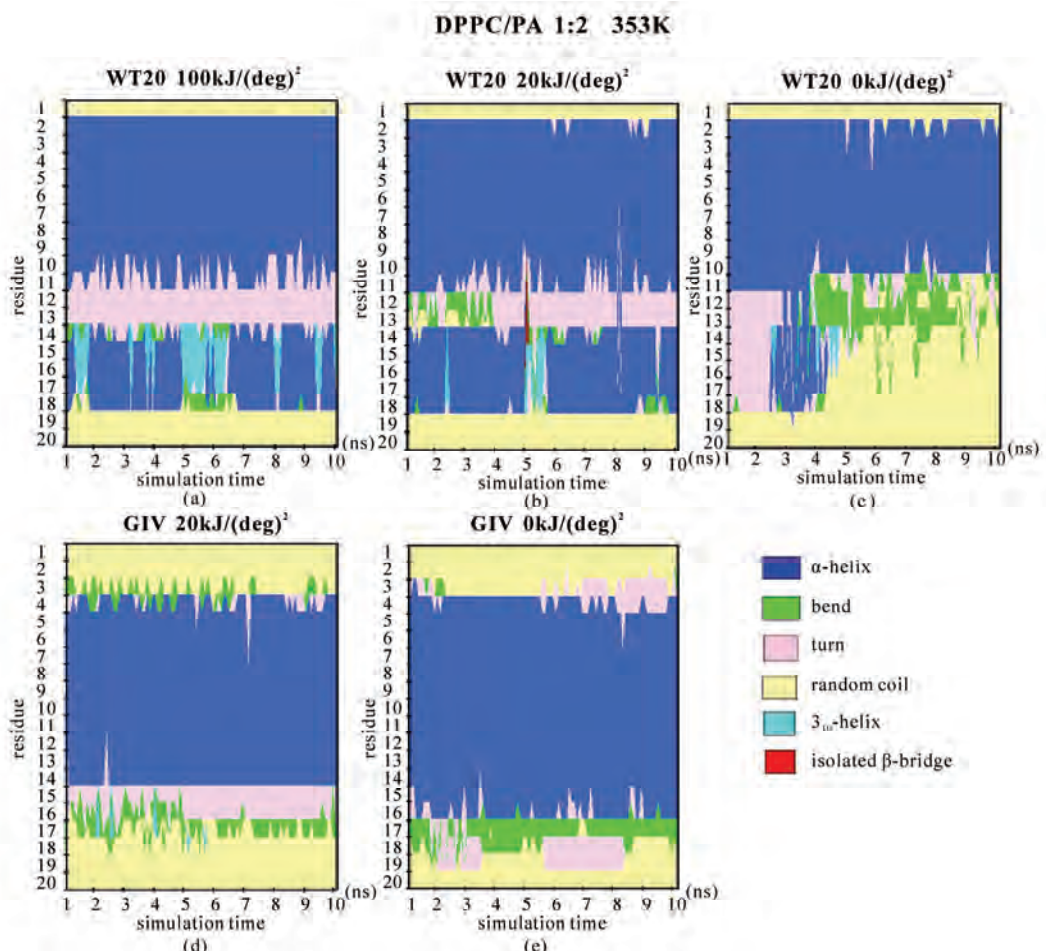


Figure 2. Secondary structure analysis of the peptide backbone based on DSSP [54]. (a, b, c) WT20 with DPPC/PA/water 1:2:40 system at 353 K. (a) Simulation with 100 kJ/(deg)² dihedral restraints. (b) Simulation with 20 kJ/(deg)² dihedral restraints. (c) Simulation with no dihedral restraints; (d, e) GIV with DPPC/PA/water 1:2:40 system at 353 K. (d) With 20 kJ/(deg)² restraints. (e) With no dihedral restraints.

no dihedral restraints were used at 353 K, the orientation was flatter and the helical content decreased to ~45% (**Figure 2(c)** and data not shown). For runs with dihedral restraints of 100 kJ/(deg)², 20 kJ/(deg)² and no restraints, the RMSDs (the average of all C_a atoms) for the last 5 ns of the 353 K pre-run were 1.9 Å, 3.4 Å and 5.2 Å, respectively, with respect to the pH5 NMR-structure (1IBN). (The RMSDs compared with the structure at t = 8 ns were 0.7 Å and 1.8 Å and 2.0 Å.)

Taken together, without the restraints, WT20 exhibits substantial deformation at 353 K from the pH 5 NMR-structure. Removal of the dihedral restraints resulted in a substantial change in the overall structure and an increase in α -helical content also in the case with G1V and W14A mutants (**Figures 1(h), 1(i), 1(k), 1(l)** and **Figures 2(d), 2(e)**). Of note, for G1V and W14A, the restraints based on the reported structures (PDB code 1XOP and 2DCI, respectively) were used. Considering the potential importance of structure, simulations were performed mainly with dihedral restraints of 20 kJ/(deg)² in the following, whereas some simulations were carried out without the restraints.

3.2. Curvature Analysis

The second line of the analyses examined the effect of WT20 on the curvature of bilayer membranes. As **Figure 3** illustrates, three WT20 molecules were embedded in the headgroup layer of each side of bilayers and 20 ns simulations were carried out at 313 K without the dihedral restraints. Intriguingly, the presence of the three WT20 molecules led to a slightly positive curvature of a DPPC/PA 1:2 bilayer, with the *d* value (**Figure 3(a)**) being ~0.53 nm (set-L1, **Figure 3(b)**). When three WT20 peptides were placed such that they aligned with the x-axis, the curvature occurred over the x-direction (set-L1). When the WT20 peptides were aligned with the y-axis, very weak positive curvature was observed over the x-direction (set-L2, **Figure 3(c)**). The positive curvature-inducing effect on a DOPE bilayer was also observed when WT20 peptides were aligned with the x-axis and also when aligned with y-axis (set-L3 and L4 in **Figures 3(d)** and **3(e)**, respectively). However, the effect on a DPPC bilayer was unstable when the WT20 molecules were aligned with the x-axis, as suggested by the large s.d. of *d* value (as shown in **Figure 3**, set-L5), whereas a negative curvature was induced when the WT20 molecules were aligned with the y-axis (set-L6 in **Figure 3**). Overall, the effect on the curvature is dependent on the lipid composition and the peptide orientation. It is currently unclear why the variance was large in the case of DPPC membrane with peptides aligned with the x-axis (set-L5). As a positive control, a DPPC bilayer containing lysophosphatidylcholine (with palmitic acid as the acyl chain) and phosphatidic acid induced curvature in 5 ns simulations of the DPPC/PA bilayer

(data not shown), and therefore at least for our setting, 20 ns simulations were likely to be sufficiently long to examine the peptide effects on membrane curvature.

3.3. Phase Analysis

The effect of WT20 on ‘phase behavior’ of the DPPC/PA/water system was analyzed in the manner described in [42]. In this method, simulations starting from random structures/positions of molecules were performed, allowing spontaneous reconstitution of a lamellar or inverted hexagonal phase (**Figure 4**). As set-R1 of **Figure 4** shows, 60% of the runs (n = 20) performed at 333 K without WT20 formed an inverted hexagonal phase, while 35% of the runs formed a lamellar (bilayer) phase consistent with previous results [42]. For the simulations performed at 333 K with a WT20 peptide (set-R2), a slight increase in the propensity for the hexagonal phase was observed; 75% of runs (n = 20) formed an inverted hexagonal phase.

The effect of WT20 was more pronounced in the simulations performed at 313 K (set-R3 and -R4) than in simulations performed at 333 K; the presence of WT20 increased the propensity of hexagonal phase formation from 35% (set-R3) to 65% (set-R4). These simulations were performed with the 20 kJ/(deg)² dihedral restraints on WT20 to the 1IBN structure. When the dihedral restraints were removed and 313 K simulations performed, the results were largely similar (set-R5) with 60% being judged to be an inverted hexagonal phase. Overall, although the effect appeared to be subtle, the presence of WT20 caused a small shift toward the hexagonal phase. One notable feature of the results was that the WT20 tended to reside in the hydrophobic part of the bilayer or hexagonal structures, protruding into the lipid acyl chains, with the N- and C-termini interacting with distinct water columns (or layers) (**Figures 4(d)** and **4(e)**). In fact, such position/orientation was observed for all the simulations that assumed an inverted hexagonal phase and for 13 out of the 14 simulations that assumed a lamellar phase. Of course, many more simulations have to be carried out to draw any conclusion regarding the equilibrium position because the amount of water seems to be a critical factor governing the equilibrium position of the peptide. Nonetheless, these features are interesting in that such versatility of WT20 positioning may be relevant to its function in later stages of membrane fusion, such as hemifusion formation and rupture of hemifusion diaphragm.

4. DISCUSSION

In the above, the results of the equilibrium analysis, the curvature analysis and the phase analysis of WT20 were shown. In the equilibrium analysis, the oblique orientation of WT20 was largely similar to that reported

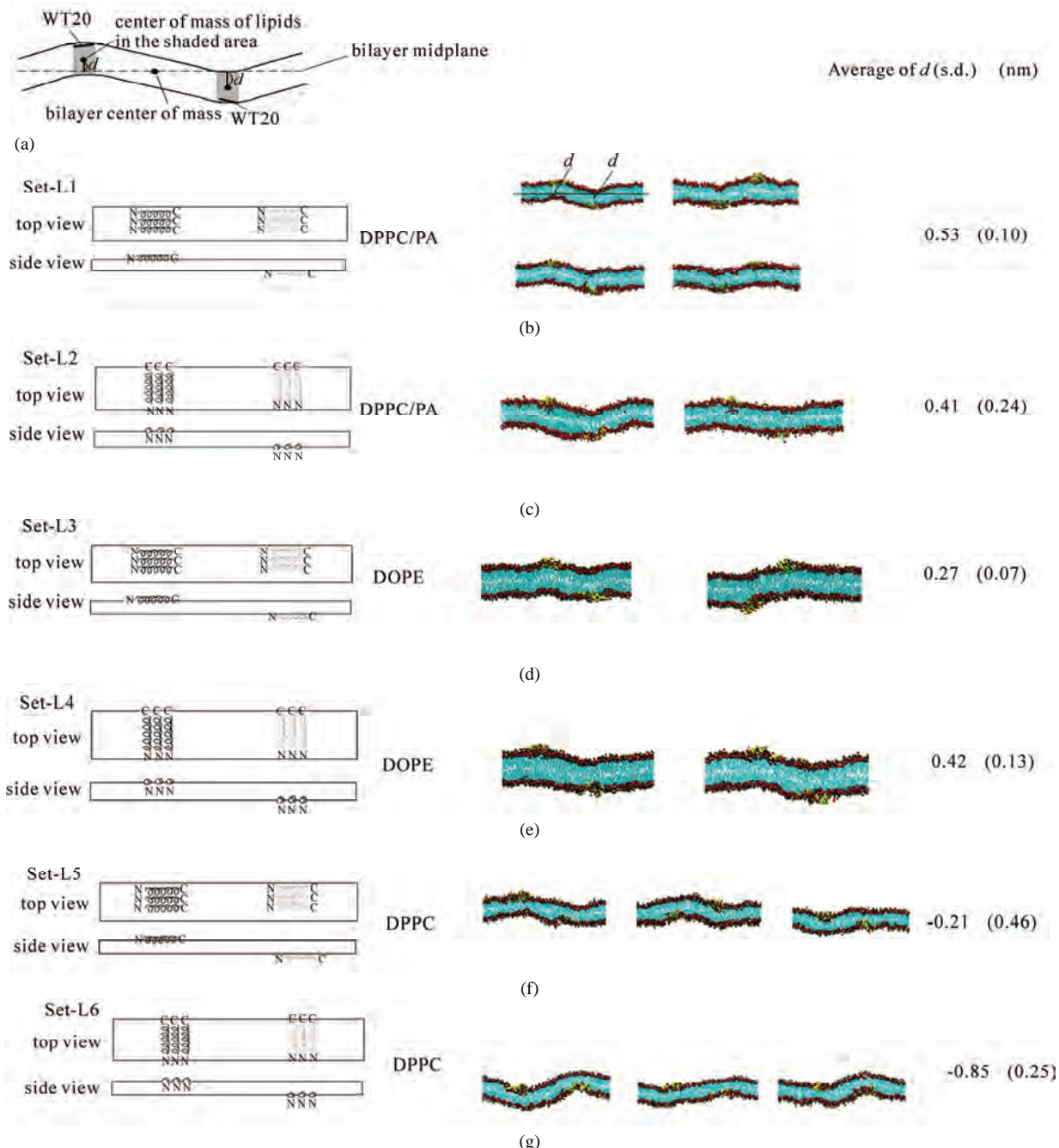


Figure 3. The effect of WT20 on the membrane curvature. (a) Scheme for peptide embedding and curvature measurement. Three WT20 molecules were embedded in the direction along the x-axis or y-axis and 20 ns simulations carried out. The curvature assessment is based on the distance d shown in the cartoon. (b-g) The average d value and representative snapshots at about 20 ns are shown for each set. If the curvature was positive, the value of the average of d becomes positive. Note that two d values per simulation were obtained and in total eight d values were obtained when four simulations were performed. Yellow trace shows the peptide backbone. Red and blue spheres show lipid oxygen and nitrogen atoms. Cyan lines show lipid acyl chains. Water molecules are hidden for clarity. (b) set-L1. Four simulations with a DPPC/PA 1:2 bilayer. WT20 molecules were oriented along the x-axis. The average of $d = 0.53$ nm with s.d. = 0.10. (c) set-L2. Same as (b) but the WT20 molecules are oriented along the y-axis. Two simulations were performed. The average of $d = 0.41$ nm. (s.d. = 0.24). (d) set-L3. DOPE membrane with the WT20 peptides oriented along the x-axis. Two simulations were performed. The average of $d = 0.27$ nm (s.d. = 0.07). (e) set-L4. Same as (d) but the WT20 peptides are oriented along the y-axis. Two simulations were performed. The average of $d = 0.42$ nm (s.d. = 0.13). (f) set-L5 DPPC membrane with the WT20 peptides oriented along the x-axis. Three simulations were performed. The average of $d = -0.21$ nm (s.d. = 0.46). (g) set-L5 DPPC membrane with the WT20 peptides oriented along the y-axis. Three simulations were performed. The average of $d = -0.85$ nm (s.d. = 0.25).

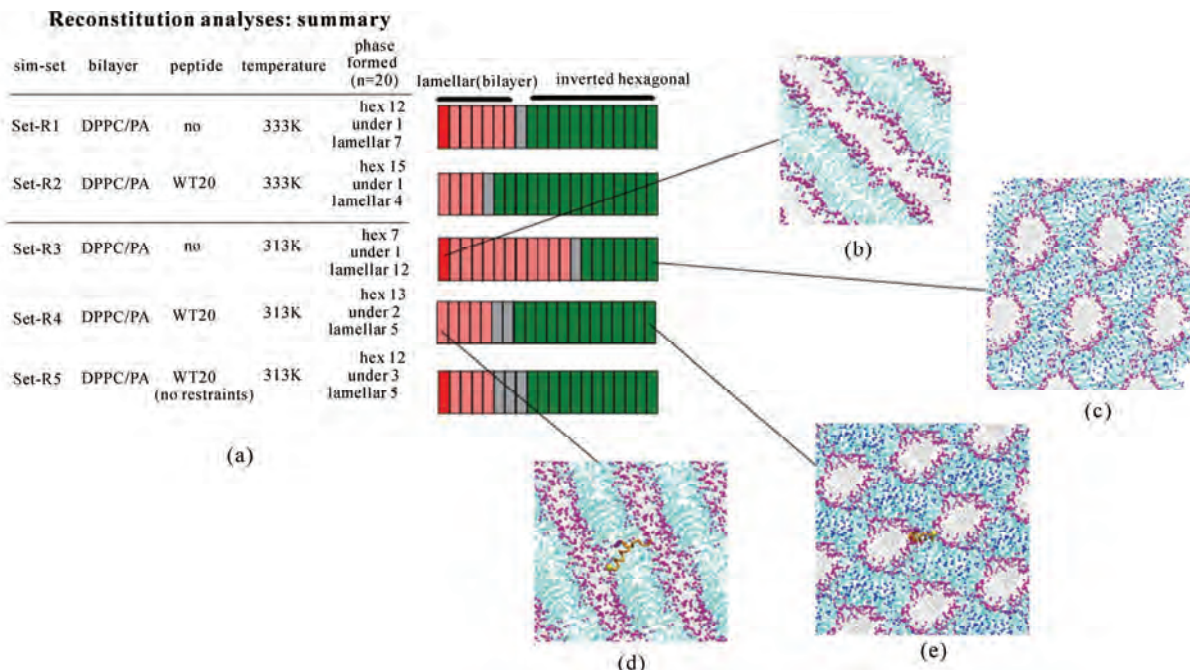


Figure 4. Analyses based on spontaneous formation of the bilayer or the inverted hexagonal phase. (a) Summary of five sets of simulations (set-R1 to R5): (set-R1) DPPC/PA/water, 333 K; (set-R2) DPPC/PA/water/WT20, 333 K; (set-R3) DPPC/PA/water, 313 K; (set-R4) DPPC/PA/water/WT20, 313 K; (set-R5) DPPC/PA/water/WT20 (no restraints), 313 K. 32 DPPC, 64 PA and 640 water molecules were used. For each set, twenty simulations were performed starting from different random structures. Note that for set-R2 and R4, the dihedral angles of WT20 were restrained ($20 \text{ kJ}/(\text{deg})^2$) to the 1IBN as the reference structure. Shown in the right column is a summary of the phases obtained in the simulations. For each set, the final phase of separate 40 ns simulations is judged to be one of an inverted hexagonal ('hex'), a lamellar phase or an undefined ('undef') phase as in [42]. A structure mainly consisting of a bilayer is judged as a lamellar phase although this phase is likely to correspond to a gel phase in [42]. A lamellar phase is indicated in red (pink denotes a defect containing lamellar phase), an inverted hexagonal phase is depicted in green. Gray denotes an undefined phase. (b-e) Representative images of the phase formed: a lamellar phase formed in a set-R3 simulation run (b), a hexagonal phase in a set-R3 run (c), a lamellar phase in a set-R4 run (d), a hexagonal phase in set-R4 run (e). In (d, e) the WT20 peptide backbone is represented by an orange trace and the N-terminus as a yellow sphere. The membrane representation is similar to that described in the legend of Figure 3.

previously, despite of our use of the DPPC/PA membrane. At the high temperature, the orientation was less oblique than at the low temperature, yet the introduction of the dihedral restraints restored the oblique angle. This finding may have technical implications for future simulation studies of peptide-induced membrane fusion.

Does WT20 alter the membrane curvature? Experiments using dipalmitoleylphosphatidylethanolamine (DiDOPE) by Epand and Epand [63] have shown that the wildtype peptide lowers the temperature of the phase transition from bilayer to hexagonal at pH 5 while it raises the temperature at pH 7.4. When added to phosphatidylethanolamine (PE), fusion peptides of some viral fusion proteins induce QII (inverted cubic) phases that do not form spontaneously without the addition of the peptides [64,65]. These and other findings suggest that HAFF lowers the activation energy for steps in the fusion process, rather than stabilizing a particular structure such as the hexagonal phase. Although the difference in lipid composition makes it difficult to compare the experimental findings with our results, our findings

suggest a possibility that MD simulations can complement experimental phase analyses in the presence of peptides. In our analyses, the WT20 effect leading to the slightly positive curvature in DPPC/PA membrane (**Figures 3(b), 3(c)**) may appear to be inconsistent with the result of the reconstitution analyses (**Figure 4**) in which the presence of WT20 led to an increased propensity of an inverted hexagonal phase. However, the peptide protruded into the hydrophobic part of the hexagonal structure with the N- and C-termini interacting with distinct water columns (**Figures 4(d), 4(e)**). Therefore, the phase behavior of the DPPC/PA membrane may be difficult to interpret simply based on the peptide effect on the curvature. The HA peptide may assume distinct orientations and functions depending on the lipid membrane composition and physical properties.

The transmembrane orientation of WT20 observed in the phase analysis may be relevant to the later steps of liposome fusion (e.g., the formation of hemifusion and the hemifusion diaphragm rupture), which deserve future analyses. The previous studies using EPR and NMR

have unambiguously shown that WT20 resides in the outer leaflet of the bilayer membranes [31]. Therefore after binding to the membrane, WT20 is most likely stay in the outer leaflet with the tilted orientation. On the other hand, it has been proposed that, after the stalk formation WT20 assumes a more vertical and/or transmembrane orientation, interacts with transmembrane domain of the fusion protein and destabilizes the stalk and/or the hemifusion diaphragm [4,5]. In this context, more analyses using the reconstitution of various lipids and peptides may give clue to peptide functions in membrane fusion.

4.1. Stalk Propensity Analysis

HAFP and many other peptides derived from virus fusion proteins exhibit lipid destabilizing and fusion activity against liposomes. So, one could be tempted to ask whether the fusogenicity of such peptides *in vitro* experiments can be studied *in silico*. For the DPPC/PA system, the stalk formation is the critical (rate-limiting) step in the transition from a lamellar to an inverted hexagonal phase [42]. For this system, stalk occurrence can easily be observed just by raising the temperature or reducing the hydration level. So, we initially attempted to analyze the peptide behavior during the very early phase of stalk formation. In this attempt, we unexpectedly found that WT20 can facilitate the stalk formation in the system. Therefore, we carried out several non-equilibrium analyses, in which one or two peptide(s) were contained in two apposed lipid monolayers. **Figures 5(a)** and **5(b)** illustrate the setting of the one- and two-peptide simulations, respectively. It may be envisaged that this set of analyses mimics the situation in which dehydration drives two liposomes containing peptides to collide with each other. The initial structures were carefully set up as commented in the Simulation Details section. **Table 1** summarizes the results of one-peptide simulations (mainly using the DPPC/PA/water/WT20 1:2:20:1 system). The stalk propensity score represents the proportion of simulations in which a stalk was formed (**Table 1**).

For all five simulations in set 1, a stalk was formed promptly at $t = \sim 1\text{-}5$ ns (**Table 1**, set 1). By contrast, the stalk propensity was weak (0.3) for the system without WT20 (set 2). When the hydration level was increased, the stalk propensity decreased (set 3 and set 4), consistent with the results reported [42]. To reduce the rate of stalk formation from that in the control (*i.e.*, set 2) simulation, we reduced the temperature, instead of increasing the hydration level. At 343 K, the stalk propensity was 0.9 for the 1:2:20:1 system (set 6), whereas it was 0.2 without WT20 (set 5). **Figure 5(a)** shows snapshots from a representative simulation of set 6. In many stalk-forming events, the polar residues belonging to the kinked region (*i.e.*, Glu11, Asn12 and Glu15) associated

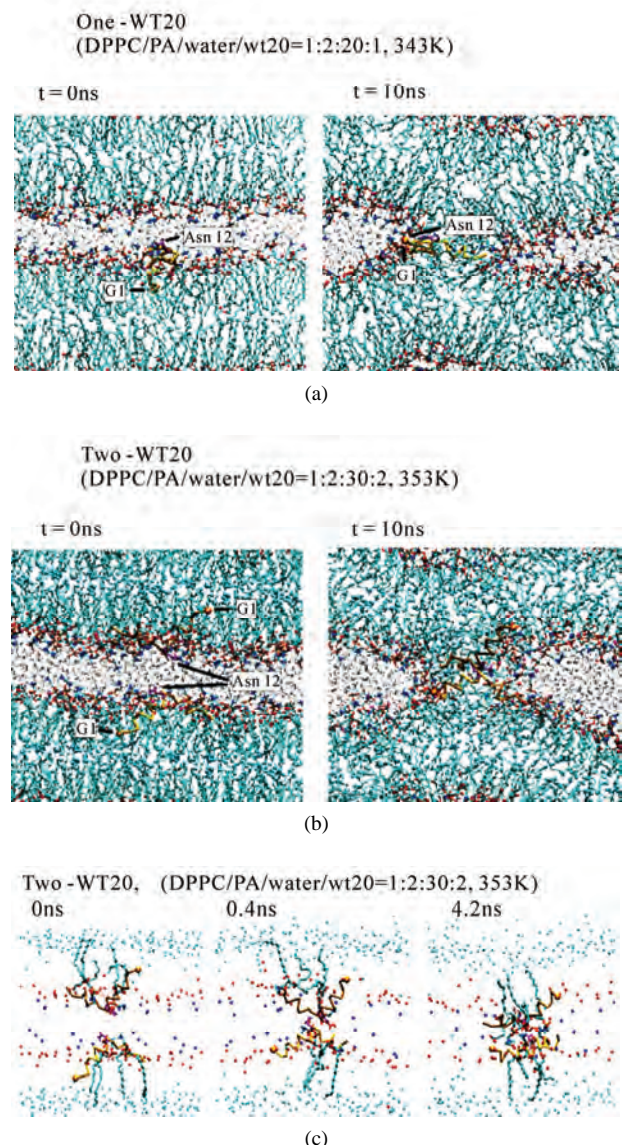


Figure 5. Stalk formation in MD simulations. Snapshots at indicated time points of representative simulations are shown. (a) DPPC/PA/water/WT20 1:2:20:1 system at 343 K (set 6). (b) DPPC/PA/water/WT20 1:2:30:2, 353 K. (c) Lipid molecule movements of a representative stalk-forming event of a 1:2:30:2 simulation. For (a, b), the thick orange trace (also the yellow trace in (b)) shows the peptide backbone. The yellow sphere shows the C_α atom of the G1 residue. Purple licorice indicates the sidechain of Asn12. Cyan lines show lipid acyl chains. The terminal C atoms of lipid acyl chains are represented as cyan balls. Red and blue spheres show lipid oxygen and nitrogen atoms. Black lines indicate water molecules. For (c), the representation scheme is similar to the one used in (a, b), but several lipid molecules are highlighted by thick licorice representation, whereas water and most of lipid acyl chains are hidden. Red licorice shows the sidechain of Glu11.

with the headgroups of lipid molecules of the apposed membrane. Our analyses showed that, once formed, a

Table 1. Stalk propensity analysis of one peptide molecule.

| set | composition | restraints ^a | temperature (K) | stalk propensity score ^b |
|-----|-----------------------------------|----------------------------|-----------------|-------------------------------------|
| 1 | DPPC/PA/water/WT20 1:2:20:1 | 1IBN | 353 | 1* |
| 2 | DPPC/PA/water 1:2:20 (no peptide) | | 353 | 0.3 |
| 3 | DPPC/PA/water/WT20 1:2:25:1 | 1IBN | 353 | 0.4* |
| 4 | DPPC/PA/water/WT20 1:2:30:1 | 1IBN | 353 | 0 |
| 5 | DPPC/PA/water 1:2:20 (no peptide) | | 343 | 0.2 |
| 6 | DPPC/PA/water/WT20 1:2:20:1 | 1IBN | 343 | 0.9 |
| 7 | DPPC/PA/water/WT20 1:2:20:1 | 1IBN, Asn12 C _a | 343 | 0.4* |
| 8 | DPPC/PA/water/WT8 1:2:20:1 | 1IBN | 343 | 0 |
| 9 | DPPC/PA/water/WT13 1:2:20:1 | 1IBN | 343 | 0.4 |
| 10 | DPPC/PA/water/WT20 1:2:20:1 | free | 343 | 0.2 |
| 11 | DPPC/PA/water/G1V 1:2:20:1 | 1XOP | 343 | 0.1 |
| 12 | DPPC/PA/water/W14A 1:2:20:1 | 2DCI | 343 | 0.1 |
| 13 | DPPC/PA/water/MPER 1:2:20:1 | 2PV6 | 343 | 0.2 |
| 14 | DOPE/water/WT20 1:15:1 | 1IBN | 353 | 0.8 |
| 15 | DOPE/water 1:15 (no peptide) | | 353 | 0.4 |

^aBasically, the restraints of 20 kJ/(deg)² were used with respect to the following reference structures: 1IBN for the pH 5 NMR structure of WT20³¹, 1XOP for G1V³³, 2DCI for W14A³⁴ and 2PV6 for MPER⁶⁰. ‘Free’ (set 10) indicates no dihedral restraints. ^b*The stalk propensity score is defined as the proportion of stalk (+) simulations out of the total number of simulations (n). For most sets n = 10. For the sets indicated by*, n = 5 (*i.e.*, set 1, 3, 7).

stalk consisting of 3-4 lipid molecules tends to grow thicker consisting of > 8 molecules. Stalk formation was typically accompanied by a subtle upward movement of WT20. When the z-position of Asn12 C_a in WT20 was restrained relative to the z-position of the COM of lipid phosphorus atoms of the same (*i.e.*, *cis*) monolayer, the stalk propensity was weak (set 7). Similar analyses were carried out for the MPER. **Figures 1(m)** and **1(n)** show the equilibrium position of the MPER at 353 K. For both cases with and without the restraints, the helical structure was stable and the orientation was largely parallel to the membrane surface. The stalk propensity of MPER was small (set 13).

The system containing one peptide in each of the apposed monolayers was also examined (*i.e.*, two-peptide analysis). Despite the relatively high hydration level was used (DPPC/PA/water/WT20 = 1:2:30:2, the same as set 4), the stalk propensity was > 0.8 regardless of the configuration. Typically, the stalk formation was preceded by self-association of WT20 (**Figures 5(b), 5(c)**). When the z-position of the Asn12 C_a of both WT20 molecules was restrained, no stalk formation occurred. Compared with the one-WT20 simulations, stalk formation was

much quicker in the two-WT20 simulations. The association between the two WT20 peptides was typically mediated by ~2-3 hydrogen bonds formed by sidechains of residues Glu11, Asn12 and Glu15 of both peptides (data not shown). When simulations were performed on WT8 (*i.e.*, a segment of eight residues at the N-terminus of WT20), no stalk propensity was found (set 8 and data not shown for the two-peptide system), consistent with the experimental finding [66]. The stalk propensity of WT13 was weak (set 9. The propensity was 0.3 for the 1:2:30:2 system). A stalk-inducing effect was also observed with two WT20 molecules in the DOPE membrane at 353 K, although the effect appears weak (set 14, 15). In several simulations, prior to the stalk formation, WT20 moved underneath the DOPE molecules. As WT20 moving to a shallower position, DOPE molecules also moved into the water layer (details not shown). Importantly, for both one- and two-peptide analysis, most of the observed stalks occurred in the proximity of the peptide. Our inspection showed that the lead-off lipid molecule (*i.e.*, the first lipid molecule that moved out of the bilayer and stayed in the stalk for > 100 ps) was frequently associated with Phe3, Phe9 and Glu15.

The following findings implicate the structure and orientation of the peptide for its ability to perturb the membrane-water interface. For most of the stalk propensity analysis, we introduced 20 kJ/(deg)² restraints on the peptide dihedral angles based on the 1IBN structure. When the restraints were removed, structural variation was large (**Figures 1(f), 1(g)** and data not shown) and WT20 showed weak stalk propensity (set 10. The stalk propensity was 0.3 for the 1:2:30:2 system). Further insights may be obtained from mutants G1V and W14A. Gly1, the residue at the N-terminus, is critical for functions of the HA protein [7,33,67]. In the equilibrium analysis, G1V adopted a linear or slightly U-shaped structure (e.g., **Figures 1(h), 1(i)**). With the 20 kJ/(deg)² dihedral restraints at its reported (linear) structure (PDB code: 1XOP), the stalk propensity of G1V was small (set 11. The stalk propensity was 0.3 for the 1:2:30:2 system). When the backbone dihedrals of WT20 were restrained to those of the NMR-determined G1V structure (*i.e.*, linear), WT20 adopted a linear structure and the stalk-inducing activity became very weak, the propensity being 0.1 for the 1:2:30:2 system. Strikingly, when the dihedrals of G1V were restrained to those of the 1IBN (*i.e.*, v-shape), the stalk propensity was high (0.9 for 1:2:30:2). When W14A was examined in the one-peptide system, the propensity was weak (set 12). When two W14A molecules in anti-parallel and parallel configurations were examined in the 1:2:30:2 system (dihedral restraints set to the reported W14A structure, 2DCI), there was no significant stalk-inducing effect, the propensity being 0.1.

Overall, these results are consistent with the experimental results [33] which argue the importance of the V-shaped structure and/or the oblique orientation for the stalk-inducing effect of the peptides. Although it is difficult to draw conclusion based on our MD simulations, our simulations showed that WT20 in the inverted V-shape has more opportunities for interaction with lipids or the peptide in the apposed monolayer membrane than G1V and W14A. The shape appears to enable the exposure of the kinked region to the water layer. However, due to the unphysiological nature of our system, this issue requires many more analyses.

4.2. Technical Limitations of Peptide-Induced Membrane Fusion Assay in Silico

While our stalk propensity results were consistent with experiments, it should be borne in mind that the membranes rich in palmitic acid or DOPE are unphysiological. It should also be stressed that, while we started simulations from lamellar structures, the membrane we used have ‘*per se*’ a propensity to form non-bilayer structures at the temperature based on the analysis by Knecht *et al.* [42]. While such non-equilibrium simulations may provide some information on kinetical effect

of the peptides, more analyses close to equilibrium conditions are necessary to draw more reliable conclusions. The use of the high temperature allowed us to obtain some statistics, but as a trade-off, restraints were introduced on the peptide backbone dihedral angles. Thus, most of the analyses are dependent on the ‘reference’ structure, instead of the equilibrium structure for the force field and conditions used. It should also be pointed out that the limited size of the simulation system can cause artifacts. The effects of the artificial setting have to be carefully examined through more rigorous future experimental and theoretical studies. Future computational approaches may include coarse-grained (CG) simulations and Brownian dynamics simulations. Recent CG-based studies of membrane fusion involve Kasson *et al.* [68]. Analyses using these methods may elucidate more robust features about the behavior of the fusion peptides.

The amount of water was critical in this study, emphasizing the importance of the dehydration for the membrane fusion. Future directions may involve oligomerization of peptides (not limited to the N-terminal fusion peptides) because the oligomerization may help the dehydration. β -sheet aggregation of HAFP may recruit HA trimers into a fusion site [66]. HAFP may also interact with the transmembrane (TM) domain or the other peptide segments contained in the external region [33]. The presence of other segments of HA protein may increase the chance for peptide oligomerization further [69]. Recent MD simulation analyses of oligomer configurations have shown that the HAFP oligomer can assume a variety of configurations (of peptide/peptide and peptide/membrane) [49]. The oligomerized peptides may have several roles ranging from stalk formation, to hemifusion, and to full fusion [e.g., 70]. Future computational efforts may well be focused on oligomerization of transmembrane peptides as well as fusion peptides (e.g., Kim *et al.* [71]).

To summarize, the dynamics of the HAFP within lipid membranes was studied. When the HAFP was located at the DPPC/PA membrane-water interface, it assumed an oblique orientation as previously reported. The HAFP exhibited a significant effect on the membrane curvature. The effect was dependent on the lipid composition of the membranes: *i.e.*, a positive curvature for the DPPC/PA membrane and the DOPE membrane whereas a negative curvature for the DPPC membrane. In the phase reconstitution analysis starting from the random DPPC/PA system, the HAFP exhibited a weak stabilization of an inverted hexagonal phase, which is suggestive of enhancement of the negative curvature. The distinct effects (*i.e.*, positive vs. negative curvature) observed in the two DPPC/PA systems is likely to be related to the result that in the latter system the HAFP assumed a transmembrane orientation more frequently than an interfacial orienta-

tion. It can be envisaged that HAFP induces different types of curvature, depending on lipid composition and on the location and orientation within membrane. HAFP also increased the rate of stalk-formation in our non-equilibrium MD simulations in which the spontaneous stalk formation is slow without peptides. However, there are clearly many difficulties if one tries to interpret rigorously the non-equilibrium simulation results. Many more efforts to bring the system closer to a physiological system and to deal with longer time scales are necessary.

5. ACKNOWLEDGEMENTS

The authors thank the anonymous reviewers for their helpful suggestions. This work was supported by Grant-in-Aid for Scientific Research from the Ministry of Education, Culture, Sports, Science, and Technology of Japan.

REFERENCES

- [1] Wilson, I.A., Skehel, J.J. and Wiley, D.C. (1981) Structure of the haemagglutinin membrane glycoprotein of influenza virus at 3 Å resolution. *Nature*, **289**(5796), 366-373.
- [2] Carr, C.M. and Kim, P.S. (1993) A spring-loaded mechanism for the conformational change of influenza hemagglutinin. *Cell*, **73**(4), 823-832.
- [3] Skehel, J.J. and Wiley, D.C. (2000) Receptor binding and membrane fusion in virus entry: The influenza hemagglutinin. *Annual Review Biochemistry*, **69**, 531-569.
- [4] Tamm, L.K., Crane, J. and Kiessling, V. (2003) Membrane fusion: A structural perspective on the interplay of lipids and proteins. *Current Opinion in Structural Biology*, **13**, 453-466.
- [5] Earp, L.J., Delos, S.E., Park, H.E. and White, J.M. (2005) The many mechanisms of viral membrane fusion proteins. *Current Topics in Microbiology and Immunology*, **285**, 25-66.
- [6] Chan, D.C., Fass, D., Berger, J.M. and Kim, P.S. (1997) Core structure of gp41 from the HIV envelope glycoprotein. *Cell*, **89**(2), 263-273.
- [7] Gething, M.J., Doms, R.W., York, D. and White, J. (1986) Studies on the mechanism of membrane fusion: Site-specific mutagenesis of the hemagglutinin of influenza virus. *The Journal of Cell Biology*, **102**(1), 11-23.
- [8] Cross, K.J., Wharton, S.A., Skehel, J.J., Wiley, D.C. and Steinhauer, D.A. (2001) Studies on influenza haemagglutinin fusion peptide mutants generated by reverse genetics. *EMBO Journal*, **20**, 4432-4442.
- [9] Chen, J., Skehel, J.J. and Wiley, D.C. (1999) N- and C-terminal residues combine in the fusion-pH influenza hemagglutinin HA(2) subunit to form an N cap that terminates the triple-stranded coiled coil. *Proceedings of the National Academy of Sciences USA*, **96**, 8967-8972.
- [10] Gallaher, W.R. (1987) Detection of a fusion peptide sequence in the transmembrane protein of human immunodeficiency virus. *Cell*, **50**(3), 327-328.
- [11] Durell, S.R., Martin, I., Ruysschaert, J.M., Shai, Y. and Blumenthal, R. (1997) What studies of fusion peptides tell us about viral envelope glycoprotein-mediated membrane fusion. *Molecular Membrane Biology*, **14**(3), 97-112.
- [12] Bosch, M.L., Earl, P.L., Farnoli, K., Picciati, S., Giombini, F., Wong-Staal, F. and Franchini, G. (1989) Identification of the fusion peptide of primate immunodeficiency viruses. *Science*, **244**(4905), 694-697.
- [13] Dürer, P., Galli, C., Hoenke, S., Corti, C., Glück, R., Vorherr, T. and Brunner, J. (1996) H⁺-induced membrane insertion of influenza virus hemagglutinin involves the HA2 amino-terminal fusion peptide but not the coiled coil region. *The Journal of Biological Chemistry*, **271**(23), 13417-13421.
- [14] Harter, C., James, P., Bächi, T., Semenza, G. and Brunner, J. (1989) Hydrophobic binding of the ectodomain of influenza hemagglutinin to membranes occurs through the "fusion peptide". *The Journal of Biological Chemistry*, **264**(11), 6459-6464.
- [15] Stegmann, T., Delfino, J.M., Richards, F.M. and Helenius, A. (1991) The HA2 subunit of influenza hemagglutinin inserts into the target membrane prior to fusion. *The Journal of Biological Chemistry*, **266**, 18404-18410.
- [16] Lear, J.D. and DeGrado, W.F. (1987) Membrane binding and conformational properties of peptides representing the NH₂ terminus of influenza HA-2. *The Journal of Biological Chemistry*, **262**(14), 6500-6505.
- [17] Murata, M., Takahashi, S., Kagiwada, S., Suzuki, A. and Ohnishi, S. (1992) pH-dependent membrane fusion and vesiculation of phospholipid large unilamellar vesicles induced by amphiphilic anionic and cationic peptides. *Biochemistry*, **31**(7), 1986-1992.
- [18] Wharton, S.A., Martin, S.R., Ruigrok, R.W., Skehel, J.J. and Wiley, D.C. (1988) Membrane fusion by peptide analogues of influenza virus haemagglutinin. *Journal of General Virology*, **69**, 1847-1857.
- [19] Burger, K.N., Wharton, S.A., Demel, R.A. and Verkleij, A.J. (1991) The interaction of synthetic analogs of the N-terminal fusion sequence of influenza virus with a lipid monolayer. Comparison of fusion-active and fusion-defective analogs. *Biochimica et Biophysica Acta*, **1065**(2), 121-129.
- [20] Soltesz, S.A. and Hammer, D.A. (1997) Lysis of large unilamellar vesicles induced by analogs of the fusion peptide of influenza virus hemagglutinin. *Journal of Colloid and Interface Science*, **186**(2), 399-409.
- [21] Epand, R.F., Macosko, J.C., Russel, C.J., Shin, Y.-K. and Epand, R.M. (1999) The ectodomain of HA2 of influenza virus promotes rapid pH dependent membrane fusion. *Journal of Molecular Biology*, **286**(2), 489-503.
- [22] Tamm, L.K. and Han, X. (2000) Viral fusion peptides: A tool set to disrupt and connect biological membranes. *Bioscience Reports*, **20**(6), 501-518.
- [23] Zhelev, D.V., Stoicheva, N., Scherrer, P. and Needham, D. (2001) Interaction of synthetic HA2 influenza fusion peptide analog with model membranes. *Biophysical Journal*, **81**(1), 285-304.
- [24] Nieva, J.L. and Aguirre, A. (2003) Are fusion peptides a good model to study viral cell fusion? *Biochimica et Biophysica Acta*, **1614**(1), 104-115.
- [25] Rafalski, M., Lear, J.D. and DeGrado, W.F. (1990) Phospholipid interactions of synthetic peptides representing the N-terminus of HIV gp41. *Biochemistry*, **29**(34), 7917-7922.

- [26] Nieva, J.L., Nir, S., Muga, A., Goni, F.M. and Wilschut, J. (1994) Interaction of the HIV-1 fusion peptide with phospholipid vesicles: Different structural requirements for fusion and leakage. *Biochemistry*, **33(11)**, 3201-3209.
- [27] Brasseur, R., Lorge, P., Goormaghtigh, E., Ruysschaert, J.M., Espion, D. and Burny, A. (1998) The mode of insertion of the paramyxovirus F1 N-terminus into lipid matrix, an initial step in host cell/virus fusion. *Virus Genes*, **1(4)**, 325-332.
- [28] Martin, I., Dubois, M.C., Defrise-Quertain, F., Saermark, T., Burny, A., Brasseur, R. and Ruysschaert, J.M. (1994) Correlation between fusogenicity of synthetic modified peptides corresponding to the NH₂-terminal extremity of simian immunodeficiency virus gp32 and their mode of insertion into the lipid bilayer: An infrared spectroscopy study. *The Journal of Virology*, **68**, 1139-1148.
- [29] Martin, I., Schaal, H., Scheid, A. and Ruysschaert, J.M. (1996) Lipid membrane fusion induced by the human immunodeficiency virus type 1 gp41 N-terminal extremity is determined by its orientation in the lipid bilayer. *The Journal of Virology*, **70**, 298-304.
- [30] Lüneberg, J., Martin, I., Nüssler, F., Ruysschaert, J.M. and Herrmann, A. (1995) Structure and topology of the influenza virus fusion peptide in lipid bilayers. *The Journal of Biological Chemistry*, **270(46)**, 27606-27614.
- [31] Han, X., Bushweller, J.H., Cafiso, D.S. and Tamm, L.K. (2001) Membrane structure and fusion-triggering conformational change of the fusion domain from influenza hemagglutinin. *Nature Structural Biology*, **8(8)**, 715-720.
- [32] Han, X. and Tamm, L.K. (2000) A host-guest system to study structure-function relationships of membrane fusion peptides. *Proceedings of the National Academy of Sciences USA*, **97(24)**, 13097-13102.
- [33] Li, Y., Han, X., Lai, A.L., Bushweller, J.H., Cafiso, D.S. and Tamm, L.K. (2005) Membrane structures of the hemifusion-inducing fusion peptide mutant G1S and the fusion-blocking mutant G1V of influenza virus hemagglutinin suggest a mechanism for pore opening in membrane fusion. *The Journal of Virology*, **79(18)**, 12065-12076.
- [34] Lai, A.L., Park, H., White, J.M. and Tamm, L.K. (2006) Fusion peptide of influenza hemagglutinin requires a fixed angle boomerang structure for activity. *The Journal of Biological Chemistry*, **281(9)**, 5760-5770.
- [35] Sáez-Cirión, A., Nir, S., Lorizate, M., Agirre, A., Cruz, A., Pérez-Gil, J. and Nieva, J.L. (2002) Sphingomyelin and cholesterol promote HIV-1 gp41 pretransmembrane sequence surface aggregation and membrane restructuring. *The Journal of Biological Chemistry*, **277(24)**, 21776-21785.
- [36] Lorizate, M., Huarte, N., Sáez-Cirión, A. and Nieva, J.L. (2008) Interfacial pre-transmembrane domains in viral proteins promoting membrane fusion and fission. *Biochimica et Biophysica Acta*, **1778(7-8)**, 1624-1639.
- [37] Charlotteaux, B., Lorin, A., Brasseur, R. and Lins, L. (2009) The “Tilted Peptide Theory” links membrane insertion properties and fusogenicity of viral fusion peptides. *Protein and Peptide Letters*, 2009; **16(7)**, 718-725.
- [38] Efremov, R.G., Nolde, D.E., Volynsky, P.E., Chernyavsky, A.A., Dubovskii, P.V. and Arseniev, A.S. (1999) Factors important for fusogenic activity of peptides: molecular modeling study of analogs of fusion peptide of influenza virus hemagglutinin. *FEBS Letters*, **462(1-2)**, 205-210.
- [39] Gray, C., Tatulian, S.A., Wharton, S.A. and Tamm, L.K. (1996) Effect of the N-terminal glycine on the secondary structure, orientation, and interaction of the influenza hemagglutinin fusion peptide with lipid bilayers. *Biophysical Journal*, **70(5)**, 2275-2286.
- [40] Marrink, S.-J., de Vries, A.H. and Tieleman, D.P. (2009) Lipids on the move: Simulation of membrane pores, domains, stalks and curves. *Biochimica et Biophysica Acta*, **1788(1)**, 149-168.
- [41] Marrink, S.-J. and Tieleman, D.P. (2001) Molecular dynamics simulation of a lipid diamond cubic phase. *Journal of the American Chemical Society*, **123(49)**, 12383-12391.
- [42] Knecht, V., Mark, A.E. and Marrink, S.-J. (2006) Phase behaviour of a phospholipid/fatty acid/water mixture studied in atomic detail. *Journal of the American Chemical Society*, **128(6)**, 2030-2034.
- [43] Marrink, S.-J. and Mark, A.E. (2004) Molecular view of hexagonal phase formation in phospholipid membranes. *Biophysical Journal*, **87(6)**, 3894-3900.
- [44] Nielsen, S.O., Lopez, C.F., Ivanov, I., Moore, P.B., Shelley, J.C. and Klein, M.L. (2004) Transmembrane peptide-induced lipid sorting and mechanism of L-alpha-to-inverted phase transition using coarse-grain molecular dynamics. *Biophysical Journal*, **87(4)**, 2107-2115.
- [45] Kamath, S. and Wong, T.C. (2002) Membrane structure of the Human Immunodeficiency Virus gp41 fusion domain by molecular dynamics simulation. *Biophysical Journal*, **83(1)**, 135-143.
- [46] Vaccaro, L., Cross, K.J., Kleinjung, J., Straus, S.K., Thomas, D.J., Wharton, S.A., Skehel, J.J. and Fraternali, F. (2005) Plasticity of influenza haemagglutinin fusion peptides and their interaction with lipid bilayers. *Biophysical Journal*, **88(1)**, 25-36.
- [47] Huang, Q., Chen, C.L. and Herrmann, A. (2004) Bilayer conformation of fusion peptide of influenza virus hemagglutinin: A molecular dynamics simulation study. *Biophysical Journal*, **87(1)**, 14-22.
- [48] Lagüe, P., Roux, B. and Pastor, R.W. (2005) Molecular dynamics simulations of the influenza hemagglutinin fusion peptide in micelles and bilayers: Conformational analysis of peptide and lipids. *Journal of Molecular Biology*, **354(5)**, 1129-1141.
- [49] Sammalkorpi, M. and Lazaridis, T. (2007) Configuration of influenza hemagglutinin fusion peptide monomers and oligomers in membranes. *Biochimica et Biophysica Acta*, **1768(1)**, 30-38.
- [50] De Vries, A.H., Mark, A.E. and Marrink, S.J. (2004) The binary mixing behavior of phospholipids in a bilayer: A molecular dynamics study. *The Journal of Physical Chemistry B*, **108(7)**, 2454-2463.
- [51] Seddon, J.M., Templer, R.H., Warrender, N.A., Huang, Z., Cevc, G. and Marsh, D. (1997) Phosphatidylcholine-fatty acid membranes: Effects of headgroup hydration on the phase behaviour and structural parameters of the gel and inverse hexagonal (HII) phases. *Biochimica et Biophysica Acta*, **1327**, 131-147.
- [52] Lindahl, E., Hess, B. and van der Spoel, D. (2001) GROMACS 3.0: A package for molecular simulation and trajectory analysis. *Journal of Molecular Modeling*, **7(8)**, 306-317.

- [53] Berger, O., Edholm, O. and Jähnig, F. (1997) Molecular dynamics simulations of a fluid bilayer of dipalmitoyl-phosphatidylcholine at full hydration, constant pressure, and constant temperature. *Biophysical Journal*, **72**(5), 2002-2013.
- [54] Sun, Z.Y., Oh, K.J., Kim, M., Yu, J., Brusic, V., Song, L., Qiao, Z., Wang, J.H., Wagner, G. and Reinherz, E.L. (2008) HIV-1 broadly neutralizing antibody extracts its epitope from a kinked gp41 ectodomain region on the viral membrane. *Immunity*, **28**(1), 52-63.
- [55] Berendsen, H.J.C., Postma, J.P.M., van Gunsteren, W.F. and Hermans, J. (1981) Intermolecular forces, interaction models for water in relation to protein hydration. D. Reidel Publishing, Dordrecht, The Netherlands.
- [56] Hess, B., Bekker, H., Berendsen, H.J.C. and Fraaije, J.G.E.M. (1997) LINCS: A linear constraint solver for molecular simulations. *Journal of Computational Chemistry*, **18**(12), 1463-1472.
- [57] Miyamoto, S. and Kollman, P.A. (1992) SETTLE: An analytical version of the SHAKE and RATTLE algorithm for rigid water models. *Journal of Computational Chemistry*, **13**(8), 952-962.
- [58] Darden, T., York, D. and Pedersen, L. (1993) Particle mesh Ewald: An Nlog(N) method for Ewald sums in large systems. *Journal of Chemical Physics*, **98**(12), 10089-10092.
- [59] Berendsen, H.J.C., Postma, J.P.M., van Gunsteren, W.F., DiNola, A. and Haak, J.R. (1984) Molecular dynamics with coupling to an external bath. *Journal of Chemical Physics*, **81**(8), 3684-3690.
- [60] Zhou, Z., Macosko, J.C., Hughes, D.W., Sayer, B.G., Hawes, J. and Epand, R.M. (2000) 15N NMR study of the ionization properties of the influenza virus fusion peptide in zwitterionic phospholipid dispersions. *Biophysics Journal*, **78**(5), 2418-2425.
- [61] Kabsch, W. and Sander, C. (1983) Dictionary of protein secondary structure: Pattern recognition of hydrogen-bond and geometrical features. *Biopolymers*, **2**, 2577-2637.
- [62] Humphery, W., Dalke, A. and Schulten, K. (1996) VMD--visual molecular dynamics. *Journal of Molecular Graphics*, **14**, 33-38.
- [63] Epand, R.M. and Epand, R.F. (1994) Relationship between the infectivity of influenza virus and the ability of its fusion peptide to perturb bilayers. *Biochemical and Biophysical Research Communications*, **202**(3), 1420-1425.
- [64] Colotto, A. and Epand, R.M. (1997) Structural study of the relationship between the rate of membrane fusion and the ability of the fusion peptide of influenza virus to perturb bilayers. *Biochemistry*, **36**(25), 7644-7651.
- [65] Siegel, D.P. and Epand, R.M. (2000) Effect of influenza hemagglutinin fusion peptide on lamellar/inverted phase transitions in dipalmitoleylphosphatidylethanolamine: implications for membrane fusion mechanisms. *Biochimica et Biophysica Acta*, **1468**(1-2), 87-98.
- [66] Han, X. and Tamm, L.K. (2000) pH-dependent self-association of influenza hemagglutinin fusion peptides in lipid bilayers. *Journal of Molecular Biology*, **304**(5), 953-965.
- [67] Qiao, H., Armstrong, R.T., Melikyan, G.B., Cohen, F.S. and White, J.M. (1999) A specific point mutant at position 1 of the influenza hemagglutinin fusion peptide displays a hemifusion phenotype. *Molecular Biology Cell*, **10**(8), 2759-2769.
- [68] Kasson, P.M., Kelley, N.W., Singhal, N., Vrljic, M., Brunger, A.T. and Pande, V.S. (2006) Ensemble molecular dynamics yields submillisecond kinetics and intermediates of membrane fusion. *Proceedings of the National Academy Sciences USA*, **103**(32), 11916-11921.
- [69] Peisajovich, S.G. and Shai, Y. (2003) Viral fusion proteins: multiple regions contribute to membrane fusion. *Biochimica et Biophysica Acta*, **1614**(1), 122-129.
- [70] Lau, W.L., Ege, D.S., Lear, J.D., Hammer, D.A. and DeGrado, W.F. (2004) Oligomerization of fusogenic peptides promotes membrane fusion by enhancing membrane destabilization. *Biophysics Journal*, **86**(1), 272-284.
- [71] Kim, J.H., Hartley, T.L., Curran, A.R. and Engelmann, D.M. (2009) Molecular dynamics studies of the transmembrane domain of gp41 from HIV-1. *Biochimica et Biophysica Acta*, **1788**(9), 1804-1812.

Mode of pollen spread in clonal seed orchard of *Pinus koraiensis*

Fu-Juan Feng¹, Xin Sui², Min-Min Chen², Dan Zhao¹, Shi-Jie Han^{2*}, Mai-He Li³

¹Northeast Forest University, Harbin, China; ffj9018@sina.com

²Institute of Applied Ecology, Chinese Academy of Sciences, Shenyang, China; *Corresponding Author: hansj@iae.ac.cn

³Swiss Federal Research Institute WSL, Birmensdorf, Switzerland

Received 14 January 2010; revised 20 March 2010; accepted 31 March 2010.

ABSTRACT

The patterns of effective pollen dispersal and the relationships between pollen dispersal and genetic composition in *Pinus koraiensis* are still unclear. Hence, we investigated the mode of pollen dispersal of *P. koraiensis* in a clonal seed orchard in Lushuihe Forestry Bureau, Jilin Province, using SSR molecular markers technique and the method of maximum likelihood. A total of 13 pairs of nuclear microsatellites polymorphic primers were used in the paternity analysis. We analyzed 100 progenies and 150 paternities. A total of 56 alleles were detected in 13 loci with 3-6 alleles (4.3 alleles in average) in a single locus. The primers of SsrPt_ctg7170 and SsrPt_ctg5333 had the maximum (6) and the minimum (3) alleles, respectively. The averaged values of observed heterozygosity, expected heterozygosity and polymorphism information content of experimental groups were 0.648, 0.601 and 0.533, respectively. The mating distance of *P. koraiensis* followed an approximately normal distribution. The most effective pollen for the female parent came from male parent trees 15-45 m away with an average mating distance of 32.60 m and the longest of 67.88 m. The pollen source of offspring was not random but greatly affected by the wind direction during the pollination season of *P. koraiensis*. These results have important implications for seed orchard design to improve the genetic quality of seeds and seed production.

Keywords: *Pinus Koraiensis*; Seed Orchard; Nuclear Microsatellites Markers; Paternity Analysis; Pollen Spread

1. INTRODUCTION

Pinus koraiensis, a national protected tree species in

China, is a dominant species in the climax vegetation, mixed needle broad-leaved forests, in eastern mountainous area in northeastern China. Currently, the distribution of this tertiary relict plant ranges from 35° to 52°N and from 126° to 143°E, concentrating mainly in Changbai Mountain, the Lesser Khingan Mountain, Wanda Mountain, and Changkuantsailing in northeastern China, northern regions in North Korea, Japan and the southern part of the Russian Far East. The slow-growing *P. koraiensis* with late sexual maturity is very difficult to regenerate in nature.

Ma et al. [1] showed that the area of natural *P. koraiensis* forest has dramatically decreased in China. Owing to the ecological and economic significance of *P. koraiensis*, plantations of this species have recently been widely establishing in northeastern China. Therefore, large amount of good seeds with good genetic properties are still urgently needed for successful afforestation. For this purpose, seed orchards of *P. koraiensis* have been established in northeastern China.

Many factors affect the physioecological quality of seeds produced in a seed orchard. For example, gene flow, to a large extent, influences the genetic structure of a forest population. Pollen movement is one of the main factors impacting the gene flow of groups. It involves the form of pollination, and number, size and shape of pollen. Pollen related to gene flow associated with the plant mating system and outcrossing rate affects the size of plant gene flow directly. The model of pollen spread determining, to a large extent, genetic compositions of open-pollinated families; can affect the levels of genetic diversity and the size of effective population [2-4]. Therefore, pollen gene flow is an important factor to impact yield and quality of seeds in seed orchards. However, the related research on *P. koraiensis* is scarce.

Recently, paternity analysis has become the most common method for directly estimating gene flow [5,6]. In the present study, SSR molecular markers technique was used to paternally identify the clonal half-sib progenies in *P. koraiensis* seed orchard, to analyze the source

of offspring pollen. The present study aimed 1) to reveal the rules of the pollen spread in *P. koraiensis* seed orchard, and 2) to quantitatively investigate outcrossing rate and self-crossing rate of progenies. The results are helpful to guide the maximum mating of the fine genotypes among the forest population, and have some significance for the design of seed orchard and the management of genetic resources [7,8].

2. MATERIALS AND METHODS

2.1. Study Site, Plant Materials and Sampling Methods

Point-centre quarter method, according to Lian *et al.* [9] and Kong [10], was used to take samples. The experimental site was set at sub-district No. 5, zone No. 2, located in the center of Hongwei Seed Orchard in Lushuihe Forestry Bureau, Jilin Province. The orchard with an area of about 10000 m² contains 727 individuals of 61 clones planted with 3 m × 3 m spacing in 1989. At the beginning of the present study, the plants grown well with an average height of 4.31 m, and an average diameter at breast height of 7.8 cm. A well-conditioned plant (plant No. of 105) located in the center of the sub-district and at the cross-point of the line 16 and row 21 was randomly selected as the female parent. The sub-district No. 5 surrounding that selected female parent was divided into 4 quadrants with a total of 149 individuals and 61 clones as male parents recorded. Sixteen, 46, 48, and 39 trees, existed in the first, second, third, and in the fourth quadrant, respectively. The clones of fourth quadrant were 15, 33, 28, and 22. The female parent was also taken into account for a possible candidate as a male parent for self-pollination. Hence, a total of 150 candidates of male parent were analyzed. A total of 100 seeds were randomly selected from the cones collected from the female parent. Embryos (offsprings) were then obtained from these seeds.

Sampling was conducted in September 2007. Annual needles collected from each male parent were stored at -40°C. The pinecones of the same year were collected from the female parent and also stored at -40°C.

2.2. DNA Extraction

DNA was extracted from the needles using the modified CTAB method [11]. Embryo DNA was extracted using the traditional method of CTAB. In the extraction process, solution was extracted for many times until no white turbidity occurred.

2.3. Statistical Analysis

Data were scored by SSR co-dominant markers. Data analyses were performed with CERVUS (Version 2.0) based on the method of maximum likelihood. The num-

ber of alleles (N_A), allele frequency (P_i), observed and expected heterozygosity (H_o , H_e), and polymorphic information content (PIC) were also calculated using CERVUS (Version 2.0).

2.4. Development of SSR Primer

A total of 13 pairs of primers were chosen from 96 pairs of allied species as described in the published documents (*Pinus pinaster* and *Pinus taeda*) [12-14]. The sequences of primers were shown in Table 1.

2.5. SSR-PCR Reaction System

The SSR-PCR reaction system was constructed as described by Lian *et al.* [9]. Amplification was carried out in an ABI 9700 Thermocycler with following PCR program: preliminary denaturation at 94°C for 4 min, 30 cycles of denaturation (1 min, 94°C), annealing (1 min, the proper temperature), extending (1 min, 72°C), and extending at 72°C for 4 min, and finally keeping at 4°C. Amplification fragments were segregated on 6% non-denatured polyacrylamide gels.

3. RESULTS

3.1. SSR Polymorphism Analysis

A total of 13 pairs of SSR primers were amplified in the male parent candidates and offsprings (a total of 250 samples). As shown in Figures 1 and 2, SSR marker in *P. koraiensis* exhibited the characteristics of good stability and repeatability as well as clear bands. A total of 56 alleles were detected in 13 loci with 3-6 alleles in a single locus and 4.3 alleles in average (Table 2). The primers of SsrPt_ctg7170 and SsrPt_ctg5333 had the maximum (6) and the minimum (3) alleles, respectively (Table 2). The averaged values of observed heterozygosity, expected heterozygosity, and polymorphism information content of the experimental groups were 0.648, 0.601, and 0.533, respectively (Table 2).

3.2. Paternal Analysis of the Open-Pollinated Progenies

Paternity analysis of the open-pollinated progenies indicated that in a 95% credibility interval, the true male parent of 53 offsprings (accounting for 53% of the total offsprings) can be inferred from the 13 SSR primers. The cumulative exclusion probability was 94.59%, of which the primer of SsrPt_ctg 7170 had the highest exclusion probability (55%). Analysis of male parent using CERVUS software showed that three clones were the same as the female parents existed in the suspected male parents of *P. koraiensis*. There were no male parents from the female parents or the same clones of female parents in the 100 open-pollinated offsprings, indicating that no self-crossing occurred in the experiment. The

Table 1. Sequence of 13 pairs of primers from the 96 pairs of allied species.

| Primer | F-Primer sequences(5'-3') | S- Primer sequences(5'-3') |
|----------------|---------------------------|----------------------------|
| SsrPt_AA739797 | ACTTTGCGGTGAATCAGACC | AAAGTAAGGCTGCTTCATGA |
| SsrPt_BF778306 | GAAGATGGAGACGAAGCAGG | TTTGCAGTCTGTTGCCTTG |
| SsrPt_ctg16811 | GTCCATGATGTTGCAGATTGG | TGTTCCCCAATGGCTGTC |
| SsrPt_ctg4363 | TAATAATTCAAGCCACCCG | AGCAGGCTAATAACAAACACGC |
| SsrPt_ctg4487a | TCTGCTGTGTGGACAAACCT | TTCTTGGCTAAAATCTCGG |
| SsrPt_ctg4698 | CGAAAAGGTGGTCTGATGG | TTTCCGCTGGATTACAC |
| SsrPt_ctg7170 | GGTTTTCGATTCTGAGGC | AACAGGTGTGCAAATAGCCC |
| SsrPt_ctg7425 | AATAAGACCCAGAGGAGCC | GACGTCTTCACCAAATCGC |
| SsrPt_ctg7731 | AGTGGTGAAGGGTCCATCTG | GCATAACACAAAAGCCAGCA |
| SsrPt_ctg5333 | GAAGGAGTCGGCGATAACAG | GGGAATTGACCTGTGAAGA |
| LOP1 | GCCTAATGGCCGGCCAGTGCT | GCGATTACAGGGTTGCAGCCT |
| LOP4 | GCCTCATCATATGAAAAGCAA | CATTGTTCTCACTACGAATGC |
| LOP8 | TATCCACCAGAAGGGCATC | CGGGAGCTTAATGATCTTC |

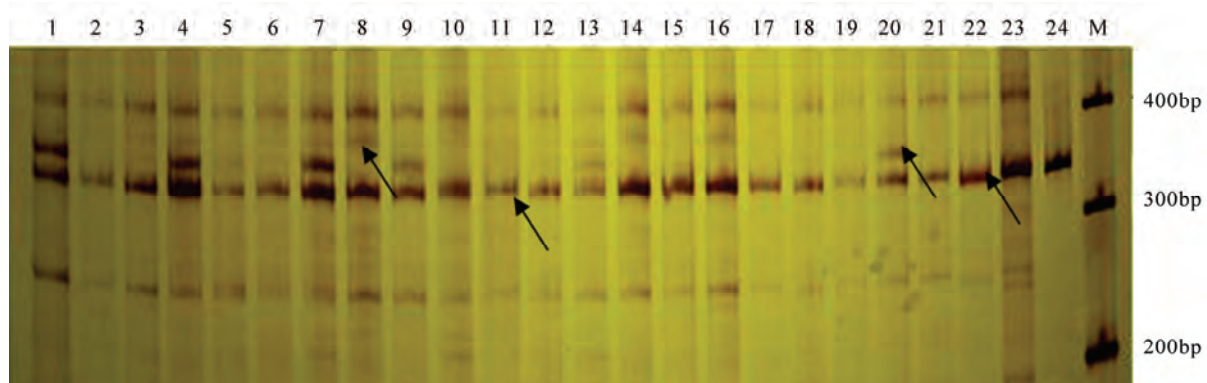
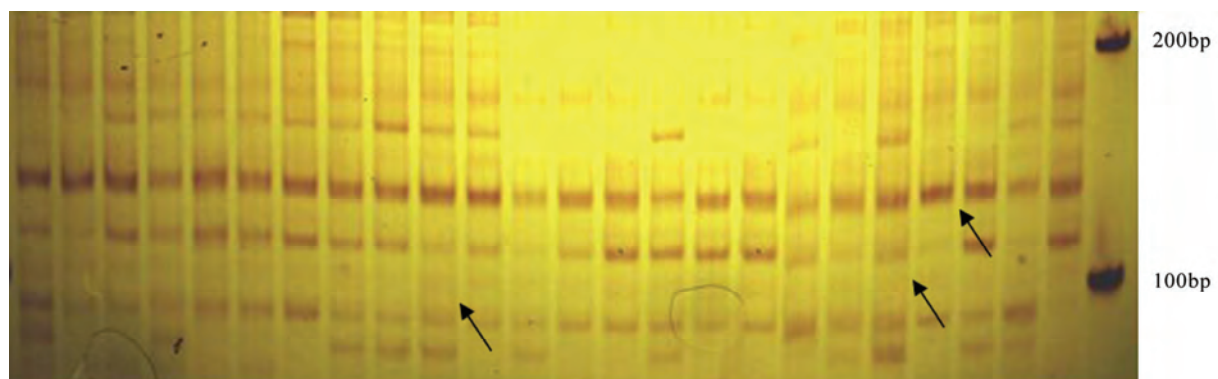
**Figure 1.** The bands of *Pinus koraiensis* amplified from the primer pairs of LOP4. Lanes 1-24 were male parents; M: marker. The arrows show the polymorphic bands.**Figure 2.** The bands of *Pinus koraiensis* amplified from the primer pairs of Ssr_ctg4363. Lanes 1-24 were male parents; M: marker. The arrows show the polymorphic bands.

Table 2. Polymorphism of SSR in *Pinus koraiensis*.

| Primer | Numbers of alleles (N_A) | Allele frequency (Range) P_i | Observed heterozygosity (H_o) | Expected heterozygosity (H_e) | Polymorphic information content (PIC) |
|-----------------|------------------------------|--------------------------------|-----------------------------------|-----------------------------------|---------------------------------------|
| SsrPt_ctg 4698 | 4 | 0.461-0.661 | 0.573 | 0.510 | 0.461 |
| SsrPt_AA739797 | 4 | 0.4386-0.561 | 0.605 | 0.494 | 0.371 |
| SsrPt_ctg 7170 | 6 | 0.0159-0.277 | 0.741 | 0.773 | 0.733 |
| SsrPt_ctg 7425 | 4 | 0.146-0.336 | 0.764 | 0.732 | 0.681 |
| SsrPt_ctg 4363 | 5 | 0.159-0.432 | 0.668 | 0.704 | 0.653 |
| SsrPt_ctg 5333 | 3 | 0.311-0.364 | 0.732 | 0.667 | 0.591 |
| SsrPt_ctg 7731 | 4 | 0.114-0.292 | 0.557 | 0.550 | 0.478 |
| SsrPt_ctg 4487b | 5 | 0.139-0.600 | 0.495 | 0.554 | 0.487 |
| SsrPt_BF 778306 | 4 | 0.111-0.704 | 0.559 | 0.458 | 0.411 |
| SsrPt_ctg 4487a | 4 | 0.0977-0.482 | 0.727 | 0.583 | 0.492 |
| Lop1 | 4 | 0.061-0.496 | 0.718 | 0.641 | 0.579 |
| Lop4 | 5 | 0.075-0.659 | 0.473 | 0.490 | 0.422 |
| Lop8 | 4 | 0.227-0.398 | 0.814 | 0.651 | 0.574 |
| Mean | 4.3 | 0.147-0.482 | 0.648 | 0.601 | 0.533 |

results reflected that outcrossing was the main mating approach of *P. koraiensis* in the open-pollinated situation.

In a 95% credibility interval, 48 male parents out of the 150 candidates (32%) produced offsprings with the female parents. Among them, the male parents of clones Nos. 149 and 126 identified three sub-generations, with a male reproductive fitness of 3%. The reproductive fitness of the rest of the male parents was 1%-2%, with an average value of 1.34%. Another 102 (68%) male candidates did not provide effective pollens for progeny groups, and the male reproductive fitness was zero.

3.3. Dispersal Patterns of Effective Pollen

The spatial distribution and mating pattern of all the candidates showed that the pollen source of offspring was not random (Figure 3). The pollen from the male candidates located in the southern quadrants 3 and 4 were significantly higher than those from trees in the northern quadrants 1 and 2. This may be closely related to the dominant wind direction affecting the pollination process of *P. koraiensis*. According to the climatological data collected in 2007, the dominant wind in the pollination season blew northeasterly (*i.e.* from the Southwest toward Northeast). Hence, pollen from the male parents in quadrants 3 and 4, which were located in the upwind direction of the female parent, can easily

reach the female parent. On the other hand, however, quadrants 1 and 2 were located in the downwind position, pollen of male parents in these quadrants were hard to reach the female parent (Figure 3).

The mating distance between parents is the dispersal distance of effective pollens, which reflects the pattern of mating within populations. *P. koraiensis* is a wind-pollinated plant species, therefore the mating distance can be well described using the flying distance of pollen. The results showed that the mating distance of *P.*

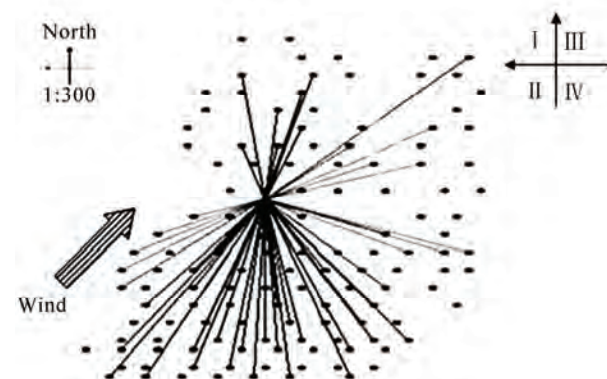


Figure 3. Spatial distribution of paternal candidates and mating pattern for the maternal tree in the experimental population of *Pinus koraiensis*.

koraiensis followed an approximately normal distribution (**Figure 4**). The proportion of successful mating of the 53 open-pollinated offsprings identified was higher in the distances of 15-30 m (36%) and 30-45 m (30%) between the female parent and the male parent, with an average mating distance of 32.60 m and the longest distance of 67.88 m (**Figure 4**).

3.4. Impact of Foreign Pollen

The impact of foreign pollen contamination was analyzed. In the results of electrophoresis of 13 pairs of SSR primers, six alleles in 25 offsprings (25% of the total offsprings) were found to be different to the male parents, which may be caused by foreign pollen contamination. The proportion of contamination was 25%.

4. DISCUSSION

4.1. Analysis of Paternal

The paternal analyses revealed the most likely parent of each offspring and the corresponding credibility (confidence probability) in an area of statistical inference. At a 95% credibility interval, 53 out of the 100 offsprings' male parents have been confirmed in the present study, indicating a high inference rate resulted from the use of 13 SSR primers. Moreover, the cumulative exclusion probability was 94.59%, also indicating that SSR codominant marker is highly appropriate for paternity analysis.

The observed heterozygosity (0.648) was higher than the expected heterozygosity (0.601), indicating that the proportion of heterozygote was relatively large within the group. This finding is consistent with other studies dealing with other tree species [15,16]. The polymorphism information content (PIC) was used as an indicator of locus diversity [17]. Botstein *et al.* [18] pointed out that the locus is high, moderate, and low polymorphic when $PIC > 0.5$, $0.25 < PIC < 0.5$, and $PIC < 0.25$, respectively. The present study showed a $PIC > 0.5$, indicating that SSR polymorphism of *P. koraiensis* is high.

The composition of male parents found in the present study was similar to the results gained from other tree species [19-22]. He *et al.* [23] based on their study of parents analysis using exclusion method, stated that the optimal number of expected parents was less than 100 in the population studied; otherwise the limitations of the analysis would increase. In the present study, a total of 150 male candidates were analyzed, thus the determination ability of the male parents may be influenced to some extent.

4.2. Spread of Effective Pollen

The characteristics, type, quantity, density, and distribution of parents, and also environmental factors determine

the spread distance and pattern of effective pollen [22]. For instance, the intensity of pollen flow and the chance of successful mating decrease with increasing pollination distance [24]. Our results showed that the spread distance of *P. koraiensis* followed an approximately normal distribution, which is similar to the results reported by Sun *et al.* [22]. The most effective pollen for the female parents came from trees with a distance of 15-45 m (**Figure 4**). Moreover, wind direction significantly affects pollination [25]. In line with this view, the receivable pollens of female parent came mainly from the southern direction associated with the dominant wind in the pollination season of *P. koraiensis*.

Of course, it is also notable that the object of this study is a man-made seed orchard of *P. koraiensis* trees. Higher density of the same tree species with similar age (maturity) can provide rich pollen, which may limit the long-distance spread of pollen.

4.3. Mating Means

The mating means are affected by many factors including pollination medium, the genetic differences between breeding individuals in groups, the spatial distribution, flowering habits, the characteristics of pollen, and climatic conditions in blooming period [22]. Our results showed that the mating means of *P. koraiensis* were dominated by outcrossing. Two possible reasons may contribute to outcrossing of *P. koraiensis*: 1) the species has dichogamy phenomena; and 2) the concentrated and homogeneous distribution of individuals in a seed orchard is beneficial to cross-pollination. Moreover, in an evolutionary view, the majority of outcrossing species would form mechanisms to avoid inbreeding depression such as self-incompatibility. Stern *et al.* [26] reported that self-sterility of conifers was mostly caused by the wilting of embryo after self-fertilization. The present study found that the self-crossing rate was nearly zero, implying that the self-incompatibility phenomenon may exist in *P. koraiensis* which needs to be tested.

4.4. Pollen Contamination

The pollen contamination level (25%) in this seed or-

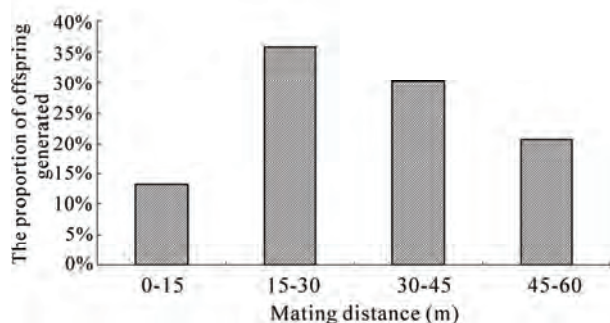


Figure 4. The dispersal distance of effective pollen.

chard was lower as compared with research results of other *Pinus* species, for example, 36%~60% for *P. taeda* [27], 84.5% for *P. elliottii* [28], and 9%~74% for *P. sylvestris* [29-31].

The unique binds for fragments found in the present study may come from other male parents outside the sampling plot (*i.e.* the sub-district No. 5). Indeed, it is most possible that the contamination pollen came from the neighboring sub-districts rather than from the surrounding natural forests since the isolation strip around the seed orchard was more than 500 m.

5. CONCLUSIONS

The present study found that the most effective pollen for the female parent came from male parent trees 15-45 m away with an average mating distance of 32.60 m and a maximum distance of 67.88 m. The pollen source of offspring was not random but greatly affected by the wind direction during the pollination season of *P. koraiensis*. These results have important implications for seed orchard design to improve the genetic quality of seeds and seed production.

6. ACKNOWLEDGEMENTS

This research was supported by Chinese Academy of Science Knowledge Innovation Sub-project, also supported by Heilongjiang Postdoctoral Research Start-up Funding.

REFERENCES

- [1] Ma, J.L., Zhang, L.W., Cheng D. and Li, J.W. (1992) Geographic distribution of *Pinus koraiensis* in the world. *Journal of Northeast Forestry University*, **20**, 40-47.
- [2] Levin, D.A. and Kerster, H.W. (1974) Gene flow in seed plants. *Evolutionary Biology*, **7**, 139-220.
- [3] Hamrick, J.L. and Schnabel, A. (1985) Understanding the genetic structure of plant populations: Some old problems and a new approach. In: Gregorius, H.R., Ed., *Population Genetics in Forestry*, Springer-Verlag, New York, **5**, 0-70.
- [4] Adams, W.T., Birkes, D.S. and Erickson, V.J. (1992) Using genetic markers to measure gene flow and pollen dispersal in forest tree seed orchards. In: Wyatt, R., *Ecology and Evolution of Plant Reproduction: New Approaches*, Chapman and Hall, New York.
- [5] Meagher, T.R. (1986) Analysis of paternity within a natural population of *Chamaelirium leuteum*. I. Identification of most-likely male parents. *American Naturalist*, **128**(2), 199-215.
- [6] Snow, A.A. and Lewis, P.O. (1993) Reproductive traits and male fertility in plants Empirical approaches. *Annual Review of Ecology and Systematics*, **24**, 331-351.
- [7] Adams, W.T. and Birkes, D.S. (1989) Matting patterns in seed orchards. *Proceedings of 20th Southern Forest Tree Improvement Conference*, Charleston, 26-30 June 1989, 75-86.
- [8] Wheeler, N.C. and Jech, K.S. (1992) The use of electrophoretic markers in seed orchard research. *New Forests*, **6**(1-4), 311-328.
- [9] Lian, C.L., Miwa, M. and Hogetsu, T. (2001) Outcrossing and paternity analysis of *Pinus densiflora* (Japanese red pine) by microsatellite polymorphism. *The Genetics Society of Great Britain*, **87**, 88-98.
- [10] Kong, F.L. (2006) Quantitative genetics in plants. China Agricultural University Press, Beijing, 20-50.
- [11] Wang, J., Yang C.P. and Liu, G.F. (2006) Extraction of genomic DNA from woody plants and its identification. *Bulletin of Botanical Research*, **26**, 589-594.
- [12] Zhou, Y., Bui, T., Auckland, L.D. and Williams, C.G. (2002) Undermethylated DNA as a source of microsatellites from a conifer genome. *Genome*, **45**(1), 91-99.
- [13] Chagné, D., Chaumeil, P., Ramboer, A., Collada, C., Guevara, A., Cervera, M.T., Vendramin, G.G., Garcia, V., Frigerio, J.M., Echt, C., Richardson, T. and Plomion, C. (2004) Cross-species transferability and mapping of genomic and cDNA SSRs in pines. *Theoretical and Applied Genetics*, **109**(6), 1204-1214.
- [14] Liewlaksaneeyanawin, C., Ritland, C.E., El-Kassaby, Y.A. and Ritland, K. (2004) Single-copy, species-transferable microsatellite markers developed from loblolly pine ESTs. *Theoretical and Applied Genetics*, **109**(2), 361-369.
- [15] Ge, S. (1998) Isozymes and studies on population genetic variation in forest trees. *Journal of Nanjing Forest University*, **1**, 68-77.
- [16] El-Kassaby, Y.A. (1991) Genetic variation within and among conifer populations: review and evaluation of methods. In: Fineschi, S., Ed., *Biochemical Markers in the Population Genetics of Forest Trees*, SPB Academic Publishing, Hague, 61-76.
- [17] Nei, M. (1972) Genetic distance between populations. *American Naturalist*, **106**, 283-292.
- [18] Botstein, D., White, R.L., Skolnick, M. and Davis, R.W. (1980) Construction of a genetic linkage maps in man using restriction fragment length polymorphisms. *American Journal of Human Genetics*, **32**(3), 314-331.
- [19] Smouse, P.E. and Meagher, T.R. (1994) Genetic analysis of male reproductive contributions in *Chamaelirium luteum* (L.) gray (Liliaceae). *Genetics*, **136**(1), 313-322.
- [20] Chen, X.Y. and Song, Y.C. (2000) Analysis of parentage for naturally established seedlings of cyclobalanopsis glauca. *Journal of Wuhan Botanical Research*, **18**, 174-180.
- [21] Sun, Y.G. and Li, H.G. (2007) The paternity analysis for open-pollination progenies of *Liriodendron* L. using SSR markers. *Chinese Bulletin of Botany*, **24**, 590-596.
- [22] Zhang, D.M., Sun, P.G., Shen, X.H. and Ru, G.X. (2009) Paternity analysis of open-and control-pollinated seeds collected from a seed orchard of *Pinus tabulaeformis*. *Chinese Journal of Plant Ecology*, **33**(2), 302-310.
- [23] He, T.H. and Ge, S. (2001) Mating system, paternity analysis and gene flow in plant populations. *Acta Phytocologica Sinica*, **25**, 144-154.
- [24] Sulaiman, Z., Collins, G., Witherspoon, J. and Sedgley, M. (2004) Identification of pollen donors for the avocado cultivar Gwen in a mixed orchard by isozyme analysis. *Journal of Horticultural Science and Biotechnology*, **79**(4), 571-575.
- [25] Wang, G.Y., Yi, H.B., Wang, B., Zhang, S.F., Wang, G.X.,

- Huang, Q.C., Zhang, G.T. and Sun, Q.Y. (1995) Study on the pollen density in the seed orchard of Korean Pine. *Journal of Northeast Forestry University*, **23**, 58-63.
- [26] Stern, K. and Roche, L. (1974) Genetics of Forest Ecosystems. Springer-Verlag, Berlin, 65-69.
- [27] Friedman, S.T. and Adams, W.T. (1985) Estimation of gene flow into two seed orchards of loblolly pine (*Pinus taeda* L.). *Theoretical and Applied Genetics*, **69(5-6)**, 609-615.
- [28] Squillace, A.E. and Long, E.M. (1982) Proportion of pollen from nonorchard sources. In: Franklin, E.C., Ed., *Pollen Management Handbook, USDA Agriculture Handbook # 587*, AVI Publishing Company Inc., Washington DC, 15-19.
- [29] Lai, H.L. and Wang, Z.R. (1997) A study on gene flow between a Masson pine seed orchard and a plantation near the orchard. *Journal of Nanjing Forestry University*, **21**, 37-41.
- [30] Harju, A. and Muona, O. (1989) Background pollination in *Pinus sylvestris* seed orchards. *Scandinavian Journal of Forest Research*, **4(1-4)**, 513-520.
- [31] Wang, X.R., Lindgren, D., Szmidt, A.E. and Yazdani, R. (1991) Pollen migration into a seed orchard of *Pinus sylvestris* and the methods of its estimation using allozyme markers. *Scandinavian Journal of Forest Research*, **6(1-4)**, 379-386.

Correlations between delayed fluorescence of chlorophyll, metabolism and yield of plants.

I. Influence of fertilizers on correlations

Armen B. Avagyan

Research and Industry Center of Photosynthesising Organisms, Feed Additives and Physiologically Active Compounds, Yerevan, Armenia; armin.av@hotmail.com

Received 7 April 2010; revised 26 April 2010; accepted 8 May, 2010.

ABSTRACT

The increase of the potash fertilizer dose induced a raise in efficiency influence of the nitrogen fertilizer, optimisation of phosphorous fertilizer effect, enhancement of leaf protein production, expansion of assimilating surface and yield growth. In the period of yield formation, the parameters of delayed fluorescence of chlorophyll (DF) of leaf wholly corresponded with key factors that had a dramatic influence on the effectiveness of yield formation. The maximum level of DF amplitude mostly depended on the activity of nitrogen metabolism and presumably on active PSII concentration changes per square unit. Half-decay time of this amplitude was predominantly identified by the level of carbohydrate metabolism in the overall plant system, including the quantity of its products and, therefore, mostly by correspondence with yield. This is a biological base triggering the use of DF parameters for system analyses of plant production process.

Keywords: Delayed Fluorescence of Chlorophyll; Metabolism; Nitrogen; Phosphorus and Potash Fertilizers; Moisture; Poisonous; Yield

1. INTRODUCTION

Plant growth is affected by numerous environmental factors. Therefore, it is difficult to predict the amount of yield, without system analyses of interaction among all key components of crop yield formation. Finding general relationship in the complex system of the plant also required selection of appropriate key objects. Our choice was PSII, which is the main producer of the DF (the level of PSI DF is several times lower [1]). DF transients have been shown to be driven by many mechanisms,

including electrical and pH gradients [2], acceptor availability, donor availability [3], and redox state of the oxygen-evolving system [4,5]. The DF induction curve, registered in a several-minute period, encompasses two major phases—a fast one taking place in the first second of induction, and a slow one, that can last for minutes. Each phase is shaped by several processes running at the same time [4,5]. When applying the phosphoroscope-based method of registration, the fast phase I observed as maximum intensity of leaf DF curve. Many authors attribute this initial phase to the light induced changes of the electrical potential and proton gradient across the thylakoid membrane, depending from the state of the PSII reaction center, which result manifests in the decrease the amount of activation energy necessary for the back reaction between QA^- and Z^+ [2,4,6] as well as may depend from quantity of oxidized QA (Figure 1).

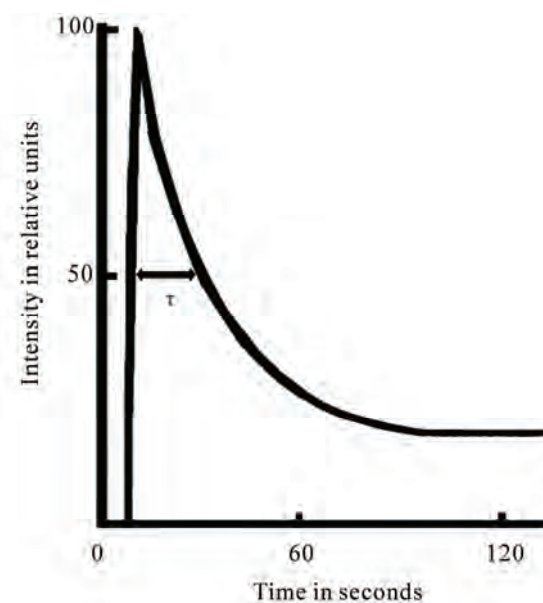


Figure 1. Induction curve of delayed fluorescence of chlorophyll.

Previously, it assumed that kinetics of fast phase further decay depend from the photosynthetic dark processes intensity [4-6]. This decay of induction curve induced the membrane energisation decreasing as result of cation efflux from thylakoids. These are a biological base triggering the use of these DF parameters in physiological research. The interest of using the parameters of DF for the diagnosis of plants state identified as the possibility of their fast measurements on intact objects by the use of comparatively simple and accessible equipment. Therefore, our goal was research the correspondence of DF parameters, metabolism and yield changes of plants in order of the use of these parameters for the system analyses of production process of field plants.

2. MATERIALS AND METHODS

2.1. Plant Material and Experimental Design

The tomato (*Lycopersicum esculentum*) variety Nver seedling and the potato (*Solanum tuberosum*) variety Pirmunes were planted on May 30 and March 30, respectively, in hot and draughty conditions of loamy clay soils of Ararat Valley, Armenia. The sprouts of pea (*Pisum sativum*) variety Pobeditel were transferred into solutions of distilled water after seeds germination (24 h up to 2-3 cm rootlets) and grown at temperature of 25°C, photosynthesis photon flux density of 605 $\mu\text{mol m}^{-2}/\text{s}$ and a photoperiod of 16/8 h. The experiment with pea performed in six replications.

The tomato sprouts planted in three replications on an each field plot of 91 m^2 . A part of nitrogen at dose of N_{30} (in kg/ha) and a full dose of phosphoric and potash fertilizers were added to the soil during the pre-sowing cultivation. The other parts of nitrogen fertilizer added twice on May 17 and June 13. For the $\text{N}_0\text{P}_0\text{K}_0$ variant, the fertilizers not added to the soil.

The potato planted in four replications on each field plot of 50 m^2 . During experiment of potato, the average air temperature was at 26°C, and the maximum air temperature was at 33.6°C. The potato plants were watered only on June 25 (on June 19 the soil humidity was 16.9%, June 24—14.0%, June 26—21.4%, July 8—14.3% and 15—12.2%).

2.2. Measurement and Sample Protocol

The yield of plants obtained per plant and for each plot. The analysis of chemical compounds quantity was performed by the use of standard methods in air-dry samples by methods of Ginsburg for leaves and Maslova (K_2O) and Arrhenius (P_2O_5) for soil [7]. The humidity of soil (in the ground layer 0-30 cm) and leaves measured through samples drying at 105°C and 80°C, respectively, in oven through 3-4 repetitions. The square of assimilat-

ing surface of plants measured by using weighing method and device AAT-5 (Hayasaki Denco Co., Japan) in four repetitions.

The parameters of the leaves DF induction curve were measured from the center of lobes by using a single-disc phosphoroskope (time between excitation and recording of DF was 7 ms) at temperature of 22°C. Exciting light was obtained from a 200 W glow lamp (KGM-200, provided maximum intensity of modulated visual light at the sample surface of 2000 $\mu\text{mol photons m}^{-2}/\text{s}$) and photodiode. Each detached-from-leaf lobe incubated about 1.5 hour in the dark between paper sheets at temperature of 4°C.

The leaf DF parameters and concentration of chemical compounds of tomato leaves measured since fructification phase, per 10 dates. The DF measurements were made with fields leaves detached from 50 tomato plants of each variant for each data of test. The calculation of yield (plot-based weighing method) and concentration of chemical compounds of fruits was carried out on 3 different dates in harvesting stage (July 25, August 6 and 18). The leaf DF parameters and concentration of chemical compounds of potato leaves were measured since bud phase, per 5 dates, concentration of chemical compounds of soil at the end of vegetation.

2.3. Statistical Analyses

The replications dates were processed from a purely mathematical standpoint by the use of the Student's and Fisher's exact test, and the standard methods of correlation analyses with 5% significance level.

3. RESULTS AND DISCUSSION

The research of the effects of mineral nutrition on DF parameters was carried out on pea germ fully provided with necessary nutrient components, contained in seed at the early stage of form-building processes. The data shows that in the growing period of germs I increased dramatically by the raise in mineral salts amounts in solution at the initial stage and then it generally fell, compared to salt-free grown plants (**Tables 1-3**). I reduction correlated with suppression level of germs' vital activity. It is well known that the increase of mineral salt concentration in the nutrient medium stimulates their quantity increase in plants [8]. In the case of an unbalanced heightened amount of separate ions in the nutrient medium, a poisonous effect on plants or unfavourable effect on their yield was observed [8-10]. In the event of addition of mineral salts to nutrition solution, the highest level of poisonous effect was detected for phosphorus anions (**Tables 1-3**). In complex with NO_3^- versus Cl^- anion cation K^+ reduced I more rapidly. This was probably based on the obtained capability of plants to

Table 1. Effect of salt concentration in solution on I of 6-day-old pea and the correlation coefficient between I and salt amount*.

| Quantity in mM | I in rel. units | | | | | Salt | Correlation coefficient in rel. units |
|-------------------|-----------------|--------|------------------|---------------------------------|-----------------------------------|-----------------------------------|---------------------------------------|
| | NaCl | KCl | KNO ₃ | KH ₂ PO ₄ | Ca(NO ₃) ₂ | | |
| 0 | 100.00 | 100.00 | 100.00 | 100.00 | 100.00 | NaCl | 0.467 |
| 2 | 93.55 | 119.82 | 105.76 | 97.24 | 101.92 | KCl | 0.295 |
| 4 | 101.61 | 114.00 | 94.93 | 89.40 | 104.26 | KNO ₃ | -0.775 |
| 20 | 101.84 | 114.29 | 90.78 | 70.28 | 113.22 | KH ₂ PO ₄ | -0.985 |
| LSD ₀₅ | 24.17 | 3.96 | 24.67 | 27.67 | 14.31 | Ca(NO ₃) ₂ | 0.992 |

*At the significance level of 5%, the critical value of correlation coefficient is 0.950.

Table 2. Temporal variation of pea I, planted in salt solution.

| Quantity in mM | I in rel. unit | | | | | |
|-------------------|-----------------------------------|--------|--------|-------------------|--------|--------|
| | Ca(NO ₃) ₂ | | | CaCl ₂ | | |
| | 6 day | 13 day | 20 day | 6 day | 13 day | 20 day |
| 0 | 100.00 | 102.56 | 84.01 | 100.00 | 103.70 | 95.91 |
| 2 | 101.02 | 106.6 | 88.05 | 103.70 | 121.60 | 98.77 |
| 4 | 104.26 | 110.02 | 105.32 | 103.77 | 125.52 | 94.44 |
| 8 | 118.33 | 110.44 | 91.47 | | | |
| 20 | | | | 105.77 | 100.00 | 84.57 |
| LSD ₀₅ | 11.10 | 14.07 | 30.39 | 14.72 | 20.53 | 20.88 |

Table 3. Correlative correspondence between pea DF I and mineral salts concentration*.

| Quantity in mM | Quantity of repetitions | Correlation Coefficient in rel. unit | | | | | |
|-------------------|----------------------------|--------------------------------------|--------|--------|-------------------|--------|--------|
| | | Ca(NO ₃) ₂ | | | CaCl ₂ | | |
| | | 6 day | 13 day | 20 day | 6 day | 13 day | 20 day |
| 0 → 4 | 3 | 0.999 | 0.999 | 0.941 | 0.779 | 0.938 | -0.569 |
| 0 → 8 | 4 | 0.959 | 0.794 | 0.402 | | | |
| 0 → 20 | 4 | | | | 0.817 | -0.530 | -0.973 |

*At the significance level of 5%, the critical value of correlation coefficient is 0.997 for three, and 0.950 for four repetitions.

reduce the effects of highly concentrated Cl⁻ anion [8]. The NO₃⁻ anion far more increased I in case of the complexity with Ca²⁺ compared with K⁺ (**Table 3**). This is probably due to the explicit favorable effect of cation Ca²⁺ on the increase of nitrate reductase activity in leaves [11]. At the same time, in the event of cation Ca²⁺ with anion NO₃⁻ induced the increase of I proves to be more prolonged than in case with anion Cl⁻ (**Tables 2 and 3**). As known, the influence of cations and anions may cause changes in the ECP (thus affecting on only the DF parameters) and quantity of active PSII [3-5], but could reflect on the interaction between weakly associate polypeptides and membrane [12], and on the packaging

of tilakoids in grana [13]. Our results confirmed that in the earlier stage of pea seedling development the mineral salts induced influence on I value mostly depended on the affects of salt concentration in solution on metabolism of plants, compared to the changes of ECP of membranes [14].

A significant reduction in N, N_p and P₁ tomato leaves of all variants was observed in field conditions from fructification stage up to harvesting (**Figure 2, Table 4**). During the experiment, it was obtained that correspondence between N and P₁ changes was significant in all variants (**Table 5**). At the same time, in all variants a reduction in N_p reliably correlated (versus the variant

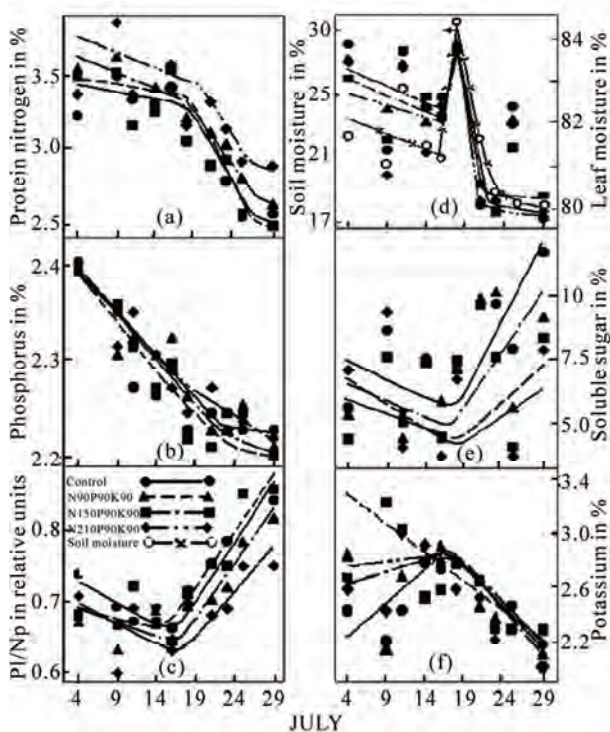


Figure 2. Temporary variation of protein nitrogen (a) and phosphorus (b) concentrations, their ratio (c), leaves and soil moistures (d), soluble sugar leaves (e) and potassium (f) amounts.

Table 4. Fertilizer dose affect on temporary variation of leaf chemical compounds quantities*.

| Coefficient Description | Correlation Coefficient in rel. unit | | | |
|--|--|---|--|--|
| | N ₀ P ₀ K ₀ | N ₉₀ P ₉₀ K ₉₀ | N ₁₅₀ P ₉₀ K ₉₀ | N ₂₁₀ P ₉₀ K ₉₀ |
| r NT | -0.880 | -0.826 | -0.889 | -0.863 |
| r N _p T | -0.854 | -0.866 | -0.885 | -0.747 |
| r P ₁ T | -0.860 | -0.920 | -0.904 | -0.930 |
| r (P ₁ /N _p)T | 0.728 | 0.768 | 0.806 | 0.531 |
| r S _f T | 0.765 | 0.561 | 0.368 | -0.014 |
| r (S _f /N _p)T | 0.797 | 0.742 | 0.605 | 0.195 |
| r K _f T | -0.227 | -0.512 | -0.732 | -0.606 |
| r K _f /N _p T | 0.556 | 0.289 | 0.166 | -0.094 |
| r M ₁ T | -0.640 | -0.711 | -0.668 | -0.570 |
| bN/T | 0.774 | 0.683 | 0.796 | 0.745 |
| bN _p /T | -0.038 | -0.036 | -0.043 | -0.028 |
| bK _f /T | -6.46 | -13.73 | -17.67 | -17.16 |
| b(P ₁ /N _p) / T | 0.007 | 0.006 | 0.009 | 0.003 |
| bM ₁ /T | -0.139 | -0.150 | -0.128 | -0.123 |

*The concentration of chemical compounds of leaves were measured at the beginning of fructification, per 10 dates. At the significance level of 5%, the critical value of correlation coefficient is 0.632.

Table 5. Fertilizer dose affect on correlative correspondence between concentrations of chemical compounds*.

| Coefficient Description | Correlation Coefficient in rel. unit | | | |
|--|--|---|--|--|
| | N ₀ P ₀ K ₀ | N ₉₀ P ₉₀ K ₉₀ | N ₁₅₀ P ₉₀ K ₉₀ | N ₂₁₀ P ₉₀ K ₉₀ |
| r N _p N | 0.885 | 0.853 | 0.845 | 0.439 |
| r N _p M ₁ | 0.497 | 0.545 | 0.521 | 0.153 |
| r N M ₁ | 0.553 | 0.655 | 0.614 | 0.740 |
| r N _p P ₁ | 0.707 | 0.691 | 0.892 | 0.731 |
| r N _p P ₁ | 0.633 | 0.783 | 0.798 | 0.560 |
| r N _p K ₁ | 0.357 | 0.527 | 0.650 | 0.442 |
| r N _p (P ₁ /N _p) | -0.950 | -0.970 | -0.968 | -0.946 |
| r M ₁ M _s | 0.613 | 0.656 | 0.768 | 0.798 |

*Experimental design of data measurements was as in **Table 4**. At the significance level of 5%, the critical value of correlation coefficient is 0.632.

N₂₁₀P₉₀K₉₀) with N and P₁ decrease (d_{P1 Np} = 61-64%, **Figures 2(a)** and **2(b)**, **Table 5**). It was previously shown that ATF, synthesised in LR, is used in phosphorylation reactions of monosaccharides at first priority [15]. Besides, a reduced mineral part of P₁ was observed in leaves, resulting from this reaction. In this case, the efficiency of phosphorylation fell significantly, inducing ADF/ATF ratio increase. As a result, it led to the inhibition of protein synthesis [16,17]. During the experiment, in case of N_p and P₁ reduction a significant P₁/N_p ratio increase was obtained in all variants, except for variants N₂₁₀P₉₀K₉₀ (**Figure 2(c)**, **Table 4**). Simultaneously, during the experiment, P₁/N_p ratio growth was reliable correspondence with N_p reduction in all variants. Thus, the N_p decrease could be induced only by the deficiency in P₁ mineral part.

The N and N_p reduction degree was higher particularly in the unfertilized N₀P₀K₀ variant and high-yield variants N₁₅₀P₉₀K₉₀, compared with other variants of the second group (**Tables 4** and **7**). Only first group variants showed a deficiency in reliable correspondence between the changes N and M₁ (**Table 5**). The existence of correspondence between the nitrogen amount in leaves and fruits and the lack of correspondence between the applied dose of nitrogen fertilizer with concentrations N, N_p and N_f were also obtained (**Tables 6** and **7**). This allows to assume that the quantity of added nitrogen fertilizer and the amount of leaf nonprotein nitrogen have not generally determined N_p differences between variants. The degree of N_p regression decrease was lowerest for N₂₁₀P₉₀K₉₀ variant (**Table 4**) (which has integrated with a high concentration of N and N_f and absence of reliable changes of M₁ and ratio P₁/N_p, as well as correspondence between N and N_p changes, compared with other variants (**Tables 4-7**) that could, presumably, be caused by

Table 6. Effect of fertilizer dose on average concentration and quantities of leaves chemical components*.

| Doze | Concentration in % | | | | | | Ratio of Amounts in rel. unit | | | Total Quantity in rel. unit | | |
|--|--------------------|----------------|----------------|------|----------------|----------------|-------------------------------|--------------------------------|--------------------------------|--------------------------------|----------------------|---------------------|
| | N | N _p | S _l | St | P _l | K _l | M _l | S _l /N _p | P _l /N _p | K _l /N _p | N _{p-total} | St _{total} |
| N ₀ P ₀ K ₀ | 3.65 | 3.07 | 7.82 | 5.73 | 2.254 | 2.47 | 81.75 | 2.63 | 0.741 | 0.812 | 43.4405 | 110.65 |
| N ₉₀ P ₉₀ K ₉₀ | 3.89 | 3.22 | 7.28 | 4.95 | 2.264 | 2.52 | 81.66 | 2.31 | 0.709 | 0.785 | 51.3912 | 116.19 |
| N ₁₅₀ P ₉₀ K ₉₀ | 3.85 | 3.10 | 6.62 | 4.84 | 2.255 | 2.64 | 81.63 | 2.19 | 0.736 | 0.856 | 72.284 | 156.5 |
| N ₂₁₀ P ₉₀ K ₉₀ | 3.95 | 3.30 | 6.74 | 3.95 | 2.265 | 2.57 | 81.36 | 2.05 | 0.690 | 0.781 | 68.607 | 140.12 |
| LSD ₀₅ | 0.19 | 0.09 | 0.96 | 0.97 | 0.022 | 0.20 | 0.33 | 0.35 | 0.024 | 0.067 | | |

*Experimental design of data measurements was as in Table 4.

Table 7. Effect of fertilizer dose on tomato fruit average chemical components concentrations, total square of leaves surface and yield*.

| Doze | Quantity in % of dry weight | | | | | Assimilation area in sq. m | Yield in centner per ha | Yield per assimilation area unit in rel. unit | S _{total} in rel. unit | S _{total/A} in rel. unit |
|--|-----------------------------|----------------|----------------|----------------|-------|----------------------------|-------------------------|---|---------------------------------|-----------------------------------|
| | N _f | P _f | S _f | K _f | VitC | | | | | |
| N ₀ P ₀ K ₀ | 4.46 | 1.02 | 53.71 | 5.54 | 3.587 | 14.15 | 445.6 | 31.491 | 23933 | 1691 |
| N ₉₀ P ₉₀ K ₉₀ | 4.89 | 1.28 | 60.94 | 7.38 | 4.457 | 15.96 | 510.6 | 31.992 | 31116 | 1950 |
| N ₁₅₀ P ₉₀ K ₉₀ | 4.84 | 1.5 | 58.64 | 8.00 | 4.648 | 23.64 | 598.9 | 25.334 | 35119 | 1486 |
| N ₂₁₀ P ₉₀ K ₉₀ | 5.34 | 1.15 | 64.33 | 8.16 | 4.292 | 20.79 | 559.0 | 26.888 | 35960 | 1730 |
| LSD ₀₅ | 0.76 | 0.43 | 8.24 | 2.85 | 1.02 | 5.28 | 42.7 | | | |

*Experimental design of data measurements was as in Table 4.

an increased dose of nitrogen fertilizer. It was previously shown that an inhibition of carbohydrate synthesis and an activation of synthesis of amino acids was caused at a high nitrogen amount (similar to the mentioned variant (**Tables 5 and 6**)) [18]. It was also detected that the activation of nitrate reductase was significantly affected by the intensity of metabolically active mineral nitrogen inflow to the leaf, which increased as the nitrate dose growth in soil [19,20].

Earlier it was showed also that in the case of M_s deficit, inhibition of protein synthesis and a reduction in N_p, as well as an increase in N were observed [21-23]. During the experiment a significant M_l decrease was obtained among leaves of variants (apart from the variant N₂₁₀P₉₀K₉₀), which, however, had a significant correlation with the changes of M_s in only fertilized variants (d_{MlMs} = 59-64%) (**Figure 2(d)**, **Table 5**). In case of the increase in the nitrogen fertilizer dose M_l determinacy from M_s change was also raised. However, in all variants the reduction of N_p, N and nonprotein nitrogen did not reliably correlate with M_s change. Significant correspondence between N and M_l values was registered only in second group variants of N₉₀P₉₀K₉₀ and N₂₁₀P₉₀K₉₀ (**Table 5**). This shows that the M_s and M_l could not be regarded as key factors causing N_p reduction, as well as P_l, K_l and S_l changes also did not depend generally on the M_s changes (**Figure 2**). At the same time, in variant

N₉₀P₉₀K₉₀, showing the highest degree of M_l reduction (**Table 4**), a reliable correspondence between changes of S_l and ratio S_l/N_p with M_l could be induced as a result of significant correlations of both N, P_l with M_l changes, peculiar only to this variant (**Tables 5 and 8**). This results show that watering plants on July 19 could be only a trigger mechanism promoting substantial changes in metabolism of plants (**Figure 2**).

It was obtained that the productivity Y/A of variants was decreasing in comparison with the increase in nitrogen fertilizer dose and in reliable correspondence with the S_l/N_p changes (**Tables 7 and 8**). At the same time, the S_{total} was increasing in parallel with the enhanced dose of nitrogen fertilizers and significantly correlated with the reduced concentration of S_l (**Figure 2(e)**, **Tables 7 and 8**). Consequently, the S_l accumulation reduction in variants was caused by the increase in requirement of assimilates by fruits. However, in N₀P₀K₀ variant, which had lower productivity, and in N₁₅₀P₉₀K₉₀ variant, which had higher productivity, the total accumulation of soluble sugars in fruits per unit of A (S_{total/A}) was less, as compared with the second group of two other variants (**Table 6**). It was obtained that these two groups of variants had differences by their N_p, P_l, P_l/N_p, S_l/N_p, K_l/N_p, N_f, and S_f (**Tables 6 and 7**). These results are consistent with previous findings that the nitrogen fertilizer effect on yield growth was achieved mostly due influence on the assimi-

Table 8. Correlation Correspondences between Tomato Average Quantities of Chemical Compounds, DF Parameters and Yield*.

| Coefficient Description (leaf) | Correlation Coefficient in rel. units | Coefficient Description (leaf-fruits) | Correlation Coefficient in rel. units | Coefficient Description (with yield) | Correlation Coefficient in rel. units |
|--|---------------------------------------|---------------------------------------|---------------------------------------|--------------------------------------|---------------------------------------|
| rN _p M _I | 0.841 | rN N _f | 0.929 | rAY | 0.950 |
| rN _p P _I | 0.970 | rN _p N _f | 0.909 | rS _I Y | -0.987 |
| rK _I S _I | 0.946 | rN _p S _f | 0.937 | rK _I Y | 0.982 |
| rS _I M _I | 0.876 | rK _I vit C | 0.975 | rN _p Y | 0.304 |
| rStM _I | 0.963 | rN _p S _{total} | 0.604 | rIY | 0.454 |
| rI τ | 0.780 | r S _I S _{total} | -0.977 | rS _I A | 0.957 |
| rIN | -0.829 | rStS _{total} | 0.896 | rN _p A | 0.175 |
| rIN _p | -0.941 | rIS _f | 0.929 | rS _I Y/A | 0.886 |
| rIS _I | 0.829 | rτS _f | 0.767 | rS/N _p Y/A | 0.962 |
| rIP _I | 0.831 | rIN _f | -0.971 | rStY/A | -0.915 |
| rIM _I | 0.974 | rIS _{total} | 0.739 | rN _p Y/A | -0.110 |
| rτN _p | 0.574 | rτS _{total} | 0.925 | rS _{total} Y | 0.943 |
| rτS _I | 0.929 | | | rτY | 0.864 |
| rIK _I | -0.302 | | | rτA | 0.877 |
| r I _{total} K _I | 0.985 | | | r I _{total} Y | 0.939 |
| rI _{total} S _{total} | 0.780 | | | | |

***Experimental design** of data measurements was as in tables 4 and 7. At the significance level of 5%, the critical value of correlation coefficient is 0.950.

lating surface square increase [24].

During the experiment, I reduction was registered in all fertilized variants (**Figure 3(a), Table 9**) and substantially correlated with the N decrease (apart from N₉₀P₉₀K₉₀ variant) (**Table 9**). I reduction reliably correlated with N_p decrease in variants of the first group – N₀P₀K₀ and N₁₅₀P₉₀K₉₀ (**Table 9**), the average ratios of I and I/N_p of which were higher (**Figures 3(a) and (b), Table 10**) as well as N_p and S_{total}/A lower (**Table 6**) compared to the second group of variants. In the mean time, in the course of the experiment only the first group variants showed a reliable I/N_p ratio growth, which was reliable correlated with N_p decrease (**Figure 3(b), Table 9**). According to the chemical kinetics laws, the reduction in concentration of interacting centers, as well as the decrease in efficiency of LR products used in DR (as a result of ribulose-1,5-diphosphate carboxylase concentration reduction) should lessen the effectiveness of coupling of LR and DR and increase of the back reaction probability between QA⁻ and Z⁺. Thus must promote certain growth of counter interaction between primary photo-oxides and photo-reducing products. *Is it possible that high levels of first group I generally determined decrease coupling between LR and DR compared to the second group?*

Over and above, it should be pointed out that Y did

not significantly correspond with concentrations N and N_p (**Table 8**). That is why the amount of average values of I variants was not significantly correspondent with Y (**Table 8**). Taking into account the fact that I indicates the activity of PSII reactions per unit of A, a calculation

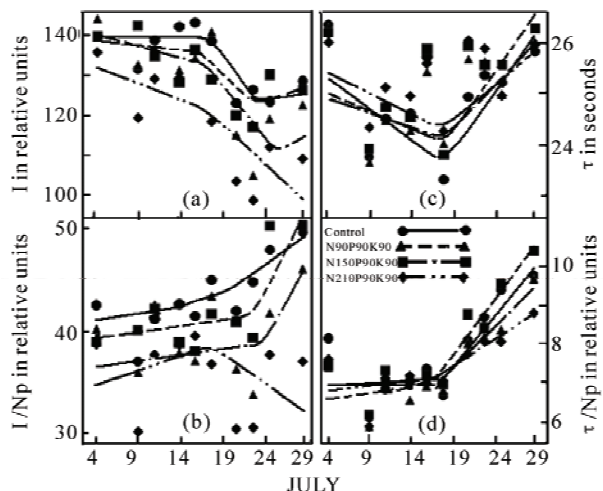


Figure 3. Temporary variation of maximal amplitude of leaf delayed fluorescence (a), I/N_p ratio (b), DF amplitude half decrease time (c) and τ/N_p ratio (d).

Table 9. Temporary variation of DF parameters' and fertilizer dose affect on correlative correspondence between DF parameters' and concentrations of chemical compounds*.

| Coefficient Description | Correlation Coefficient in rel. units | | | |
|--|--|---|--|--|
| | N ₀ P ₀ K ₀ | N ₉₀ P ₉₀ K ₉₀ | N ₁₅₀ P ₉₀ K ₉₀ | N ₂₁₀ P ₉₀ K ₉₀ |
| rIT | -0.625 | -0.729 | -0.712 | -0.669 |
| r (I/N _p)T | 0.780 | 0.227 | 0.675 | -0.148 |
| rτT | 0.118 | 0.262 | 0.327 | 0.233 |
| r (τ/N _p)T | 0.702 | 0.765 | 0.820 | 0.708 |
| rIN | 0.779 | 0.567 | 0.823 | 0.797 |
| rIN _p | 0.756 | 0.595 | 0.655 | 0.498 |
| r (I/N _p)N _p | -0.885 | -0.507 | -0.847 | -0.216 |
| rτN | -0.293 | -0.668 | -0.286 | -0.343 |
| rτN _p | -0.302 | -0.323 | -0.314 | -0.276 |
| rIP ₁ | 0.368 | 0.781 | 0.796 | 0.610 |
| r (I/N _p)(P ₁ /N _p) | 0.802 | 0.626 | 0.923 | 0.420 |
| rτP ₁ | 0.235 | -0.077 | -0.112 | 0.003 |
| r (τ/N _p)(P ₁ /N _p) | 0.906 | 0.897 | 0.922 | 0.852 |
| rIM ₁ | 0.708 | 0.879 | 0.582 | 0.672 |
| rτM ₁ | -0.175 | -0.468 | -0.510 | -0.390 |
| rτS ₁ | -0.016 | 0.224 | -0.147 | 0.115 |
| rHK ₁ | 0.497 | 0.600 | 0.662 | 0.711 |
| rτK ₁ | -0.507 | 0.085 | -0.638 | -0.201 |
| r (τ/N _p) K ₁ | -0.451 | -0.401 | -0.767 | -0.504 |
| rIT | -0.103 | -0.275 | -0.298 | -0.189 |
| bIT | -0.630 | -1.174 | -0.733 | -1.216 |
| b(I/N _p)T | 0.351 | 0.112 | 0.384 | -0.070 |
| bτT | 0.0143 | 0.0304 | 0.0387 | 0.0204 |
| b(τ/N _p)T | 0.0572 | 0.0565 | 0.0728 | 0.0381 |
| bI N _p | 17,15 | 22.59 | 13.99 | 24.46 |
| bIM ₁ | 3.3059 | 6.727 | 3.1207 | 5.6734 |

*Experimental design was as in **Table 4**. At the 5% significance level the critical value of the correlation coefficient is 0.632.

was made for total I produced by all PSII of A per variants (Table 10). In this case I_{total} of variants highly determined their Y (d_{I_{total}} Y = 88.2%) and simultaneously significantly correlated with average K₁ values (**Table 8**). On the other hand, average K₁ did not significant affect the changes of I average levels per unit of assimilating surface between the variants (**Table 8**). These results allowed to exclude the general influence of K₁ on I as

Table 10. Fertilizer dose influence on tomato DF parameters average values*.

| Doze | I in rel.units | τ in seconds | I/N _p | τ/N _p | I _{total} in rel. units |
|--|----------------|--------------|------------------|------------------|----------------------------------|
| N ₀ P ₀ K ₀ | 133.1 | 23.90 | 43.68 | 7.90 | 1883.365 |
| N ₉₀ P ₉₀ K ₉₀ | 127.9 | 24.06 | 39.91 | 7.56 | 2041.284 |
| N ₁₅₀ P ₉₀ K ₉₀ | 130.1 | 24.42 | 42.39 | 8.02 | 3075.564 |
| N ₂₁₀ P ₉₀ K ₉₀ | 119.3 | 24.60 | 36.23 | 7.52 | 2480.247 |
| LSD ₀₅ | 5.7 | 0.48 | 2.47 | 0.32 | |

*Experimental design of data measurements was as in **Table 4**.

direct result of K₁ induced changes on an ECP of chloroplast membrane. Despite it during the experiment a significant correspondence was obtained between I and K₁ changes in N₁₅₀P₉₀K₉₀ and N₂₁₀P₉₀K₉₀ variants (**Table 9**). A significant decreasing of K₁ in leaves was obtained exclusively for variant N₁₅₀P₉₀K₉₀ (**Figure 2(f)**, **Table 4**), which reliably correlated with the N_p reduction again in only this variant (**Table 5**), depending, presumably, on higher K₁ amount among variants at the initial period of the experiment (**Figure 2(f)**). It may stimulate an intensive carbohydrate metabolism and assimilate transport in the earlier period, versus other variants. As it is well known, the increase of K₁ promotes the phloem transport raising [24]. These factors could cause accelerated senescence of N₁₅₀P₉₀K₉₀ variant, proved also by the VitC accumulation degree in fruits of variants (**Tables 6 and 7**). Significant correlation between average values of K₁ and VitC was also registered between variants (**Tables 6, 8 and 10**). It is well known that VitC increase in Y correlated with intensive decrease of N_p in senescent leaves [15,25]. Consequently, the binding force between I_{total} and K₁ was, generally, stipulated by the K₁ affect on metabolism of plants. On the other hand, the high values of I in first group variants, compared to second group of variants, could not result solely from the decrease coupling between LR and DR generally due to dark reaction productivity deactivation, since in case of elimination of photosynthetic efficiency influence per unit of A, a reliable dependence on the I increase persisted in case of N_p reduction (rIN_p (S_{total}/A) = -0.995, rIN_p (Y/A) = -0.981). This shows that the high average values of I in variants could principally stipulate a high concentration of active PSII per unit of A.

During the experiment, the difference in N_p between two groups of variants was visualized as well by the fact that in the first group variants of N₀P₀K₀ and N₁₅₀P₉₀K₉₀ registered lower values of I regression coefficient and a significant increase I/N_p in concurrently higher N_p regression coefficient, versus the second group variants (**Tables 4 and 9**). The similar changes of I/N_p in variants (**Table 9**), confirmed that N_p reduction was probably caused generally by carbohydrate metabolism enzyme

quantity decrease, because as previously reported, at the end of the vegetation N_p decrease is basically caused by the reduction in ribulose-1,5-diphosphate carboxylase amount, leading also to a reduction of photosynthesis intensity [21,26-29]. Furthermore, the fact that the changes in phosphate status have only small effect on the photochemical apparatus of leaves was also previously confirmed [30]. Our data also shows that in case of nitrogen fertilizer affect the total concentration of LR centers is likely to constitute a negative feedback with Y of variants per unit of assimilating surface square ($rI_{total} Y/A = -0.944$).

Theoretically, it was assumed that the τ (Figure 1), in general, depended on the activation of phosphorylation reaction of sugars in Calvin cycle, which led to proton gradient reduction as a result of ATP use and described the intensity of LR and DR of photosynthesis coupling [4-6]. The obtained results showed that the τ values of variants were not in significant correspondence with N_p , M_l , S_l , but in contrast to I, were determined mostly by the level of carbohydrate metabolism end products per unit of A ($R_{\tau} (S_{total}/A St) = 1.000$) (Figure 3(c), Table 8). The average values τ of variants were highly determined by the S_{total} in fruits ($d_{\tau S_{total}} = 85.6\%$) (Tables 7, 8, 10). This is why in the event of elimination of effect of starch formation processes the values τ significantly correlated with quantity of S_{total} ($r_{\tau S_{total}} (St) = -0.997$), which was generally determined by the Y of variants (Table 8), being previously caused by the reliable binding force $r_{\tau Y/A (St)} = -0.995$. Besides, in case of the increase S_{total} , a significant reduction in S_l and S_t raise in leaves was registered between variants (Table 8). This clearly shows the interaction between the Y formation and the photosynthetic production process in leaves and its affect on τ values.

Thus, I and τ parameters of tomato variants were stipulated substantially by different key factors. Therefore, there was not a reliable correspondence between their average values (Table 8) and within those parameters in the stages of fructification up to harvesting (Table 9). During the experiment, reduction in LR/DR coupling efficiency in case of N_p decrease was confirmed by the increase in ratio τ/N_p and its reliable correlation with ratio P/N_p changes in all variants (Figure 3(d), Table 9), as well as by the fact that in the first group with a low protein amount (Table 4), the average τ/N_p ratio was higher compared to the second group variants (Table 10). However, it is important to point out that during the experiment significant increases of τ was showed only per unit of N_p and, on the other hand, temporal significance change of τ of variants was not obtained (Table 9). This could be caused by τ high dependence on carbohydrate metabolism end products accumulation in fruits.

The data also shows that during the experiment I decrease generally correlates with M_l reduction of variants

(Table 9), which appears to be the key generator for reliable correlation between their averaged values (Table 8). It is well known that nitrogen fertilization affects on the osmotic adjustment of tomato plants [31]. Water deficit stimulated both leaf relative water amount decrease, osmotic potential, as well as increase in glycinebetaine and sugar leaf amounts [32]. Simultaneously, a marked increase in electrolyte leakage, decrease in amounts of chlorophylls a and b, and inhibition of PSII activity were observed. Thus, the previously analysis data showed that the amounts of major PSII proteins, including D1 and D2 proteins in PSII reaction centre and light-harvesting Chl *a/b*-protein complex (LHC2) in periphery, declined in case of water stress increasing [33,34]. Therefore, it is possible that M_l changes were not a key factor stipulating degradation of the main part of N_p pool (Table 5), but in case of PSII, had their own input in deactivation of those centers. Indeed, in case of elimination of M_l affect on I the binding force between I and N_p was increased, I also reliably determined changes of both N_p and M_l ($rIN_p (M_l) = -0.995$, $RI (N_p M_l) = 1.000$). In that event, during the experiment, the high degree of I reduction especially in second group variants of $N_{90}P_{90}K_{90}$ and $N_{210}P_{90}K_{90}$ (Figure 3(a), Table 9) was determined by water stress influence increase as a result of higher concentrations of N compared with plants of first group variants (Table 6) and more intensive M_l reduction in $N_{90}P_{90}K_{90}$ variant (Table 4). This assumption is also confirmed by the significant correlation between N and M_l , which is obtained only in second group of variants (Table 5). Previously, it was shown that in case of dehydration of cut-off leaves of potato both I growth and τ reduction were seen at the initial stage, which was caused by the influence of osmotic or ionic potentials on an ECP change [35]. This study showed that more than 3.2-3.8 % leaf moisture loss induced I reduction resulting from PSII deactivation. In the present experiment on tomato, the differences between average initial and end levels of M_l variants are 4% (apart form the variant $N_{150}P_{90}K_{90}$ (around 3%)) (Figure 2(d)). Therefore, this assumption has certain reasons. Some input in I reduction via changes of ionic potential during water loss which may be caused by the disturbance of interaction between weakly associated proteins and membranes in a case of salt concentration increase [12] or through explicit effects of osmotic potential on genetic apparatus was possibly made in vivo moisture decrease (northern hybridization indicated that progressive water stress remarkably reduced amounts of the chloroplast gene *psbA* and *psbD* and nuclear gene *cab* transcripts) [34]).

It is well known that in a number of events the level of Y may be stipulated by the resistance of metabolism and photosynthetic apparatus toward unfavourable environmental impacts [7,36,37]. Therefore, the next experiment was carried out to study the potato production processes

in the period between bud and harvesting stages. The resistance of plants to drought was modified by various doses of phosphorus and potash fertilizers in water deficit conditions (**Table 11**). During this experiment, it was observed that P_1 concentration did not depend on P_s , so N was determined by phosphorus amount in leaves and soil ($RN(P_1P_s) = 0.974$) (**Tables 11 and 12**). Besides, N concentration increased in case of P_s amount growth ($rNP_s (P_1) = 0.955$), and, in contrast, during P_1 increase, N amount reduced accordingly ($rNP_1 (P_s) = 0.968$). At the same time, K_s increment reliably increased K_i , which significantly correlated with P_1 increase (**Table 12**).

$P_{120-150}$ doses are heightening for potato plants [9]. In case of such doses, a decrease in drought resistance of plants and yield falls were obtained [7,22,23,36], which probably depended on the decrease in free water concentration in cells [31,37]. The above-mentioned is also proved by I dependence on the dose of phosphorus anion in nutrient medium (**Table 1**). Previous studies have proved that water deficit induced the N increase that accompanied with N_p reduction as a result of inhibition of protein synthesis [22,23]. Evidently, these were dominant cause for productivity decrease in potato variants of $N_{150}P_{120}K_{45}$ and $N_{150}P_{120}K_{60}$, showing increased N (**Table 11**). As described previously K_s stimulates increase of photophosphorylation efficiency, assimilates transport intensity and nitrogen metabolism [6,25,38]. In addition, it was assumed that the favourable effects of K_i on plants in droughty conditions may be promoted via affection on exchange of cytoplasmic K^+ and H^+ cations of stroma [39]. Generally, while eliminating the effects of leaves moisture changes caused by the unfavourable impact of increased P_s doses on plants, the K_s increase significant correlated with the N decrease ($rNK_s (M_i) = -0.906$). This result confirmed that the increased dose of potash fertilizer induced optimization of nitrogen metabolism, and drought resistance enhancement among variants. A further proof of this was also the increased P_1

amount and yield (**Tables 11 and 12**). This assumes harmony with previously studies results [38].

In the end of vegetation it was obtained that both I and τ values of potato variants were highly determined by N ($d_{IN} = 87.6\%$, $d_{tN} = 76.0\%$), so the values of both DF parameters reliably correlated (**Table 12**), as opposed to the experiment on tomato (**Table 8**). In the meantime, the I of variants was substantially growing, and the τ was reliably decreasing in case of K_s increase (**Table 12**). The average values of both I and τ values of variants significantly correlated and each of these parameters reliably correlated with the Y of variants (also, as opposed to the experiment on tomato variants) (**Table 12**). As known, in droughty conditions PSII deactivation and electron transport inhibition were confirmed [40,41]. Although the positive correlation between I and Y of variants indicated that the Y increase mostly depended on nitrogen metabolism optimization, which probably resulted in the increase of photosynthesis primary reaction centers concentration.

4. CONCLUSIONS

The raised quantity of potash fertilizer induced increase in the efficiency of nitrogen fertilizers effect resulted by enhancement of protein production ($rK_i N_{p-total} = 0.954$), ripening A ($rN_{p-total} A = 0.985$, $rK_i A = 0.983$), Y ($rN_{p-total} Y = 0.973$, $rK_i Y = 0.982$) and the total amount of starch accumulated in leaves ($rN_{p-total} S_{total} = 0.970$, $rK_i S_{total} = 0.979$) of tomato plants. However, nitrogen fertilizer induced falling of the yield per unit of A ($rN_{p-total} Y/A = -0.952$). Besides, K_i had a significant impact on the yield generation per unit of A ($rK_i Y/A = -0.915$).

Generally, accumulation of soluble sugars in tomato fruits determined Y of variants, however, total N_p and K_i of plant did not significantly correlate with the S_{total} and the efficiency of its formation per unit of A ($rN_{p-total} S_{total} = 0.933$, $rN_{p-total} S_{total}/A = -0.549$, $rK_i S_{total} = 0.863$, $rK_i S_{total}/A = -0.615$). As for potato, the data shows that in

Table 11. Fertilizer doze affect on chemical components quantities, yield and DF parametres of potato*.

| Fertilizer Doze | Quantity in leaves in % of dry weight | | | | Quantity in soil in % of dry weight | | Yield in centner per ha | I in rel. units | | τ in seconds | |
|------------------------|--|-------|-------|-------|--|-------|-------------------------------|-----------------|------------------|-------------------|------------------|
| | N | P_1 | K_i | M_i | P_s | K_s | | $I_{average}$ | I_{end} | $\tau_{average}$ | τ_{end} |
| $N_0P_0K_0$ | 0.28 | 0.28 | 5.7 | 83.7 | 67.4 | 108.2 | 256.3 | 95.91 | 73.1 ± 2.4 | 21.9 | 17.28 ± 1.26 |
| $N_{150}P_{90}K_{45}$ | 0.28 | 0.30 | 5.9 | 79.6 | 69.2 | 112.3 | 316.9 | 110.87 | 80.1 ± 3.2 | 20.16 | 15.36 ± 1.62 |
| $N_{150}P_{120}K_{60}$ | 0.34 | 0.25 | 5.6 | 81.0 | 65.6 | 110.2 | 305.3 | 112.17 | 75.0 ± 3.2 | 19.56 | 15.9 ± 1.38 |
| $N_{150}P_{150}K_{75}$ | 0.28 | 0.30 | 6.2 | 81.5 | 68.0 | 113.4 | 339.8 | 112.91 | 75.73 ± 3.7 | 18.96 | 14.88 ± 1.02 |
| $N_{150}P_{120}K_{45}$ | 0.84 | 0.25 | 5.4 | 79.0 | 69.4 | 106.1 | 294.7 | 102.33 | 61.18 ± 3.13 | 21.36 | 19.5 ± 1.44 |

*The leaf DF parameters of leaves were measured since bud stage, per 5 dates, and concentration of chemical compounds of leaves and soil at the end of vegetation. The deviation of average values of DF parameters' did not exceed 3-5% of its average value.

Table 12. Correlative correspondence between chemical compounds amounts in leaves and soil, DF parameters' and yield of potato*.

| Coefficient Description (leaves) | Correlation coefficient In rel. units | Coefficient Description (leaves-fruits-yield) | Correlation coefficient In rel. units |
|--|---------------------------------------|---|---------------------------------------|
| rN M _I | -0.608 | rN _p P _s | 0.457 |
| rN P _I | -0.655 | r P _I P _s | 0.339 |
| rN K _I | -0.706 | rK _I K _s | 0.910 |
| rK _I P _I | 0.888 | rN P _s | 0.457 |
| rP _I M _I | 0.223 | rN K _s | -0.754 |
| rK M _I | 0.260 | rP _I K _s | 0.757 |
| rI N | -0.936 | rM _I P _s | -0.540 |
| rτ N | 0.872 | rI K _s | 0.927 |
| rI τ | -0.929 | rτ K _s | -0.966 |
| rI K _I | 0.629 | rI P _s | -0.294 |
| rτ K _I | 0.838 | rI _{average} Y | 0.915 |
| rI P _I | 0.690 | rτ _{average} Y | -0.902 |
| rI _{average} τ _{average} | -0.909 | | |

*Experimental design of data measurements was as in table 11. At the significance level of 5%, the critical value of correlation coefficient is 0.950.

frames of moisture deficit, aggravated and implemented by unbalanced increased doses of phosphorus fertilizer, the optimization of metabolism and yield of variants were ensured by the increase in potash fertilizer dose.

During both field experiments, I mostly depended on the activity of nitrogen metabolism and probably determined changes of active PSII concentrations per unit of A. The amounts of I average values of variants did not have a significant correlation with Y for tomato plants, as their productivity did not depend from N_p and on production process intensity per unit of A. Simultaneously, total I from full A of tomato plant significant correlated with the productivity of variants (**Table 8**). In case of potato, the production process mostly depended on the degree of water deficit influence on plants' through affect on nitrogen metabolism, thus leading to the correlation between I and τ as well as their both correspondence with Y of variants as opposed to tomato experiment.

It was observed that the values τ predominantly depended on the level of carbohydrate metabolism in the whole plant system, including the quantity of its end products, therefore resulting in correlation with Y of both tomato and potato variants as opposed to their I.

Thus, the results showed that the DF parameters are closely intertwined with metabolism and formation of yield. This is a biological base triggering the use of these

parameters in system analysis of production process. The combined use of the both DF parameters allows generating complete information about key affects on the production process. Fast measurement of DF parameters, the availability of portable devices designed for this goal, as well as the possibility of saving of resources and time versus the chemical-analytical method, allow to recommend the use of DF parameters for the system analyses of production process and the diagnosis of physiological state of plants.

5. ACKNOWLEDGEMENTS

Thanks to Drs L.P. Gorbunova, G.A .Gabrielyan, K.V. Stepanyan for assistance in chemical analyses.

REFERENCES

- [1] Mar, T., Brehlner and J., Roy, G. (1975) Induction kinetics of delayed light emission in spinach chloroplasts. *Biochimica et Biophysica Acta*, **376**, 345-353.
- [2] Wraight, C. A., Crofts, A. R. (1971) Delayed fluorescence and the high-energy state of chloroplast. *European Journal of Biochemistry*, **19**, 386-397.
- [3] Malkin, S. (1977) Delayed luminescence. In: Barber, J. Ed., *Primary Processes of Photosynthesis*, Elsevier, Amsterdam, 349-431.
- [4] Goltsev, V., Zaharieva, I., Lambrev, P., Yordanov, I. and Strasser, R. (2003) Simultaneous analyses of prompt and delayed chlorophyll a fluorescence in leaves during the induction period of dark to light adaptation. *Journal of Theoretical Biology*, **225**, 171-183.
- [5] Goltsev, V., Chernev, P., Zaharieva, I., Lambrev, P. and Strasser, R. J. (2005) Kinetics of delayed chlorophyll a fluorescence registered in milliseconds time range. *Photosynthesis Research*, **84**, 209-215.
- [6] Matorin, D. N., Venedictov, P. S., Timofeev, K. N. and Rubin, A. B. (1978) Research of delayed fluorescence induction curves of green plants. Russian Scientific Report of High School. *Biological Sciences*, **2**, 35-41.
- [7] Peterburgskiy, A. V. (1976) Practical work of agrochemistry.
- [8] Gurbickiy, Z. I. (1963) Physiological and agronomical base for using fertilizers. Academy of Science, Moscow.
- [9] Peterburgskiy, A. V., Asarov, C. K. and Pleshkov, B. P. (1964) Agrochemistry.
- [10] Mrah, S., Ouergh, Z., Eymery, F., Rey, P., Hajji, M., Grignon, C. and Lachaal, M. (2006) Efficiency of biochemical protection against toxic effects of accumulated salt differentiates *Thellungiella halophila* from *Arabidopsis thaliana*. *Journal of Plant Physiology*, **164**, 375-384.
- [11] Davidian, J. C. and Salsac, L. (1979) Interaction anions-cations (Ca²⁺, K⁺, NO₃⁻, Cl⁻) et influence sur induction de l'activity nitrate reductase dans les racines exercices de maïze. *Physiology Vegetable*, **17**, 375-385.
- [12] Avagyan, A. B., Venedictov, P. S., Dobrecov, G. E., Rubin, A. B. (1983) Influence of uni- and divalent cations on interaction ANS and rodamin 6g fluorescent probes with chloroplasts. *Biological Sciences*, **5**, 33-36.

- [13] Barber, J. (1982) Influence of surface charges on thylakoid structure and function. *Annual Review of Plant Physiology*, **33**, 261-268.
- [14] Avagyan, A. B. (1988) Influence of mineral salts on leaves delayed fluorescence. *Biological Journal of Armenia*, **41**, 487-492.
- [15] Brivare, V. N., Nimbacar, J. D. and Chavan, P. D. (1987) Products of $^{14}\text{CO}_2$ labelling in senescent leaves of French bean. *Photosynthetica*, **21**, 360-362.
- [16] Plant, Z., Mayoral, M. L. and Reinold, L. (1987) Effect of altered sink-source ratio on photosynthetic metabolism of source leaves. *Plant Physiology*, **85**, 786-791.
- [17] Woodrow, I. E. (1986) Control of the rate of the photosynthetic carbon fixation. *Biochimica et Biophysica Acta*, **851**, 181-192.
- [18] Mohamed, A. H. and Graham, A. A. (1979) Possible mechanism of ammonium regulation of photosynthetic carbon flow in higher plants. *Plant Physiology*, **64**, 263-268.
- [19] Ingemarson, B. (1987) Nitrogen utilization in Lemma. I. Relations between net nitrate flux, nitrate reduction and in vivo activity and stability of nitrate reductase. *Plant Physiology*, **85**, 856-859.
- [20] Shander, D. L. and Boyer, J. S. (1976) Nitrate reductase activity in maize leaves II. Regulation by nitrate flux at low leaf potential. *Plant Physiology*, **58**, 505-509.
- [21] Bertamini, M., Zulini, L., Muthuchelian, K., Nedunchezian, N. (2006) Effect of water deficit on photosynthetic and other physiological responses in grapevine (*Vitis vinifera* L. cv. Riesling) plants. *Photosynthetica*, **44**, 51-54.
- [22] Isikeev II. (1985) Mineral nutrition and irrigation influence on proteins and noncontiguous amino acids amounts in cereal grass. *Russian Agrochemistry*, **10**, 78-91.
- [23] Vodianic, A. S., Vodianic, T. M. (1984) About pea overhead organs nitrogen metabolism in case of unfavorable moistering condition. *Russian Agricultural Biology*, **10**, 12-15.
- [24] Hunt, E. R., Weber, J. A., Gates, D. M. (1985) Effects of nitrate application on *Amaranthus powelli* wats. *Plant Physiology*, **79**, 619-624.
- [25] Maharashtra, D. (1999) Quality aspects of k nutrition in horticultural crops. In: Imas, P. Ed., *Recent trends in nutrition management in horticultural crops*. International Potash Institute, Israel. http://www.ipipotash.org/presen_tn/qaknhc.html
- [26] Peterson, L. W. and Huffaker, R. C. (1975) Loss of ribulose-1, 5-diphosphate carboxylase and increase in proteolytic activity during senescence barley leaves. *Plant Physiology*, **55**, 1109-1015.
- [27] Wittenbach, V. A. (1979) Ribulose biphosphat carboxylase and proteolytic activity in wheat leaves from anthesis through senescence. *Plant Physiology*, **64**, 884-887.
- [28] Friedrich, J. W., Huffaker, R. C. (1980) Photosynthesis, leaf resistance and ribulose-1,5-biphosphate carboxylase degradation in senescing barley leaves. *Plant Physiology*, **65**, 1103-1007.
- [29] Mae, T. N., Kay, N., Makino, A. and Ohira, K. (1984) Relation between ribulose biphosphate carboxylase content and chloroplast number in naturally senescing primary leaves of wheat. *Plant Cell Physiology*, **25**, 333-336.
- [30] Abadia, J., Rao, M. and Terry, N. (1987) Changes in leaf phosphate status have only small effect on the photochemical apparatus of sugar beet leaves. *Plant Science*, **50**, 49-55.
- [31] García, A. L., Fuentes, V. and Gallego, J. (1996) Influence of nitrogen supply on osmoregulation in tomato (*Lycopersicon esculentum* Mill.) plants under moderate water stress. *Plant Science*, **115**, 33-38.
- [32] Martinez, J. P., Lutts, S., Schanck, A., Bajji, M. and Kinet, J. M. (2004) Is osmotic adjustment required for water stress resistance in the Mediterranean shrub *Atriplex halimus* L. *Journal of Plant Physiology*, **161**, 1041-1051.
- [33] Gaspar, L., Sarvari, E., Molnar, I., Stehli, L., Molnar-Lang, M., Galiba, G. (2002) Structural changes of the photosynthetic apparatus under osmotic stress in different *Triticum aestivum* and *Aegilops biuncialis* genotypes. *Acta Biologica Szegediensis*, **46**, 91-93.
- [34] Liu, W., Yuan, S., Zhang, N., Lei, T., Duan, H., Liang, H. and Lin, H. (2006) Effect of water stress on photosystem 2 in two wheat cultivars. *Biologia Plantarum*, **50**, 597-602.
- [35] Avagyan, A. B. (1991) Study of dehydration effects on the photosynthetic apparatus of detached leaves at different temperatures by the method of delayed fluorescence. *Russian Biophysics*, **36**, 885-890.
- [36] Bacanov, N. S. (1970) Potato.
- [37] Proshkin, A. V. (1973) Influence of mineral nutrition on state of water in spring wheat leaves. *Biological Sciences*, **4**, 90-93.
- [38] Abdel-Wahab, S. (1995) Potassium nitrution and nitrogen fixation by nodulated legumes. *Nutrient Cycling in Agro-ecosystems*, **8**, 9-20.
- [39] Pier, P. A. and Berkowitz, G. A. (1987) Modulation of water stress effects on photosynthesis by altered leaf K^+ . *Plant Physiology*, **85**, 665-661.
- [40] Potter, J. R. and Boyer, J. S. Chloroplast response to low leaf potentials. II. Role of osmotic potentials. *Plant Physiology* 1973, **51**, 993-997.
- [41] Powless, S. B. and Bjorkman, O. (1982) Hight light and water stress effects on photosynthesis in *Nerium oleander*. II. Inhibition of photosynthesis reaction under water stress: Interaction with light level. In: Carnegie Institution Year Book, **81**, 76-77.

Abbreviations:

| | |
|---|--|
| A – total square of leaves surface of plants | M_s – soil humidity, |
| DF – delayed fluorescence of chlorophyll | N – leaf nitrogen |
| I – maximum amplitude of leaves DF | N_p – leaf protein |
| I_{total} – total I from A emitting surface | N_f – fruit nitrogen |
| τ – time of half decrease of I | $N_{p-total}$ – total protein of leaves |
| LR – light reactions of photosynthesis | P_l – leaf phosphorus |
| DR – dark reactions | P_f – fruit phosphorus |
| ECP – electrochemical potential | P_s – soil phosphorus |
| r – correlation coefficient | K_l – leaf potassium |
| b – regression coefficient | K_f – fruit potassium |
| d – determination coefficient | K_s – soil potassium |
| R – multiple correlation coefficient | S_l – leaf soluble sugars |
| NPK – added amount of fertilizers in N:P ₂ O ₅ :K ₂ O in kg/ha | S_f – fruit soluble sugars |
| T – vegetation period | S_{total} – total quantity of soluble sugars accumulated in yield ($S_f \times Y$) |
| Y – yield | St – leaf starch |
| Y/A – productivity per unit of A | VitC – fruit vitamin C |
| M_l – leaf humidity | |

Correlations between delayed fluorescence of chlorophyll, metabolism and yield of plants. II. Influence of moisture of leaf and temperature condition on delayed fluorescence of leaves

Armen B. Avagyan

Research and Industry Center of Photosynthesizing Organisms, Feed Additives and Physiologically Active Compounds, Yerevan, Armenia; armin.av@hotmail.com

Received 22 April 2010; revised 28 April 2010; accepted 8 May, 2010.

ABSTRACT

During various temperatures of incubation the dehydration of leaves up to 3.2-3.8% mainly induced increase maximum amplitude of delayed fluorescence of chlorophyll. It was shown that moisture loss with this range could be determined for the most part by the growth of the electrochemical potential of thylakoid membranes. The further incubation of detached leaves at 36°C temperature, with more notable moisture loss, resulted in specific its decline as opposed to cases of 22 and 6°C of thermal incubation. It was confirmed that the increased temperatures and moisture loss damage of the cells of plants occurred together induce a greater influence on plants than in case of occurring apart. The results allow to suppose that this can be mostly caused weakly associated polypeptides fallen out from the chloroplast membrane, which may be stipulated by high temperature combined with change ionic and osmotic stresses due moisture loss. Simultaneously, the results showed that the exposure of the critical lowered air temperature led to considerable typical changes of leaves delayed fluorescence parameters of field plants. Therefore, their use can constitute new approaches to elucidate the molecular basis of plant freezing tolerance in a timely manner, based on concentration-related changes and the efficiency of coupling between light and dark processes of plants.

Keywords: Delayed Fluorescence of Chlorophyll; Temperature; Moisture; Frost; Weakly Associated Polypeptides

1. INTRODUCTION

The optimum temperature for various reactions of photosynthesis of plants generally varies from 20 to 35 C. In case of short treatment time the increased temperature induced energy metabolism activation of chloroplasts [1,2]. It is well known that water deficit in plants can induce change of osmotic potential [3]. During dehydration of leaves the intensity of photosynthesis increases noticeably at first (up to 4% of moisture loss, named effect of Brilliant) and at second stage it inhibits in case of more moisture loss. The electro-microscopic research showed that at the first period only small changes of packaging the lamellae grains and stroma were obtained, and since the moisture loss of 4% already significant swellings in the lamellae system and infringements of membrane structures were observed [1]. It is noteworthy that in case of interaction between the increased temperatures and the drought the structural organization and regular processes in the cells of plants were broken in more degree [3,4]. Simultaneously, in condition of the water loss of wheat leaves, the roots of which were submerged into polyethylene glycol solutions, an increase in electrolyte leakage, decrease in contents of chlorophylls *a* and *b*, major PSII proteins, including the D1 and D2 proteins in the PSII and the LHC2 and I, whole inhibition of PSII activity were obtained [5]. Northern hybridization showed that progressive water stress remarkably reduced contents of the chloroplast gene *psbA* and *psbD* and nuclear gene *cab* transcripts [5] and 62 genes differentially expressed under osmotic stress [6]. On the other hand, it was assumed that water stress had no effects on the primary photochemistry of PSII, but modified the PSII photochemistry in the light-adapted leaves and such modifications may be a mechanism to down-regulate the photosynthetic electron transport to match a decreased CO₂ assimilation [7]. It was also assumed that PSII is to be highly drought-

resistant: even a drastic desiccation in the air of detached leaf samples only marginally affected the quantum yield for photochemistry in PSII, and water stress markedly modified the responses of PSII to superimposed constraints [9]. The stability of PSII to heat was observed in leaves exposed to water stress conditions: heat treatments (e.g. 42°C in the dark), which caused a complete and irreversible inhibition of PSII in well-watered leaves, resulted in a small and fully reversible reduction of the photochemical efficiency of PSII in drought-stressed leaves. These results allow to suppose that water stress enhanced resistance of PSII to constraints (heat, strong light at high temperature) that are usually associated with drought in the field [8].

PSII is the main producer of DF (the intensity of the PSII delayed fluorescence is several times lower [9], which possesses raised sensitivity to the action of plant metabolism changes and various environmental factors [10]. DF transients have been shown to be driven by many mechanisms, including electrical and pH gradients [11], acceptor availability, donor availability [12], and redox state of the oxygen-evolving system [13,14]. The delayed fluorescence induction curve, registered in a several minutes time period, encompasses two major phases—a fast one, taking place in the first second of induction, and a slow one, that can last for minutes (**Figure 1**). Each phase is shaped by several processes running at the same time [13,14]. Those initial phases of the induction which many authors attribute to the changes of the electrical potential, depending on the size of ECP on a membrane on the state of the PSII reaction center, since the light induced potential difference and the proton gradient across the thylakoid membrane are thought to reduce the amount of activation energy necessary for the back reaction between QA^- and Z^+ to occur and on the other hand, the I level follows the extent of the variable component of fluorescence and has been suggested to be proportional to the amount of oxidized QA at the beginning of illumination [11,13,14], as well as the concentration of active centers of the PSII [11]. It was previously assumed that the time course of DF after the maximum (**Figure 1**) is possibly influenced by a number of dark photosynthetic processes (directly or indirectly modifying the characteristics of PSII) [13,14]. The decay of induction curve was generally explained by a decrease in the membrane energization as a result of secondary cation efflux from thylakoids [13,14]. Our results showed that half time of I decay— τ describe the level of interaction LR with dark processes of plants [10]. These are a biological base triggering the use of these DF parameters in physiological research.

Thus, our goal was to study the correlations between values of DF parameters and both temperature and moisture influences on leaves.

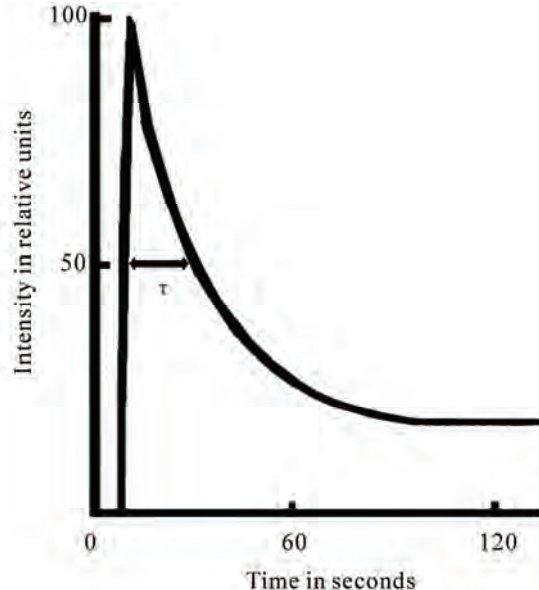


Figure 1. Induction curve of delayed fluorescence of chlorophyll.

2. MATERIALS AND METHODS

2.1. Plant Material and Experimental Design

The potato (*Solanum tuberosum*) variety Priekulsky and the pea (*Pisum sativum*) variety Pobeditel were grown on the clay loam soils in the Armenian Ararat Valley, with the soil moisture of 67-71% of field water capacity. The potato was planted on August 24, and the pea was sown on July 30.

2.2. Measurement and Sample Protocol

The moisture of leaves was identified by their drying at 80°C in oven. The thermal influence was measured on leaves with the initial average moisture of 86.01%, which were detached from field plants in the early hours at air temperature of 22-24°C. In each replicates of thermal treatment of variants the measurement was done on 40 unpaired lobes from the same quantity of plants, with 4 replicates. Each detached from-leave lobe was incubated and measured at various standing temperature of variant.

The influence of frosts was measured on leaves of the field potato (in a plot of 19 plants) and pea plants (in a plot of 33 plants), which had not a visual trace of damage. Each detached from-leave lobe was incubated about 1.5 hour in the dark between paper sheets at temperature of 22°C.

The parameters of the leaves DF induction curve were measured from the center of lobes by using a single-disc phosphoroscope (time period between excitation and recording of DF was 7 ms), Exciting light was obtained

from a 200 W glow lamp (KGM-200, provided maximum intensity of modulated visual light at the sample surface of 2000 $\mu\text{mol photons m}^2/\text{s}$) and photodiode at temperature of 22°C.

2.3. Statistical Analyses

The data were processed from a purely mathematical standpoint, using the Student's and Fisher's exact test, with 5% significance level, and by the use of the standard methods of correlation analyses.

3. RESULTS

In case of incubation at 22 and 6°C temperature affects the dehydration of detached leaves with range up to 3.2-3.8% induced the I significant increase (**Tables 1-3**, $r_{IM(T)}$ at incubation of 130 and 220 min). In the event of elimination of moisture loss affect the temperature increase induced significant rise of I in all variants (**Tables 1** and **3**, $r_{IT(M)}$). The incubation of detached leaves at 36°C with further more notable moisture loss resulted in I decline as opposed to variants with other thermal treatment (**Tables 1-3**, $r_{IM(T)}$ at incubation of 400 min). It depends on the size of ECP on a membrane [11,13,14] donor availability [11-13], as well as possible concentration of active PS II [10]. Our results have shown that half time of I decay— τ describe the level of interaction LR with dark processes of plants [10]. In cases of eliminating the τ or M influences on I a significant correspondence was obtained between I changes with the moisture decrease, as well as with τ of variants (**Tables 1** and **2**).

The moisture loss induced reliable τ increase in cases of elimination of I influence (**Tables 2** and **3**, $r_{tM(I)}$, $r_{tM(T)}$). On the other hand, the induced I increase by moisture loss with range up to 3.2-3.8% stipulated τ reliable decrease (**Table 2**, $r_{IT(M)}$ in case of 22 and 6°C temperature effects, **Table 3**, $r_{tM(T)}$). Only in case the incubation of detached leaves at 36°C temperature effect with more notable moisture loss, I declines accompanied

by τ significant increase (**Table 2**, $r_{IT(M)}$, **Table 3** $r_{IT(T)}$). The incubation temperature increase induced I growth, as well as stipulated τ decrease of variants (**Table 3**).

After the preliminary incubation in extreme temperatures in 90 minutes, their affects on DF parameters were excluded through leaves subsequent adaptation to 22°C (**Table 1**). In this case, after the subsequent 1.5-hour incubation at 22°C no significant distinctions for the DF parameters of leaves up to 4% moisture loss were obtained. Consequently, moisture loss in such leaves did not induce significant influence on the concentration of the PSII and the level of interaction between LR and DR. Therefore, this result showed that in this range of moisture loss, I growth was caused by the increased ECP on thylakoid's membranes due to water loss. These results are consistent also with previous electronic-microscopic finding that the changes obtained in this range of moisture are analogous to those induced by plasmolytic agent's effect on structural organization of thylakoid membranes [1]. Previously also was shown that the short-term influence of high temperatures and the small dehydration of leaves did not cause a substantial change in the activity of the DR key enzymes [15]. Henceforth it was possible to conclude that the enhancement of the LR and DR interaction efficiency in the case of 1.7-2.5% moisture loss could for the most part be determined by the growth of the thylakoid's membranes ECP. Therefore, it is apparent that the effect named Brilliant was induced due ECP growth in case of small moisture loss.

After the preliminary incubation of leaves at 375 minutes in extreme temperatures, the thermal effects on leaves' DF parameters were excluded through leaves subsequent adaptation to 22°C (**Table 1**). In this case, after the 1.5-hour incubation of leaves at 22°C the leaves, which earlier were processed at 36°C, showed a significant reduction in I, compared with other both variants (**Tables 1**). On the other hand, it was previously obtained that leaves incubated at 22°C showed I reduction only after loosing over 35-40% moisture [16]. Therefore,

Table 1. Temporary variation of DF parameters and leaf moisture during incubation at different temperatures.

| Time in min | I in relative units | | | | τ in seconds | | | | Moisture in % | | | |
|-------------|---------------------|--------|--------|---------------------|-------------------|-------|-------|---------------------|---------------|-------|-------|---------------------|
| | 36°C | 22°C | 6°C | LSD _{0.05} | 36°C | 22°C | 6°C | LSD _{0.05} | 36°C | 22°C | 6°C | LSD _{0.05} |
| 130 | 120.30 | 93.61 | 74.72 | 10.89 | 15.74 | 23.91 | 26.02 | 3.36 | 83.53 | 85.10 | 84.57 | 0.46 |
| 220 | 122.80 | 101.40 | 85.00 | 5.68 | 17.79 | 21.39 | 23.80 | 1.06 | 81.77 | 84.31 | 83.59 | 0.80 |
| 400 | 111.81 | 109.81 | 96.01 | 5.61 | 18.59 | 22.50 | 25.91 | 3.34 | 79.46 | 83.39 | 82.33 | 1.38 |
| 90+180* | 109.11 | 107.01 | 106.02 | 6.17 | 21.91 | 21.31 | 21.96 | 1.87 | - | - | - | - |
| 375+130* | 114.97 | 124.38 | 121.95 | 7.97 | 22.64 | 24.76 | 21.73 | 3.18 | 78.40 | 82.57 | 81.58 | 1.62 |

*The thermal effects on DF parameters were measured after the preliminary incubation of leaves at its treatment temperature (first time number) and subsequent adaptation at 22 °C (second time number).

Table 2. Correlative correspondence between DF parameters and leaf moisture in variants of different temperature treatments*.

| Coefficient Description | Correlation Coefficient in rel. unit | | |
|-------------------------|--------------------------------------|--------|--------|
| | 36°C | 22°C | 6°C |
| r_{IM} | 0.802 | -0.995 | -0.978 |
| $r_{IM(\tau)}$ | 1.000 | -1.000 | -1.000 |
| r_{IT} | -0.546 | -0.542 | -0.026 |
| $r_{IT(M)}$ | 1.000 | -0.998 | -1.000 |
| r_{tM} | -0.938 | -0.456 | -0.044 |
| $r_{tM(I)}$ | -1.000 | -0.998 | -1.000 |

*The critical size of correlation coefficient at 5% reliability level is equal to 0.997.

Table 3. Correlative correspondence of DF parameters and temperature and leaf moisture between variants during Incubation at different temperatures.

| Coefficient Description | Correlation Coefficient in rel. units | | |
|-------------------------|---------------------------------------|--------|--------|
| | 130 min | 220 | 400 |
| r_{IM} | -0.720 | -0.726 | -0.374 |
| $r_{IM(\tau)}$ | -1.000 | -1.000 | 1.000 |
| $r_{IM(T)}$ | 1.000 | 1.000 | 1.000 |
| r_{IT} | 0.991 | 0.993 | 0.933 |
| $r_{IT(M)}$ | 1.000 | 1.000 | 1.000 |
| $r_{IT(t)}$ | 1.000 | 1.000 | 1.000 |
| r_{tT} | -0.934 | -0.989 | -0.997 |
| $r_{tT(M)}$ | -1.000 | -1.000 | -1.000 |
| $r_{tT(I)}$ | 1.000 | 1.000 | -1.000 |
| r_{tM} | 0.859 | 0.751 | 0.737 |
| $r_{tM(T)}$ | 1.000 | 1.000 | 1.000 |
| $r_{tM(I)}$ | -1.000 | -0.998 | -1.000 |
| r_{IT} | -0.974 | -0.999 | -0.902 |
| $r_{IT(M)}$ | -1.000 | -1.000 | -1.000 |
| $r_{IT(T)}$ | -1.000 | -1.000 | 1.000 |

*The critical value of the correlation coefficient at the 5% significance level is equal to 0.997.

taking into account the well-known higher DR key centers resistance to increased temperature affect [15], our results showed that obtained specific correlations between parameters of I decrease at 36°C with more notable moisture loss, caused by both temperature and moisture loss specific influence on PSII quantity reduction

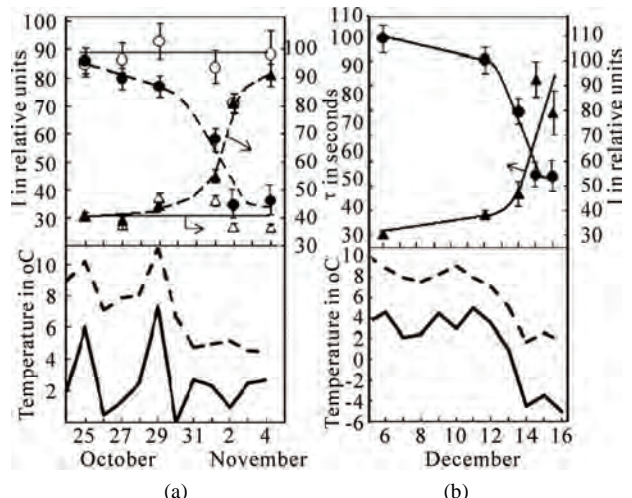


Figure 2. Temporary variation DF parameters (A. potato (\bullet , \blacktriangle) and pea (\circ , Δ), B. pea) and minimal and mean air temperatures. Air temperature is presented by the data of State Hydrometeorological service.

per unit of area.

The critical range of resistance to low temperature is 0 °C for potato and from -4 up to -6°C for pea plants [17]. During the vegetation, the first fall to 0°C of the minimum daily temperature was observed on October 30. After the frost a gradual I decrease and τ increase were observed in potato leaves, while no significant changes in DF parameters were obtained for the pea leaves (Figure 2(a)). After October 30, the average daily air temperature was about 5°C that allowed to exclude the influence of the reactivation process on the changes in the potato leaves' parameters, since the depression of its vital activity occurs already up to an air temperature of 7-8°C [17]. The lack of significant changes in the pea leaves' DF parameters was observed (Figure 2(a)) because it's vital activity reduction occurs at 2°C of air temperature. However, after the exposures to frost with intensity ranging from -4 to -5°C a subsequent decrease of I and growth of τ were observed in pea leaves (Figure 2(b)). After frost affects the average daily air temperature was at a lower level, which was necessary for reactivation processes of plant (Figure 2(b)).

4. DISCUSSION

The effect of high temperatures on the photosynthetic apparatus of the leaves and isolated chloroplasts were also performed through their 5-min thermal treatment [16,18]. After subsequent adaptation leaves to the temperature of 22°C intensity of chlorophyll fluorescence of isolated chloroplasts, Hill's reaction indicated the damage in the area of PSII at processing above 40°C. The amplitude of electro paramagnetic resonance Signal II (g

$\Delta H_{\max} = 2.0026$, $\Delta H_{\max} = 7-8$ Gs), caused by the functioning of the water-splitting system of PSII, increased above 40°C thermal affect on chloroplast. In the meantime, the microcalorimetric observation of isolated chloroplasts warmed-up at 45°C has not shown significant damages in the structural organization of basic membranes. Other studies reported that in case of thermal treatment using the water-splitting system was damaged in the first place [19,20]. Our investigation by using fluorescent probe method showed that at the temperature of above and more than 40°C the weakly associated polypeptides had fallen out from the chloroplast membrane [21-23]. After the separation of chloroplasts from incubation medium content of the obtained weakly associated with membrane polypeptides was 5-6% of the total protein amount in non separated suspension (or 17-20% of membrane whole weakly associated polypeptides). There was also polypeptide of 12-34 kdalton in the separated solution and among them later it was identified 17.2 kdalton thermolabile weakly associated polypeptide of the water-splitting system [24].

Previously it was described that the mineral salts' induced influences on I mostly depends on the effects of salt concentration on concentration of active PSII, compared to the changes of ECP of membranes [10]. Under high salt conditions, plant growth is severely inhibited due to both osmotic and ionic stresses [6]. In case of salt stress, osmotic stress is triggered by an excess of salt in the soil, and ionic stress is caused by the over-accumulation of salt in the cells and recovery is greater under osmotic stress than in case of salt stress [6]. It was shown that the weakly associated polypeptides had fallen out of the chloroplast membrane also in case of increase in amount of mineral salts in suspension of chloroplast [25]. Last findings showed that in the leaf thermograms curve of DF, stationary level decline was observed starting from temperature at 35°C, which was interpreted as a result of PSII oxygen-evolving system inhibition [26]. These results allow to suppose that the specific effect of both increased temperature and moisture loss could be stipulated by the PSII activity in consequence of disturbance in interaction between weakly associated polypeptides with chloroplast membrane.

Experiments were shown that initial moisture loss could be determined for the most part by the growth of the thylakoid membranes ECP. Therefore, it is apparent that the effect named Brilliant was mainly resulted from the ECP growth. Simultaneously our results confirmed that the combined effects of drought and high temperature were much more severe than those of each separate treatment cells of plants [3,4] may be case of deactivation of water-splitting reaction center. Obtained data allow to suppose that both the increased temperature and moisture loss specific effect could be stipulated by the PSII deactivation through the weakly associated poly-

peptides fallen out from the chloroplast membrane.

It was shown that frost induced the water crystal formation and as a result increased the cell hydrolytic processes, observed in the content of lipid falls and registered deactivation of PSII and PSI [27-29]. The obtained data conform to the results of both photosynthesis intensity inhibition and PSII activity loss in case of frost. Therefore, our results allow to conclude that the exposure of the critical low air temperature led to considerably typical changes of DF parameters of leaves, which may be then associated with the deactivation of PSII and whole damage of photosynthetic apparatus. The obtained results confirmed our previous assumption that changes in active PSII concentrations and interaction between LR centers and dark processes of plant affect on parameters of DF and moisture loss to stimulate a deactivation of PSII in leaves [10]. Therefore, the use of DF parameters can constitute new approaches to elucidate the molecular basis of plant freezing tolerance in a timely manner, based on concentration-related changes and the efficiency of coupling between LR and dark processes of plants. At the same time, our experiments showed the targets of additional applications of DF parameters aimed at the thermal and moisture influences research. The interest of using the parameters of this luminescence for the diagnosis of plants' state is identified also by the possibility of their fast measurements on intact objects by the use of comparatively simple and accessible equipment.

REFERENCES

- [1] Niculina, G. N. and Semichatova, O. A. (1983) Influence of a heat on the contents of adenylate in leaves of peas. The influence of a high temperature on the contents of the adenylates in pea leaves. *Russian Plant Physiology*, **30**, 998-1005.
- [2] Tezara, W., Mitchell, V., Driscoll, S. P. and Lawlor, D. W. (2002) Effects of water deficit and its interaction with CO₂ supply on the biochemistry and physiology of photosynthesis in sunflower. *Journal of Experimental Botany*, **53**, 1781-1791.
- [3] Polimbetova, F. A., Mamonov, L. K. and Kim, G. G. (1974) Estimation of cereal crops to drought and heat resistance in field conditions. *Russian Agricultural Biology*, **9**, 235-237.
- [4] Nicolas, M. E., Gleadow, R. M. and Dalling, M. J. (1984) Effects of drought and high temperature on grain growth in wheat. *Australian Journal of Plant Physiology*, **11**, 553-566.
- [5] Liu, W., Yuan, S., Zhang, N., Lei, T., Duan, H., Liang, H. and Lin, H. (2006) Effect of water stress on Photosystem 2 in two wheat cultivars. *Biologia Plantarum*, **50**, 597-602.
- [6] Ueda, A., Kathiresan, A., Inada, M., Narita, Y., Nakamura, T., Shi, W., Takabe, T. and Bennett, J. (2004) Osmotic stress in barley regulates expression of a different set of genes than salt stress does. *Journal of Experi-*

- tal Botany*, **55**, 2213-2218.
- [7] Lu, C. and Zhang, J. (1999) Effects of water stress on Photosystem II photochemistry and its thermostability in wheat plants. *Journal of Experimental Botany*, **50**, 1199-1206.
- [8] Havaux, M. (1992) Stress tolerance of Photosystem II in vivo. Antagonistic effects of water, heat, and photoinhibition stresses. *Plant Physiology*, **100**, 424-443.
- [9] Mar, T., Brehlner, J., Roy, G. (1975) Induction kinetics of delayed light emission in spinach chloroplasts. *Biochimica et Biophysica Acta*, **376**, 345-353.
- [10] Avagyan, A. B. (2010) Correlations between Delayed Fluorescence of Chlorophyll, Metabolism and Yield of Plants. I. Influence of Fertilizers on Correlations. *Journal of Biophysical Chemistry*, **1**. (in press)
- [11] Wright, C. A. and Crofts, A. R. (1971) Delayed fluorescence and the high-energy state of chloroplast. *European Journal of Biochemistry*, **19**, 386-397.
- [12] Mar, T., Brehlner, J. and Roy, G. (1975) Induction kinetics of delayed light emission in spinach chloroplasts. *Biochimica et Biophysica Acta*, **376**, 345-353.
- [13] Goltsev, V., Zaharieva, I., Lambrev, P., Yordanov, I. and Strasser, R. (2003) Simultaneous analysis of prompt and delayed chlorophyll a fluorescence in leaves during the induction period of dark to light adaptation. *Journal of Theoretical Biology*, **225**, 171-183.
- [14] Goltsev, V., Chernev, P., Zaharieva, I., Lambrev, P., Strasser, R. J. (2005) Kinetics of delayed chlorophyll a fluorescence registered in milliseconds time range. *Photosynthesis Research*, **84**, 209-215.
- [15] Avagyan, A. B. (1986) Effect of air temperature and soil moisture content on delayed fluorescence in *Pisum sativum* leaves in field conditions. *Russian Fiziologiya Rastenii*, **33**, 23-28. <http://cat.inist.fr/?aModele=afficheN&cpsidt=8764680>
- [16] Berry, J. A and Downton, W. J. S. (1987) Photosynthesis dependence from influence of environment factors. *Photosynthesis*, **2**, 276-354.
- [17] Korovin, A. I. (1984) Plants and extreme temperatures. Gidrometizdat, Sankt Petersburg.
- [18] Avagyan, A. B., Venedictov, P. S., Dobrecov, G. E. and Rubin, A. B. (1982) Influence heat damage of pea chloro-
- plasts on their interaction with fluorescent probe ANS. *Biological Sciences*, **11**, 30-35.
- [19] Muller, A., Witt, H. T. (1961) Trapped primary product of photosynthesis in green plants. *Nature*, **189**, 944-945.
- [20] Kafalieva, D. N. and Bushuev, M. C. (1979) Influence of temperature on photoinduced proton gradient in isolated chloroplasts. *Russian Biophysics*, **24**, 676-680.
- [21] Avagyan, A. B., Venedictov, P. S. and Rubin, A. B. (1982) Interaction between fluorescent probe ANS and chloroplasts. *Russian Biophysics*, **27**, 415-419.
- [22] Avagyan, A. B., Venedictov, P. S., Rubin, A. B. (1984) Application of rodamin 6g as a fluorescent probe for study of chloroplast membranes. *Russian Biophysics*, **29**, 980-983.
- [23] Avagyan, A. B. (1987) The application of the method of fluorescent probes in research of chloroplast membrane properties. *Biological Journal of Armenia*, **40**, 443-448.
- [24] Becker, D. W., Callahan, F. E. and Chiniae, G. M. (1985) Photoactivation of NH₂OH-treated leaves: reassembly of realized extrinsic PSII polypeptides and relegation of Mn catalyst of water oxidation. *FEBS Letters*, **192**, 209-214.
- [25] Avagyan, A. B., Venedictov, P. S., Dobrecov, G. E., Rubin, A. B. (1983) Influence uni- and bivalence cations on interaction fluorescent probe ANS and rodamin 6g with chloroplasts. *Biological Sciences*, **5**, 33-36.
- [26] Zaharieva, I. and Goltsev, V. (2003) Advances on Photosystem II investigation by measurement of delayed chlorophyll fluorescence by a phosphoroscopic method. *Photochemistry and Photobiology*, **77**, 292-298.
- [27] Neuner, G. and Pramsohler, M. (2006) Freezing and high temperature thresholds of Photosystem II compared to ice nucleation, frost and heat damage in evergreen subalpine plants. *Physiologia Plantarum*, **126**, 196-204.
- [28] Yi, X. F. and Zhang, Z. B. (2008) Influence of insect-infested cotyledons on early seedling growth of Mongolian oak, *Quercus mongolica*. *Photosynthetica*, **46**, 139-142.
- [29] Ehlert, B. and Hincha, D. K. (2008) Chlorophyll fluorescence imaging accurately quantifies freezing damage and cold acclimation responses in *Arabidopsis* leaves. *Plant Methods*. www.plantmethods.com/content/4/1/12

Abbreviations:

PSII – photosystem II

LHC – light harvesting complex

ECP – electrochemical potential

DF – delayed fluorescence of chlorophyll

I – maximum amplitude of DF curve

τ – time of I half decay

LR – light reactions of photosynthesis

DR – dark reactions

M – leaf moisture

T – temperature

r – correlation coefficient

Correlations between delayed fluorescence of chlorophyll, metabolism and yield of plants. III. Influence of viral infection on field plants and new technology of clone selection of virus-free planting potato

Armen B. Avagyan

Research and Industry Center of Photosynthesizing Organisms, Feed Additives and Physiologically Active Compounds, Yerevan, Armenia; armin.av@hotmail.com

Received 22 April 2010; revised 28 April 2010; accepted 8 May, 2010

ABSTRACT

At the end of potato plants vegetation virus infection induced both decrease in maximum amplitude of delayed fluorescence maximal amplitude and increase half time of its decrease, as well as reduction in the amount of stems, plants' height and assimilation area surface, yield, acceleration of plants development and their early die-off. The differences of DF parameters and yields between strongly and weakly infected plants increase in case of a combined virus infection. In industrial test of the selection of virus-free planting potato by the use of DF parameter, a rise in the yield and decrease degree of viral infection of crops was obtained.

Keywords: Potato; Delayed Fluorescence Of Chlorophyll; Virus; Phonological Stage; Yield; Clone Selection; Virus-Free Planting Potato

1. INTRODUCTION

About 20 viruses cause diseases of potato and these diseases are one of the major causes of the potato yield reduction [1]. The most widespread and harmful potato virus of mosaic group (X, S, M (PVX, PVS, PVM)) can reduce yields from 5% up to 40%, others, such as potato leaf roll virus (PLRV) or combined infections of potato viruses X and Y, cause yield losses up to 90% [1,2]. Furthermore, damage of metabolism and decrease in potato productivity are much greater in case of the combined virus infection in comparison with single-virus diseases [1,2]. What is most important: when the virus-free seed potato of this reproduction is used, plants

of the first reproduction are infected in the current of vegetation, and in following reproductions the infected plants quantity progressively increases which correlates with the reduction of crops. This progressively increases rate of viral infection and its effect on yield rice in hot climate [1,2].

In practice, virus-infected plants cannot be "cured" [1,2]. At present level of virus-free seed potato output via tissue culture has not so far managed to address the global solution of the problem connected with virus-free industrial production. Indiscriminate production of virus free seed can be undesirable and costly [1]. The prime cause of this is the lack of a well-developed elite seed farm designed to produce a necessary quantity of virus-free seed potato in many countries. As a whole selection technique should combine high sensitiveness with simplicity of application and low cost [1]. For virus-free planting tubers selection microprecipitation, although least sensitive, compared with latex and ELISA tests, is useful when laboratory facilities are not available to conduct the other tests [1]. Both microprecipitation and latex test may show non-specific flocculation to sap components other than the target virus [1]. Our research results showed that at the latex serological test preferred for virus diagnosis are less reliable for industrial virus-free seed potato selection in field condition, which has also been agreed with the data presented by other researchers [3,4]. The accuracy in serologic analyses was relatively higher for bud and flowering stages of potato plants [2-4]. However, it seems not reasonable to use the analyses results of these periods for clone selection of virus-free seed potato in harvesting period, since the new infection risk at the end stage of vegetation is high [2].

Currently, many countries have to export virus-free potato planting tubers, although this is likely to increase

the domestic production cost. Over and above, problems concerning small industrial sowings (farms, etc.) that do not have a constant access to virus-free seed potato as well as laboratory facilities for the serological diagnostics of viruses. In the meantime, these farms may be one of the greatest reasons for the spread of virus diseases. The selection of preventive measures against viruses requires labour input and, therefore, the development methods for mass selection of virus-free seed potatoes for planting are of great importance.

Virus infection also led to a decrease in plants' photosynthetic potential resulting from the reduction in their assimilating surface square, photosynthetic rate, ribulose-1, 5-diphosphate carboxylase activity, contents of chlorophylls and xanthophylls cycle pigments, and concentration and activity of PSII [2,5-8]. As the disease developed, the maximum carboxylation velocity of ribulose-1, 5-diphosphate carboxylase and the maximum electron transport rate contributing to ribulose-1,5-diphosphate carboxylase regeneration gradually decreased, followed by substantial reductions in the relative quantum efficiency of PSII electron transport, the efficiency of excitation energy capture by open PSII reaction centers [6]. It was assumed that viral infection depressed photosynthesis mainly by interfering with the enzymatic processes in the Calvin cycle, which resulted in a down-regulation of electron transport [6].

PSII is the main producer of DF (the intensity of the PSI DF is several times lower [9]), which possesses raised sensitivity to the action of plant metabolism changes and various environmental factors. DF transients have been shown to be driven by many mechanisms, including electrical and pH gradients [10], acceptor availability, donor availability [9], and redox state of the oxygen-evolving system [11,12]. DF induction curve, registered in a several minutes time period, encompasses two major phases—a fast one, taking place in the first second of induction, and a slow one, that can last for minutes (**Figure 1**). Each phase is shaped by several processes running at the same time [11,12]. When applying the phosphoroscope-based method of registration, the maximum intensity of leaf DF curve (I, fast phase), the phases of which many authors attribute to the changes of the electrical potential, depending on the size of ECP on a membrane on the state of the PSII reaction center, since the light induced potential difference and the proton gradient across the thylakoid membrane are thought to reduce the amount of activation energy necessary for the back reaction between QA^- and Z^+ to occur and on the other hand, the I level follows the extent of the variable component of fluorescence and has been suggested to be proportional to the amount of oxidized QA at the beginning of illumination [10-12], as well as the concentration of active centers of the PSII [13,14]. Previously, it was assumed that the time course of DF

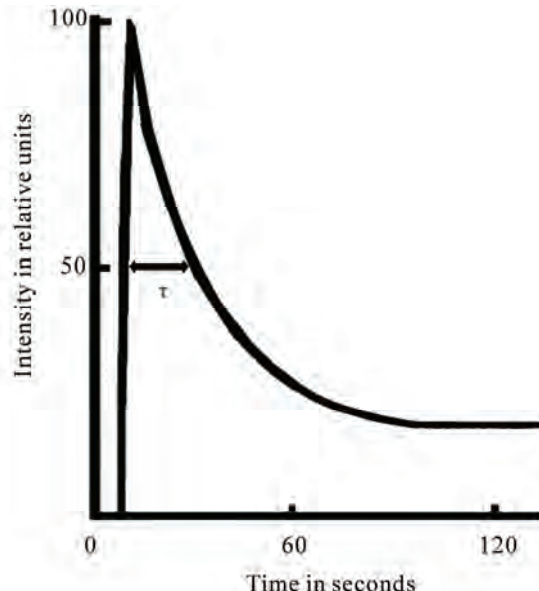


Figure 1. Induction curve of delayed fluorescence of chlorophyll.

after the maximum is possibly influenced by a number of DR (directly or indirectly modifying the characteristics of PSII) [11,12]. The decay of induction curve was generally explained by a decrease in the membrane energization as a result of secondary cation efflux from thylakoids [11,12]. Our results showed that half time of I decay— τ describe the level of interaction LR and DR of plants [13,14]. This is a biological base triggering the use of these DF parameters in physiological research. The interest of using the parameters of this luminescence for the diagnosis of plants' state is identified also by the possibility of their fast measurements on intact objects by the use of comparatively simple and accessible equipment. Thence, our goal was to research the effects of viral infection influences on potato plants by the use of DF parameters as well as to develop new method for selection of virus-free planting potato.

2. MATERIALS AND METHODS

2.1. Plant Material and Experimental Design

The Industrial Test objects were the potato (*Solanum tuberosum*) of following varieties: Pirmunes and Domodedovskiy (tubers planted on March 30), Byelorussian Early (tubers planted on March 30 and July 12, two-harvest culture per year) planted in dry and hot climatic conditions of the Armenian Ararat Valley, and variety Lorgh, the tubers of which were planted on May 5 in the temperate climate of the Sevan basin.

2.2. Measurement and Sample Protocol

The degree of infection among potato plants (the viruses

X, S, M and Y) was determined in bud and flowering stages through the latex serological test [1,2] by the use of the serum, produced in the Russian Potato Research Institute.

The parameters of DF induction curve of the leaves without virus infection symptoms were measured from the center of lobes by using a single-disc phosphoroscope (time period between excitation and recording of DF was 7 ms), exciting light was obtained from a 200 W glow lamp (KGM-200, provided maximum intensity of modulated visual light at the sample surface of 2000 $\mu\text{mol photons m}^{-2}/\text{s}$) and photodiode at temperature of 22 °C. Each detached-from-leave lobe was incubated about 1.5 hour in the dark between paper sheets at temperature of 22 °C.

2.3. Statistical Analyses

The data were processed from a mathematical standpoint by using the Student's and Fisher's exact test, with 5% significance level, as well as based on the standard methods of correlation analyses.

3. RESULTS

Significant differences of DF parameters between strongly (variants A) and weakly infected variants (variants B) were observed only at the end of the plant vegetation period (**Table 1**). The plants of the variety Domodedovskiy of the variant A had a low height by 20%, less stem amount by 28% per shrub and a productivity reduction by 29%, in comparison with the plants of the B. Correspondingly, for the plants of the variety Byelorussian Early of the variant A, these indicators were lowered by 7%, 28% and 27% as compared to its variant B.

In conditions of the Ararat Valley the plants of the variant A of the variety Domodedovskiy achieved the full seedling stage at 3 days earlier, and the full bud and flowering stages at 4 days earlier as compared to its variant B. In temperate climate of the Sevan basin, the beginning of the full phenological stages of variant A was at 2-3 days earlier, compared to its variant B.

Early death also shortens bulking time and limits overall productivity of potato [15]. The decrease in the amount of stems may be caused by accelerated early ripening planting tubers, which might then lead to a reduction in both the assimilation area and the harvesting of potato plants [16]. In case of less developed shrub, the tuberization processes grow faster [17], and the more developed tubers have a relatively lower post-harvesting resting stage [18]. At end of storage the height of stolons of the variant A of variety Domodedovskiy was 1.5-2 times as much in spring as compared to its variant B. This showed that the high infection rate in sowings stimulates accelerated development and early die-off of potato plants. Therefore it is most probable that the lack of reasonable differences of the leaf DF parameters in the flowering stage between the variants A and B of varieties (**Table 1**) can be resulted mainly both from the ontogenetic development rate and the well known active PSII concentration reduction [5-8], which further promotes emergence of significant distinctions of leaf DF only in the end of the vegetation period. So, at this period of each a variants I was higher and τ was lower compared to their B variants (**Table 1**). Simultaneously, I was higher and τ was lower in case of N decreasing in a plant (**Tables 2 and 3**). These DF parameters differences could be stipulated a well known reduction in active PSII content by virus infections and inhibition of carbohydrate metabolism [5-8]. DF parameters typical

Table 1. Influence of Virus Infection on DF Parameters of Potato*.

| Variety | Phenological Stage | Variant | Registration Data | Plants Quantity | I in rel. units | I_A/I_B | τ in s | τ_A/τ_B |
|---------------------|--------------------|---------|-------------------|-----------------|-----------------|-----------|-------------|-----------------|
| Domodedovskii | Flowering | A | June 9 | 65 | 122.4 ± 3.4 | 1.084 | 28.1 ± 0.4 | 0.920 |
| | | B | | 78 | 112.9 ± 3.1 | | 30.6 ± 0.5 | |
| | Harvesting | A | June 13 | 46 | 120.8 ± 3.6 | 1.088 | 29.6 ± 0.6 | 1.021 |
| | | B | | 30 | 111.0 ± 3.8 | | 29.0 ± 0.7 | |
| Lork | Harvesting | A | July 6 | 60 | 119.8 ± 5.3 | 0.761 | 26.2 ± 0.7 | 1.056 |
| | | B | | 70 | 157.5 ± 5.0 | | 24.8 ± 0.8 | |
| | Flowering | A | August 13 | 39 | 70.4 ± 2.0 | 0.963 | | |
| | | B | | 22 | 73.1 ± 5.3 | | | |
| Belorussian earlier | Harvesting | A | September 9 | 25 | 71.4 ± 3.2 | 0.887 | | |
| | | B | | 25 | 80.5 ± 3.5 | | | |
| | Harvesting | A | October 3 | 183 | 81.9 ± 0.7 | 0.889 | | |
| | | B | | 184 | 92.8 ± 0.7 | | | |
| | | A | October 17 | 65 | 76.0 ± 3.3 | 0.866 | | |
| | | B | | 86 | 87.8 ± 2.1 | | | |

*For the variant A of the variety Domodedovskiy, the amount of infected plants was 58% (viruses X – 46%, S – 6%, M – 25% and Y – 5%), and for the variant B – 5% (viruses X – 5%, S – 1, 2% and M – 2, 6%). Accordingly, for the plants of the variety Lork, was 18% (viruses X – 7.7%, S – 7.7% and M – 10.3%) and 2% (virus X – 2%), and for those of the variety Byelorussian Early – 52% (viruses X – 42%, S – 7%, M – 11% and Y – 2%) and 30% (viruses X – 24%, S – 4% and M – 5%), respectively.

Table 2. Influence of combined virus infection on DF and productivity of the potato variety Pirmunes.

| Quantity of Strain | Quantity of Plant | I in rel. units | τ in seconds | Productivity per plant in g |
|--------------------|-------------------|-----------------|-------------------|-----------------------------|
| 0 | 27 | 149.2 ± 5.1 | 23.10 ± 0.73 | 435 ± 35 |
| 1 | 35 | 132.8 ± 5.6 | 23.28 ± 0.68 | 374 ± 32 |
| 2 | 19 | 124.9 ± 6.2 | 25.14 ± 1.31 | 277 ± 28 |

Table 3. Influence of combined virus infection on DF of the potato variety Domodedovskiy.

| Quantity of Strain | Quantity of Plant | I in relative units | τ in seconds |
|--------------------|-------------------|---------------------|-------------------|
| 0 | 53 | 153.9 ± 7.6 | 25.38 ± 0.60 |
| 1 | 49 | 149.3 ± 7.6 | 24.96 ± 0.76 |
| 3 | 8 | 114.9 ± 13.0 | 27.00 ± 2.27 |

changes correlated with yield reduction for the strongly-infected variants and in case of the number of virus strains increased in plant (**Tables 1, 2 and 4**). This confirmed the previous conclusion that the combined virus infection induces more significant fall in yield of potato [1,2].

During the experiment, the interaction between the key LR and DR centers may induce I and τ changes [13,14]. The elimination of τ values influences could eliminate the DR affect on I [13,14]. During the experiment, the accumulation of changes in active PSII concentration in the end of the vegetation period was indicated by the reduced ratio of I_A/I_B ($r_{IA/IB} = -0.989$), the correspondence of which was significant in case of eliminating the effect of the degree of interaction between LR and DR ($r_{IA/IB}(\tau_A/\tau_B) = -1.000$) (**Table 1**). In the event of eliminating τ influence I reduction significance correlated with the N increase in plant and yield decrease (**Table 4**).

The observed correspondences allow us to develop a new method of clone selection of virus-free seed potatoes. For this goal, an independent Industrial Test was

performed via the primary selection of the first spring planting batches of Byelorussian early variety, based on the I values of leaves of 500 plants (degree of virus infection of crop was 33%). Its average I value was 97.7 ± 0.4 rel. units. For 50 plants of the variant 1 and 50 plants of the variant 2 selected from these 500 plants, I was 153.8 ± 2.1 and 58.6 ± 1.2 rel. units, respectively. The average productivity of the plant for 1 and 2 variants was 820 and 600 g per plant, respectively, which may also indicate the lower infection level of plants of the variant 1 as compared with the variant 2. The tubers of these selected variants were planted out in summer both alongside the nearby field industrial reproduction, and in an isolated plot. In field conditions the degree of virus infection for the reproduction of plants grown from the tuber of the variant 1 was less on 15% and 22% compared with industrial plants of second reproduction and the tubers of variant 2, respectively, (**Table 5**). In the isolated plot, the infection degree of plants grown from the tubers of the variants 1 and 2 was lowered to 4 and 6%, respectively, as compared with these values obtained in the industrial field conditions (**Tables 5 and 6**). It agrees with the well known reduction of the infection transfer probability in the isolated plot [2]. At the end of the vegetation period I of variant 1 was higher on 16% compared variant 2 (**Table 5**). These results also indicate the lower infection rate of plants by the variant 1 as compared with the industrial and variant 2 sowings.

For the tuber-grown plants of the variant 1 being cultivated both in industrial fields and isolated plots, the height of batches was higher by 7.2-9.1%, and the quantity of stems per batch was more by 28.8-32.8% compared with the plants being cultivated from tubers of the variant 2 (**Tables 5 and 6**). This also indicates a virus infection lower degree in plants grown from tubers of the variant 1, as well as rate of yield (**Table 5**).

The amplitude I for the leaves of 180 batches of this reproduction of the variant 1 was measured before harvesting, which amounted to an average of 92.0 ± 2.1 rel. units. For 45 selected batches, the amplitude I was, on

Table 4. Correlative correspondence between parameters of DF, number of strain in plant and yield of the potato varieties Pirmunes and Domodedovskiy.

| Coefficient Description | Pirmunes | Domodedovskiy | Coefficient Description | Pirmunes |
|-------------------------|----------|---------------|-------------------------|----------|
| r_{IN} | -0.980 | -0.975 | r_{IP} | 0.968 |
| r_{tN} | 0.903 | 0.867 | r_{tP} | -0.926 |
| r_{It} | -0.800 | -0.954 | $r_{IP(\tau)}$ | 1.000 |
| $r_{IN(t)}$ | -1.000 | -1.000 | r_{NP} | 0.998 |

*The critical value of the correlation coefficient at 5 % significance level is 0.997.

Table 5. Description of field reproduction results in case of using the DF for selection of potato planting materials.

| Variant | Quantity of Plants | Virus Infection Degree in % | I in relative units | Batch Height in cm | Stems Quantity per batch in items | Yield per batch in g |
|------------|--------------------|-----------------------------|---------------------|--------------------|-----------------------------------|----------------------|
| Industrial | 180 | 45 | | | | 342 |
| Variant 1 | 180 | 30 | 87.8 ± 0.7 | 44.4 ± 0.5 | 2.35 ± 0.06 | 449 |
| Variant 2 | 88 | 52 | 76.0 ± 3.3 | 41.4 ± 0.8 | 1.77 ± 0.07 | 330 |

Table 6. Description of isolated plots reproduction results in case of using the DF for selection of potato planting materials.

| Variant | Quantity of Plants | Virus Infection Degree in % | Batch Height in cm | Quantity of Stems per batch in items |
|-----------|--------------------|-----------------------------|--------------------|--------------------------------------|
| Variant 1 | 37 | 26 | 34.8 ± 1.3 | 2.86 ± 0.15 |
| Variant 2 | 21 | 46 | 31.9 ± 1.3 | 1.77 ± 0.15 |

average, 132.0 ± 3.4 rel. units. In the second spring field reproduction the selected planting tubers from 45 batches, as well as the harvesting industrial tubers were planted out in three repetitions per 50 items. The productivity of the plant grown from the selected planting materials of 45 batches amounted, on the average, to 750 g, while the batch yield for the industrial field variant was 583 g ($LSD_{05} = 21$ g). Hence, these industrial tests showed that the selection at the end of the vegetation of planting materials by leaves amplitude I will ensure a 26.4% of additional yield.

4. DISCUSSION

The data show that the well known damage of nitrogen metabolism in plants, induced by mosaic viruses [1,2, 5,19,20], remarkably affected the DF parameters. The distinctions of strongly and weakly infected plants grow higher particularly in case of a combined virus infection. Virus infection induces acceleration of plants development and their early dying, both I decrease and τ increase in the end of vegetation, reduction in the amount of stems, plants' height and assimilatory area surface as well as yields. Analogous changes of plant morphology and yield was registered also in other reports [5,7,19]. This allows us recommended the use of DF I for selecting virus-free planting materials. On other hand, after the infection of cotton-plant by fungus *Verticillium* resulting from continuous development of virus disease, a decrease in I was also observed [21]. Therefore this allows us to assume that the use of parameters DF can find a broader application. The use of the new method enables to select potato tubers as much as possible free from diseases, thereby raising the industrial yield of the potato reproductions. Therefore this biophysical method may be recommended also to be applied in small farms. One of the most noteworthy advantages of this method is its easy-to-apply technology based on the use of up-to-date

portable phosphoroscopes.

Under continuous influence of virus infection, changes in the DF parameters were observed analogously, caused by water stress on potato, modified by doses of phosphorus fertilizers [13], leaf prolonged dehydration and frosts influence [14], which also being correlated with the changes of yield. Therefore, these results allow recommend the use of DF parameters in the systems analysis of production process.

5. ACKNOWLEDGEMENTS

Author thanks Dr. A. Sahakyan for assistance in serological analysis.

REFERENCES

- [1] Salazar, L. F. (1982) Virus detection in potato seed production. *Technical information Bulletin*, **18**. <http://www.cipotato.org/library/pdfdocs/TIBen21141.pdf>
- [2] Zikin, A. G. (1976) Viral Diseases of the Potato. Sankt Petersburg, Kolos.
- [3] Avagyan, A. B. and Sahakyan, A. D. (1987) About a degree of reliability of serological method using for diagnostics of potato virus diseases in hot climate conditions. *Russian Agricultural Biology*, **8**, 63-64.
- [4] Avagyan, A. B. and Sahakyan, A. D. (1991) Diagnostics of mosaic viruses in potato plants by the use of serological method. *Russian Agricultural Biology*, **3**, 123-127.
- [5] Chia, T. F. and He, J. (1999) Photosynthetic capacity in Oncidium (Orchidaceae) plants after virus eradication. *Environmental and Experimental Botany*, **42**, 11-16.
- [6] Zhou, Y. H., Peng, Y. H., Lei, J. L., Zou, L. Y., Zheng, J. H. and Yu, J. Q. (2004) Effects of potato virus Y^{NTN} infection on gas exchange and Photosystem II function in leaves of *Solanum tuberosum* L. *Photosynthetica*, **42**, 417-423.
- [7] Guo, D. P., Guo, Y. P., Zhao, J. P., Liu, H., Peng, Y., Wang, Q. M., Chen, J. S. and Rao, G. Z. (2005) Photosynthetic rate and chlorophyll fluorescence in leaves of stem mustard (*Brassica juncea* var. *tsatsai*) after turnip

- mosaic virus infection. *Plant Science*, **168**, 57-63.
- [8] Synkova, H., Semoradova, S., Schnablova, R., Muller, K., Pospisilova, J., Ryslava, H., Malbeck, J. and Serovska, N. (2006) Effects of biotic stress caused by Potato virus Y on photosynthesis in *ipt* transgenic and control *Nicotiana Tabacum* L. *Plant Science*, **171**, 607-616.
- [9] Mar, T., Brehner, J. and Roy, G. (1975) Induction kinetics of delayed light emission in spinach chloroplasts. *Biochimica et Biophysica Acta*, **376**, 345-353.
- [10] Wraight, C. A. and Crofts, A. R. (1971) Delayed fluorescence and the high-energy state of chloroplast. *European Journal of Biochemistry*, **19**, 386-397.
- [11] Goltsev, V., Zaharieva, I., Lambrev, P., Yordanov, I. and Strasser, R. (2003) Simultaneous analysis of prompt and delayed chlorophyll a fluorescence in leaves during the induction period of dark to light adaptation. *Journal of Theoretical Biology*, **225**, 171-183.
- [12] Goltsev, V., Chernev, P., Zaharieva, I., Lambrev, P., Strasser, R. J. (2005) Kinetics of delayed chlorophyll a fluorescence registered in milliseconds time range. *Photosynthesis Research*, **84**, 209-215.
- [13] Avagyan, A. B. (2010) Correlations between Delayed Fluorescence of Chlorophyll, Metabolism and Yield of Plants. I. Influence of Fertilizers on Correlations. *Journal of Biophysical Chemistry*, **1**. (in press)
- [14] Avagyan, A. B. (2010) Correlations between Delayed Fluorescence of Chlorophyll, Metabolism and Yield of Plants. II. Influence of Moisture of Leaf and Temperature Condition on Delayed Fluorescence of Leaves. *Journal of Biophysical Chemistry*, **1**. (in press)
- [15] Dwelle, R.B. and Love, S. L. (2009) Potato Growth and Development. University of Idaho. <http://www.ag.uidaho.edu/potato/production/files/Growth%20and%20Development%20chapter-%20web.pdf>
- [16] Tucci, R.D. (1966) Influence of steams development at planting on the subsequent growth and a crop of tubers. In: Growth and Development of a Potato, Moscow, 107-126.
- [17] Milthorp, F. L. (1989) Growth of the potato. In: Burton, W. G. Ed., The potato, Longman Scientific & Technical., 189-284.
- [18] Burton, W. G. (1989) Representations about a dormant period of tubers and its mechanism. In: Burton, W. G. Ed. The potato, 3rd Edition, Longman Scientific & Technical, 31-59.
- [19] Kobayashi, K., Sarrobert, C., Ares, X., Rivero, M. M., Maldonado, S., Robaglia, C. and Mentaberry, A. (2004) Over-expression of potato virus X TGBp1 movement protein in transgenic tobacco plants causes developmental and metabolic alterations. *Plant Physiology and Biochemistry*, **42**, 731-738.
- [20] Ayako, Y. K., Shinpei, K., Hirofumi, Y., Noriyuki, D. and Kazuhito, K. (2006) Nitrate reductase is responsible for elicitor-induced nitric oxide production in *Nicotiana benthamiana*. *Plant & Cell Physiology*, **47**, 726-735.
- [21] Makarova, E. N., Abrarov, A. A., Veselovskiy, V. A. and Vecelova, T. V. (1980) Delayed light of cotton leave depending from wilt resistance. *Russian Plant Physiology*, **27**, 413-418.

Abbreviations:

LR – light reactions of photosynthesis

DR – dark reactions

PSII – photosystem II

DF – delayed fluorescence of leaf chlorophyll

I – maximum amplitude of DF

τ – time of I half decrease

T – vegetation period

N – quantity of virus strains in plant

P – yield

r – correlation coefficient

A Plasmid vector encoding functional human keratinocyte growth factor gene in vitro

—Functional human KGF gene expression in vitro

Lin Qiu, Chunbao Guo*

Laboratory of Surgery, Children's Hospital of Chongqing Medical University, Chongqing, China; *Corresponding Author: gchunbao@yahoo.com.cn

Received 9 February 2010; revised 7 March 2010; accepted 2 April, 2010

ABSTRACT

In this study, we cloned human KGF (hKGF) genes using RT-PCR techniques and developed a eukaryotic expression plasmid vector capable of directing the expression of functional hKGF. Monolayer culture of human embryo lung fibroblast (HLF) was used for isolation of total RNA. Then the total RNA was purified and reverse-transcribed into cDNA using an oligo (dT) primer. A full PCR fragment for hKGF was generated and cloned. Restriction digestion and nucleotide sequence analysis validated the complete hKGF transcription. The hKGF cDNA fragment was inserted into pEGFP-C2 vector by means of recombinant DNA technology and verified by restriction analysis and sequencing. We have constructed pEGFP-C2-hKGF encoding the green fluorescent protein (GFP). Furthermore, hKGF had the effect on AEC II proliferation. These results suggest that the potential application of a hKGF plasmid of gene expression should be useful for sustained AEC proliferation, and its in vivo efficacy needs to be validated.

Keywords: Human Embryo Lung Fibroblast; Gene Clone; Reverse Transcriptase Polymerase Chain Reaction; Eukaryotic Expression Vector

1. INTRODUCTION

It has become clear that type II alveolar epithelial cell (AEC II) proliferation is not only important in physiological processes of fetal and neonatal lung development in association with somatic growth, mechanical stretching, physical, chemical and biological stimulation, but also plays a pivotal role in pathological conditions, such as lung inflammation, injury and reparation due to hyperoxia and hypoxia, barotrauma and volutrauma, radiation, and other natural or iatrogenic hazards [1,2,3].

Growth factors that are mitogenic for adult rat, rabbit, or human AEC II in vitro include epidermal growth factor, transforming growth factor- α (TGF- α), insulin, and acidic and basic fibroblast growth factor (FGF).

Keratinocyte growth factor (KGF; also known as FGF-7), a member of the FGF family, is a potent mitogen specific for epithelial cells [4]. Unlike other members of this family, KGF is produced by cells of mesenchymal origin of several stromal fibroblast lines derived from embryonic, neonatal, and adult sources [5,6]. In these tissues, KGF functions in mesenchymal induction of epithelial growth as a stromal-derived paracrine regulator of epithelial proliferation. It is important in fetal pulmonary growth and differentiation [7]. A protective role of KGF to block apoptosis and to prevent oxidative damage has also been suggested for AECs, hepatocytes, and keratinocytes [1,2,8,9]. KGF induces AEC II proliferation in vitro and in vivo [3,10,11]. Furthermore, lungs of transgenic mice expressing a dominant negative for the KGF receptor (FGF receptor 2-IIIb) under control of the surfactant protein C promoter have grossly abnormal lung development, with only two primordial epithelial tubes and no branching morphogenesis [12]. Transgenic mice overexpressing KGF exhibit lethal papillary cystadenoma, with marked enlargement of the bronchial air spaces [13].

In recent years, the therapeutic potential of these growth factors in lung disease, especially in lung injury and reparation, has yet to be fully explored [3]. KGF has been best studied and has impressive protective effects against a wide variety of injurious stimuli when given as a pretreatment in animal models. Whether this protective effect could translate into a treatment effect in humans with acute lung injury (ALI) needs to be investigated [3,14]. Regardless of their therapeutic potential, studies of the unique roles played by these growth factors in the pathogenesis and the resolution of ALI and other lung diseases will continue to enhance our understanding of the complex pathophysiology of inflammatory injury and repair in the lung. Recombinant eukaryotic expres-

sion vector is one of the most popular and promising tools for gene delivery [15]. But how to construct a proper recombinant vector carrying the interested gene has become the bottle neck which restricts the application of the vector in clinical gene therapy. In the present study we sought to construct a eukaryotic expression vector containing hKGF gene, which was capable of introducing exogenous gene in vitro, so as to enable further experimental foundation for ALI study.

2. MATERIALS AND METHODS

2.1. Bacterial Strains, Plasmids, and Cultivation

For preparation of total DNA, human embryo lung fibroblast was cultivated. *E. coli* DH5 α and an expression vector pMD18-T Vector (Takara Bio, Dalian, China) were used for cloning and expression studies. *E. coli* DH5 α and an expression vector pEGFP-C2 used for eukaryotic expression. *E. coli* strain were cultivated in Luria-Bertani (LB) medium supplemented with antibiotics (100 μ g/ml ampicillin and/or 35 μ g/ml chloramphenicol) when they were required. The recombinant plasmid pEGFP-C2-hKGF includes hKGF genes from human embryo lung fibroblast in pEGFP-C2. The nucleotide sequence of hKGF is available from GenBank under Accession No. M60828.

2.2. Human Embryo Lung Fibroblast Cell Culture

Human embryo lung fibroblast were cultivated were obtained from cell Bank and seed into 12-well plates and cultured in growth medium DMEM supplemented with 10% heat-inactivated fetal bovine serum (FBS), 100 U/mL penicillin, and 100 μ g/mL streptomycin in a humidified atmosphere containing 5% CO₂ and 95% air at 37°C. After six days of differentiation, human embryo lung fibroblast were grown in monolayers until they reached a confluence of 70~80%.

2.3. RNA Isolation and cDNA Synthesis

Total RNA was isolated from monolayers of human embryo lung fibroblast using the guanidine isothiocyanate based TRIzol solution (GIBCO-BRL, Burlington, ON, Canada) according to the manufacturer's specifications. The RNA samples were resuspended in 100% formamide and quantified spectrophotometrically at 260 nm. All RNA isolates had an OD₂₆₀:OD₂₈₀ between 1.8 and 2.0, indicating clean RNA isolates. The RNA quality was also checked by 1.0% agarose gel electrophoresis, stained with 1 μ g/ml ethidium bromide. Oligo-(dT)₁₈ (Invitrogen, Burlington, ON) was used as primer in the first step of cDNA synthesis. Total RNA (5 μ g) was combined with 0.5 μ g oligo-dT, 200 μ M dNTPs and H₂O

and preheated at 65°C for 2 min to denature secondary structures. The mixture was then cooled rapidly to 20°C and then 10 μ l 5 × RT Buffer, 10 mM DTT and 200 U MMLV Reverse Transcriptase (Sigma-Aldrich, Oakville, ON, Canada) was added for a total volume of 50 μ l. The reverse transcription mix was incubated at 37°C for 90 min. then stopped by heating at 95°C for 5 min. The cDNA stock was stored at -20°C. The yield of cDNA was measured according to the PCR signal generated from the internal standard house-keeping gene β -actin amplified from 18 to 24 cycles starting with 0.1 μ l of the cDNA solution. The volume of each cDNA pool was adjusted to give the same exponential phase PCR signal strength for β -actin after 20 cycles.

2.4. Amplification of the hKGF Gene

The hKGF gene (GenBank Accession No. M60828) was amplified by PCR from the cDNA solution as described above, using two oligonucleotide primers P1 (5'-CCT AGA TCT GCC ACC ATG CAC AAA TGG ATA CTG AC-3', the *Bgl*II restriction site is underlined and the ATG initiation codon is indicated by boldface type) and P2 (5'-CCT CTC GAG TTA AGT TAT TGC CAT AGG AAG-3', the *Xho*I restriction site is underlined and the TTA termination codon is indicated by boldface type), with the aid of the computer program Primer Premier 5.0. The sense primer is homologous to nucleotides 1 to 20 in the hKGF open reading frame and contains a consensus (GCCACC) Kozak sequence immediately upstream of the initiation codon. In addition, a *Bgl*II site was inserted at the 5'-terminus to facilitate cloning. The antisense primer is homologous to nucleotides 565 to 585 and contains an *Xho*I recognition sequence at its 5' terminus. These primers allowed amplification of a 609-bp cDNA fragment¹⁶. The PCR process involved at 95°C for 2 min, and then 35 cycles of 95°C for 30 s, 60°C for 1 min, 72 °C for 1 min. at the last cycle, PCR products were extended by keeping the temperature at 72°C for 10 min. Then 10 μ l of each PCR product was electrophoresed on 1% agarose gel containing 0.5 μ g/mL EB, and PCR products were then purified from agarose gel according to the protocol of DNA purification kit. The resulting PCR fragment was blunted by T4 DNA polymerase, phosphorylated by T4 polynucleotide kinase, and ligated to the *Scal*I-digested and phosphorylated pMD18-T Vector by T4 DNA ligase. The resulting recombinant plasmid was mixed with *E. coli* DH5 α cells (1:19), on ice for 30 min, 42°C 2 min, then added 2 ml LB, ice for 2 min, 37°C 80 min, and added to X-gal 40 μ l, IPTG 20 μ l, 37°C overnight. Transformed cells were spread onto LB medium agar plates for blue-white blot screening. The positive clones were selected from the transfected *E. coli* DH5 α cells. Blue colonies due to indigo production on LB agar plates were selected as candidates for cells car-

rying hKGF gene from *E. coli* DH5 α cells. The recombinant plasmid was isolated from *E. coli* DH5 α cells using Plasmid Extract Kit. The insert was digested and sequenced to ensure that the correct construction had been obtained.

2.5. Construction of an Expression Vector

The amplified recombinant plasmid was digested with endonucleases *Bgl*/II and *Xho*I then followed with electrophoresis. The amplified hKGF fragment was retrieved using PCR Fragment Recovery Kit (Takara, Bio, Dalian, China) according to manufacturer's guide. Recovery hKGF cDNA was ligated to pEGFP-C2 digested by *Bgl*/II and *Xho*I. Briefly, 1 μ l pEGFP-C2, 1 μ l cDNA fragment and 5 μ l Universal Buffer were mixed at 4 °C overnight. The pEGFP-C2 plasmid inserted with correct hKGF gene was simultaneously introduced into *E. coli* DH5 α cells. The recombinant plasmid was isolated, digested and sequenced to get correct construction plasmid of pEGFP-C2-hKGF.

2.6. S-D Rat AECII Cells Isolation

Alveolar epithelial cells were isolated from pathogen-free male Sprague-Dawley rats (180-200 g) as previously described [10]. The cell pellet (70% purity, > 95% viability, 8-10 \times 10⁶ cells/rat) was plated at a density of 7-10 \times 10⁵ cells/cm² in six-well culture dishes. Culture medium consisted of DMEM containing 25 mM D-glucose, 10 mM HEPES, 23.8 mM NaHCO₃, 2 mM L-glutamine, 10% FCS, 50 U/ml penicillin, 50 μ g/ml streptomycin, and 10 μ g/ml gentamicin incubated in a 5% CO₂-95% air atmosphere. Culture medium was changed 24 h after isolation and then on alternate days.

2.7. Cell Transfection, Cell Count

Cells were seeded in a 6-well plate with 2 \times 10⁵ cells per well 24 h prior to transfection when they were cultured to a confluence of about 90%. Cell transfection was performed according to the manufacturers instructions. Briefly, a transfection mixture was prepared by adding 6 μ g of plasmid DNA and 20 μ l lipofectame (GIBCO BRL) to 500 μ l serum-free RPMI1640. After incubated at room temperature for 20 min, the transfection mixture was added to the cells to be cultivated for 4 h at 37°C when the media containing the transfection mixture was exchanged for growth medium. After transfection cells were observed and photographed by fluorescence microscope and counted at 24, 48, 72, and 96 h.

2.8. Expression Analysis by Immunohistochemistry

The gene transferred AECII cells were washed and fixed with 4% paraformaldehyde then incubated with the 1:200 dilution of rabbit anti human primary antibody to KGF (Santa Cruz Biotechnology, Santa Cruz, CA) or

control IgG (1:1000) overnight at 4°C. The tissue sections were washed in PBS, then incubated with a 1:300 dilution of biotinylated secondary sheep anti-rabbit or goat anti-rabbit IgG. After washing with PBS, tissue sections were incubated with an avidin-biotin complex and developed in 0.075% (w:v) 3, 3 diaminobenzidine (DAB). After lightly counterstaining with haematoxylin, the sections were dehydrated. The intensity of immunostaining around the stent struts was scored as follows: 0, no staining; 1, minor staining only; 2, moderate staining; and 3, heavy staining. Scoring was performed on every third strut in each vessel beginning with the strut closest to the top of the slide by an investigator blinded to the treatment allocation.

2.9. Akt Kinase Assay

Akt kinase assay was performed using Akt Kinase Assay kit (Cell Signaling Technology, Beverly, MA), following the manufacturer's instructions. In brief, soluble extract of lung tissue was prepared by using Triton X-100-containing extraction buffer and used for immunoprecipitation of Akt with anti-Akt antibody conjugated to agarose beads. The immunoprecipitated Akt was incubated with glycogen synthase kinase (GSK)-3 protein in kinase assay buffer containing ATP. After centrifugation, an aliquot of the supernatant was removed and tested for the presence of phospho-GSK-3 by western blotting using anti-phospho-GSK-3 α/β (Ser 21/9) antibody. Equal amounts of soluble extracts were immunoprecipitated with anti-Akt Ab, and The Akt bound to the agarose beads was released by boiling in SDS-sample buffer and subjected to western blot analysis.

3. RESULTS

3.1. The HKGF Gene Fragment Amplified by PCR from Human Embryo Lung Fibroblast

To clone the full sequence gene encoding human KGF protein for functional expression, standardized RT-PCR assay was performed for cloning the gene from the cDNA of human embryo lung fibroblast. Total cellular RNA was purified and RT-PCR was performed using primers based on the published hKGF cDNA sequence, as described in methods. Conditions and cycle number were optimized for primer. This yielded target fragments of hKGF gene with expected 609 bp in length that was subsequently TA-cloned into a pMD18-T vector (Figure 1).

3.2. Enzyme Digestion Analysis of the Recombinant Plasmid

We next analyzed the sequence of the fragment of PCR-amplified hKGF cDNA (609 bp). The recombinant

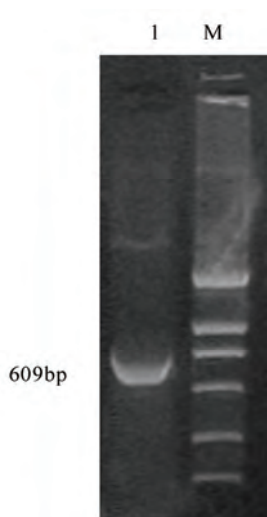


Figure 1. Generation of hKGF cDNA amplified from human embryo lung fibroblast. M: marker (500bp DNA ladder), 1: Lane 1 shows the PCR product (arrow shown), corresponding to the hKGF cDNA (609 bp). Samples were run on a 3% agarose gel with a DNA ladder.

plasmid inserted hKGF cDNA were both doubly digested with *PST1/ECOR1* (**Figure 2**). A 601 bp fragment was released from pMD18-T. This feature of exogenous gene fragment introduced argues in favor of a successful clone.

3.3. Nucleotide Sequence Analysis

Further analysis of the nucleotide sequences of *hKGF* gene in pMD18-T revealed that the sequences of the cloned gene was completely coincidence with the published *hKGF* sequences [16].

3.4. Insertion of HKGF Gene into PEGFP-C2 Plasmid

To construct eukaryotic expression vector, PCR products were subcloned into a pEGFP-C2 vector. The construction strategies of recombinant exogenous *hKGF* gene and eukaryotic expression plasmid pEGFP-C2-hKGF are described elsewhere. Recombinant gene hKGF was 609 bp with *PST1/ECOR1* restriction site on each side, the size of pEGFP-C2-hKGF was 5.3 kb.

3.5. Identification of Eukaryotic Expression Vector AEGFP-C2-HKGF

The eukaryotic expression vector pEGFP-C2-hKGF was identified by restriction endonucleases cut with *PST1/ECOR1* and electrophoresis generating a 601 bp fragment according to the result from GeneBank (**Figure 3**). By nucleotide sequencing, coinciding completely with the sequence from GeneBank. There were no endonuclease cut sites of *PST1/ECOR1* by zymogram analysis.

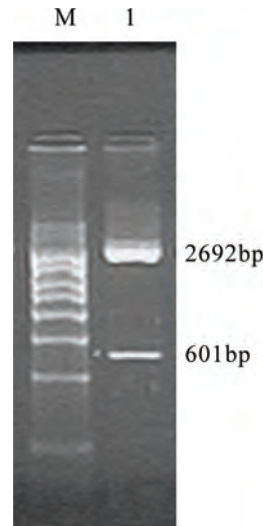


Figure 2. The recombinant plasmid was doubly-digested with *PST1/ECOR1*. M: marker (1 kb DNA ladder), 1: the product of PCR doubly digested with *PST1/ECOR1*, yielding expected 601 bp and 2692bp cDNA fragments.

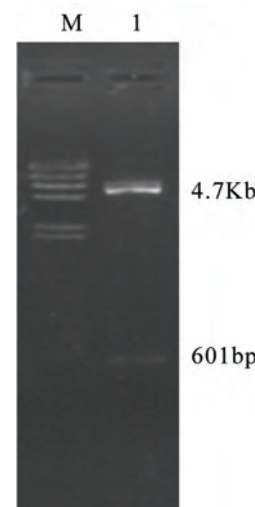


Figure 3. Expressing vector pEGFP-C2-hKGF was digested by *PST1/ECOR1*. M: Marker (1 kb DNA ladder); 1. 601 bp and 4.7 kb DNA fragments were appeared as expected.

3.6. Expression of the Target HKGF Protein by Immunohistochemistry

AECII cells from S-D rat transfected by either pEGFP-C2-hKGF (the experimental group) or pEGFP-C2 (the control group) for 24, 48, 72 h were fixed, paraffin embedded, and then immunostained with an antibody raised against KGF and KGFR, which cross-reacts with porcine KGF and KGFR. We found scattered AECII staining at 24 h group (mean score 0.5 ± 0.5). Expression appeared strong at 48 h (mean score 1.8 ± 0.8) and appeared to

peak at 72 h (mean score 2.1 ± 0.8) (**Figure 3(b)**). But, there was no statistical significant between 48 h and 72 h groups (**Figure 4**, $P > 0.05$). KGF expression was undetectable at 24 h and 48 h control groups. The results of fluorescence expression were similar to that of immunohistochemistry (**Figure 5**).

3.7. Effect of HKGF on AECII Cell Growth

Cell growth was measured by cell count. The cell numbers were 2.8×10^6 , 3.6×10^6 , and 5.0×10^6 in the experimental group and 2.6×10^6 , 3.2×10^6 , and 3.9×10^6 in the control group at 24, 48, and 72 h respectively. The growth of AECII was stimulated by KGF in a time-dependent manner (**Figure 6**, $P < 0.05$).

3.8. KGF-Induced Activation of Akt in Vivo

We next have investigated whether high KGF expression follow up a dramatic increase in Akt activation as evaluated by Akt kinase assay. We have shown that expression of constitutively active Akt appeared strong transfected by eukaryotic expression vector pEGFP-C2-hKGF (**Figure 7**). Thus, one possible explanation for KGF-mediated effect is associated with activation of the Akt signaling axis.

4. DISCUSSION

This Eukaryotic expression plasmid vector expressing

KGF in our study was designed for two purposes. The first was to study the underling mechanism of KGF such as producing extensive type II cell hyperplasia. It is much more difficult to find this extensive type II cell hyperplasia in rodent lungs with a variety of injuries, including bleomycin. Therefore in rodents, it has been difficult to investigate the biologic properties of hyperplastic type II cells and their ability to alter the inflammatory and fibroproliferative response. Type II cells can augment fibrotic reaction by producing PDGF, TGF- α , and TGF- β [17-20]. However, type II cells also inhibit fibroblast proliferation [21]. Exogenous KGF should make it possible to study the biologic properties of hyperplastic type II cells. The second purpose was to have a means of delivering KGF for a sustained period in a local area for the treatment of lung injury. Currently, because of the inflammation induced by adenoviral vectors, therapy of acute lung injury may not be possible. Another approach is to decrease the host response by using plasmid vector.

Over the past 10 yr, it has become increasingly clear that KGF play important roles in both the normal and the injured lung and ultimately may have therapeutic potential as a targeted therapy to facilitate lung epithelial repair in lung disease. KGF has been shown to increase the expression of SP-A and SP-D in cultured alveolar type II cells *in vitro* [22,23]. Administration of KGF has been

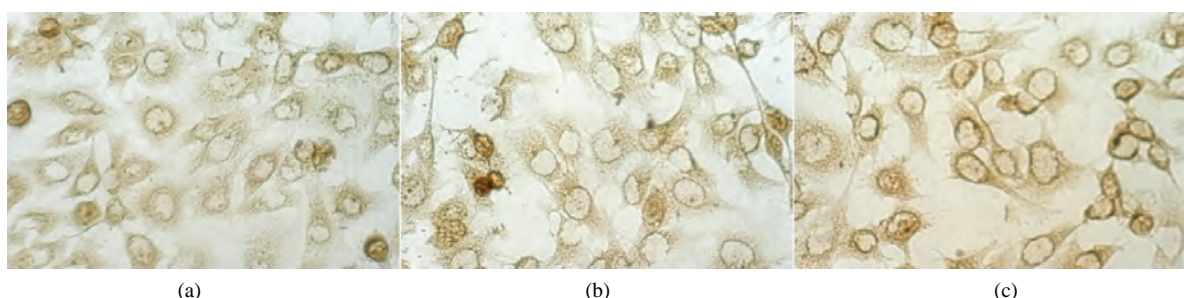


Figure 4. Immunolocalization of KGF in S-D AECII cells. Positively stained cells appear brown color. Positive immunoreactivity to KGF is present in surrounding cytomembrane and is weak in the cytoplasm. The control group data did not show. Note the strong cytomembrane staining in S-D AECII cells 72 h transfection with hKGF vector (c), whereas moderate in S-D AECII cells 48 h transfection with hKGF vector (b) and weak in S-D AECII cells 24 h transfection with hKGF vector (a). Original magnification $\times 200$.

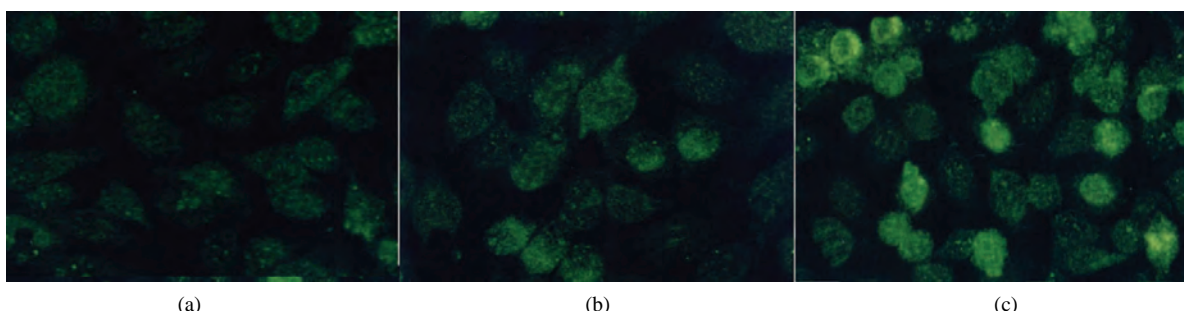


Figure 5. Fluorescence expression in S-DAECII cells. Positively stained is weak at 12 h (a), and strong at 48 h (b), peak at 72 h (c). The control group data did not show. Original magnification $\times 200$.

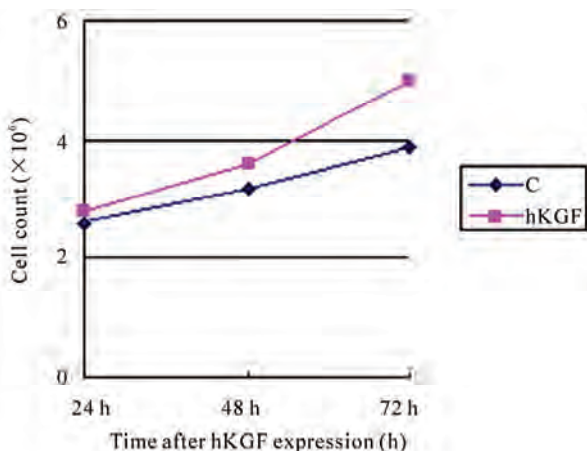


Figure 6. Cell count of AECII cells transfected by eukaryotic expression vector pEGFP-C2-hKGF in different time ($\times 10^6$). Each point is mean \pm SE from 6 observations from a representative experiment. Where no error bars are shown, they are included in the point. Similar results were obtained in 2 further experiments.

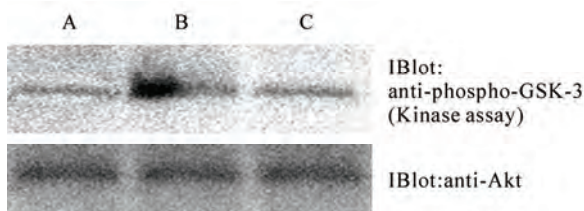


Figure 7. Activity of Akt kinase in the AECII by eukaryotic expression vector pEGFP-C2-hKGF. Akt kinase activity of AECII transfected with eukaryotic expression vector pEGFP-C2-hKGF for 72 h (b) was detected in a high level as compared with normal AECII (a) and vector control (c). The blot was stripped and probed with anti-Akt Ab as described in Materials and Methods and shown equal amounts of Akt in immunoprecipitates. Three observations were included per condition and data shown are representative of two independent experiments.

shown to protect the lung from a variety of insults including oxygen, radiation and chemotherapy. In bleomycin-induced lung injury, KGF was shown to decrease lung edema.

However, the KGF has had to be given before the injury in order to be effective. A more sustained delivery of KGF or expression of KGF might allow for successful post-treatment therapy. Gene transfer into specific tissues or cell types is a key technique in the development of gene delivery strategies study, gene function research and gene therapy. Adenoviral vectors can efficiently transfer foreign genes into lung tissue *in vivo* [24,25]. However, adenovirus-mediated gene expression is transient and may be associated with a significant inflammatory response, depending on the viral dose [26]. Unfortunately, this inflammatory response limits the use of

these vectors in treating acute lung injury. The host response is mainly to the virus.

Eukaryotic expression plasmid vector capable of directing the expression of exogenous gene has been found to be potentially valuable for the study of specific gene function and for gene therapy [27-29]. We described the establishment of a eukaryotic expression system, which allows us to express hKGF in S-D rat AECII. The versatility of this system is evident in our ability to express hKGF. Because our objective in this study was to study the effects of KGF, it was important to develop this system. The results of immunohistochemistry performed in this study demonstrate that the constructed eukaryotic expression system pEGFP-C2-hKGF efficiently produces hKGF gene. And cell count result suggested that hKGF could induce S-D rat AECII cell proliferation.

As plasmid vector gene transfer is one of the most reliable and convenient methods for introducing genes into almost all types of mammalian cells and for expressing the genes at high levels since many cells receive multiple copies of the recombinant genome [30-32]. Gene delivery using eukaryotic expression plasmid vector that propagates in cultured cells might be an effective way for research [33,34]. In order to increase the effect of putative gene therapy, in this study, primers containing specific enzyme-cutting sites were designed to amplify the 0.6 kb *hKGF* from human genome, and the 0.6 kb sequence was cloned into the eukaryotic plasmid. The *hKGF* gene, cloned from human embryo lung fibroblast, showed high homologies of nucleotide and putative amino acid sequences compared with the published corresponding sequences [35,16].

It was shown that there are several different signal transduction pathways to be stimulated by growth factors (36) and through Akt signaling to transmit induced apoptosis signaling to link life and death decisions (37). Our data support the idea that high levels of KGF positively regulate Akt during lung development. KGF-induced Akt activation may play an important role in inhibiting lung alveolar cell death thereby preserving the lung architecture and function during oxidative stress (38). At present, we have no simple explanation for how KGF modifies the response of Akt signal. Future insight into the relationships between KGF and Akt *in vivo* will come from functional and biochemical studies on the pathway of the two ligands, and from the study of both KGF-deficient and KGF, Akt double null mutant mice.

In summary, we succeeded in constructing the hKGF eukaryotic expression vector pEGFP-C2-hKGF acting as a mediating mesenchymal-epithelial interactions, and studied its bioactivity of induction type II cell proliferation. But the molecular mechanisms of pEGFP-C2-hKGF mediated proliferation of AECII cells still need to be established.

5. ACKNOWLEDGEMENTS

We thank Prof. Wang Fu-Liang for providing technical assistance and insightful discussions during the preparation of the manuscript. This work was supported by National Scentific Foundation of China (No: 30030781).

REFERENCES

- [1] Haddad, I. Y., Milla, C., Yang, S., Panoskaltsis-Mortari, A., Hawgood, S., Lacey, D. L. and Blazar, B. R. (2003) Surfactant protein A is a required mediator of keratinocyte growth factor after experimental marrow transplantation. *American Journal of Physiology. Lung Cell Molecular Physiology*, **285**, L602-L610.
- [2] Yi, E. S., Williams, S. T., Lee, H., Malicki, D. M., Chin, E. M., Yin, S., Tarpley, J. and Ulich, T. R. (1996) Keratinocyte growth factor ameliorates radiation- and bleomycin-induced lung injury and mortality. *American Journal of Pathology*, **149**, 1963-1970.
- [3] Keijzer, R., van Tuyl, M., Meijers, C., Post, M., Tibboel, D., Grosveld, F. and Koutsourakis, M. (2001) The transcription factor GATA6 is essential for branching morphogenesis and epithelial cell differentiation during fetal pulmonary development. *Development*, **128**, 503-511.
- [4] Ware, L. B. and Matthay, M. A. (2002) Keratinocyte and hepatocyte growth factors in the lung: Roles in lung development, inflammation, and repair. *American Journal of Physiology. Lung Cell Molecular Physiology*, **282**, L924-L940.
- [5] Ray, P., Devaux, Y., Stoltz, D. B., Yarlagadda, M., Watkins, S. C., Lu, Y., Chen, L., Yang, X. F. and Ray, A. (2003) Inducible expression of keratinocyte growth factor (KGF) in mice inhibits lung epithelial cell death induced by hyperoxia. *Proceedings of the National Academy of Science*, **100**, 6098-6103.
- [6] Atabay, K., Ishigaki, M., Geiser, T., Ueki, I., Matthay, M. A. and Ware, L. B. (2002) Keratinocyte growth factor can enhance alveolar epithelial repair by nonmitogenic mechanisms. *American Journal of Physiology. Lung Cell Molecular Physiology*, **283**, L163-L169.
- [7] Hohlfeld, J. M., Hoymann, H. G., Tschernig, T., Fehrenbach, A., Krug, N. and Fehrenbach, H. (2004) Keratinocyte growth factor transiently alters pulmonary function in rats. *Journal of Applied Physiology*, **96**, 704-710.
- [8] Buckley, S., Barsky, L., Driscoll, B., Weinberg, K., Anderson, K. D. and Warburton, D. (1998) Apoptosis and DNA damage in type 2 alveolar epithelial cells cultured from hyperoxic rats. *American Journal of Physiology. Lung Cell Molecular Physiology*, **274**, L714-L720.
- [9] Senaldi, G., Shaklee, C. L., Simon, B., Rowan, C. G., Lacey, D. L. and Hartung, T. (1998) Keratinocyte growth factor protects murine hepatocytes from tumor necrosis factor-induced apoptosis in vivo and in vitro. *Hepatology*, **27**, 1584-1591.
- [10] Portnoy, J., Curran-Everett, D., Mason, R. J. (2004) Keratinocyte growth factor stimulates alveolar type II cell proliferation through the extracellular signal-regulated kinase and phosphatidylinositol 3-OH kinase pathways. *American Journal of Respiratory Cell and Molecular Biology*, **30**, 901-907.
- [11] Fehrenbach, A., Bube, C., Hohlfeld, J. M., Stevens, P., Tschernig, T., Hoymann, H. G., Krug, N. and Fehrenbach, H. (2003) Surfactant homeostasis is maintained in vivo during keratinocyte growth factor-induced rat lung type II cell hyperplasia. *American Journal of Respiratory and Critical Care Medicine*, **167**, 1264-1270.
- [12] Chedid, M., Rubin, J. S., Csaky, K. G. and Aaronson, S. A. (1994) Regulation of keratinocyte growth factor gene expression by interleukin 1. *Journal of Biological Chemistry*, **269**, 10753-10757.
- [13] Simonet, W. S., DeRose, M. L., Bucay, N., Nguyen, H. Q., Wert, S. E., Zhou, L., Ulich, T. R., Thomason, A., Danilenko, D. M. and Whitsett, J. A. (1995) Pulmonary malformation in transgenic mice expressing human keratinocyte growth factor in the lung. *Proceedings of the National Academy of Science*, **92**, 12461-12465.
- [14] Spilde, T. L., Bhatia, A. M., Marosky, J. K., Preutt, B., Kobayashi, H., Hembree, M. J., Prasad, K., Daume, E., Snyder, C. L. and Gittes, G. K. (2003) Fibroblast growth factor signaling in the developing tracheoesophageal fistula. *Journal of Pediatric Surgery*, **38**, 474-477.
- [15] Fu, Y. G., Qu, Y. J., Wu, K. C., Zhai, H. H., Liu, Z. G. and Fan, D.M. (2003) Apoptosis-inducing effect of recombinant Caspase-3 expressed by constructed eukaryotic vector on gastric cancer cell line SGC7901. *World Journal of Gastroenterology*, **9**, 1935-1939.
- [16] Morikawa, O., Walker, T. A., Nielsen, L. D., Pan, T., Cook, J. L. and Mason, R. J. (2000) Effect of adenovector-mediated gene transfer of keratinocyte growth factor on the proliferation of alveolar type II cells in vitro and in vivo. *American Journal of Respiratory Cell and Molecular Biology*, **23**, 626-635.
- [17] Paine, R. 3rd., Rolfe, M. W., Standiford, T. J., Burdick, M. D., Rollins, B. J. and Strieter, R. M. (1993) MCP-1 expression by rat type II alveolar epithelial cells in primary culture. *Journal of Immunology*, **150**, 4561-4570.
- [18] Li, C., Zhu, N. L., Tan, R. C., Ballard, P. L., Deryck, R. and Minoo, P. (2002) Transforming growth factor-beta inhibits pulmonary surfactant protein B gene transcription through SMAD3 interactions with NKX2.1 and HNF-3 transcription factors. *Journal of Biological Chemistry*, **277**, 38399-38408.
- [19] Beers, M.F., Solarin, K.O., Guttentag, S.H., Rosenblum, J., Kormilli, A., Gonzales, L.W. and Ballard, P. L. (1998) TGF-beta1 inhibits surfactant component expression and epithelial cell maturation in cultured human fetal lung. *American Journal of Physiology. Lung Cell Molecular Physiology*, **275**, L950-L960.
- [20] Zhao, Y., Young, S. L., McIntosh, J. C., Steele, M. P. and Silbajoris, R. (2000) Ontogeny and localization of TGF-beta type I receptor expression during lung development. *American Journal of Physiology. Lung Cell Molecular Physiology*, **278**, L1231-L1239.
- [21] Mason, R. J., Lewis, M. C., Edeen, K. E., McCormick-Shannon, K., Nielsen, L. D. and Shannon, J. M. (2002) Maintenance of surfactant protein A and D secretion by rat alveolar type II cells in vitro. *American Journal of Physiology. Lung Cell Molecular Physiology*, **282**, L249-L258.
- [22] Xu, X., McCormick-Shannon, K., Voelker, D. R. and Mason, R. J. (1998) KGF increases SP-A and SP-D mRNA levels and secretion in cultured rat alveolar type

- II cells. *American Journal of Respiratory Cell and Molecular Biology*, **18**, 168-178.
- [23] Chelly, N., Mouhieddine-Gueddiche, O. B., Barlier-Mur, A. M., Chailley-Heu, B., Bourbon, J. R. (1999) Keratinocyte growth factor enhances maturation of fetal rat lung type II cells. *American Journal of Respiratory Cell and Molecular Biology*, **20**, 423-432.
- [24] Xing, Z., Braciak, T., Jordana, M., Croitoru, K., Graham, F. L. and Gauldie, J. (1994) Adenovirus-mediated cytokine gene transfer at tissue sites. Overexpression of IL-6 induces lymphocytic hyperplasia in the lung. *Journal of Immunology*, **153**, 4059-4069.
- [25] Yei, S., Mittereder, N., Wert, S., Whitsett, J. A., Wilmott, R. W. and Trapnell, B. C. (1994) In vivo evaluation of the safety of adenovirus-mediated transfer of the human cystic fibrosis transmembrane conductance regulator cDNA to the lung. *Human Gene Therapy*, **5**, 731-744.
- [26] Roy, S., Gao, G., Lu, Y., Zhou, X., Lock, M., Calcedo, R. and Wilson, J. M. (2004) Characterization of a family of chimpanzee adenoviruses and development of molecular clones for gene transfer vectors. *Human Gene Therapy*, **15**, 519-530.
- [27] Ebelt, H. and Braun, T. (2003) Optimized, highly efficient transfer of foreign genes into newborn mouse hearts in vivo. *Biochemical and Biophysical Research Communications*, **310**, 1111-1116.
- [28] Bosma, P. T., van Eert, S. J., Jaspers, N. G., Stoter, G. and Nooter, K. (2003) Functional cloning of drug resistance genes from retroviral cDNA libraries. *Biochemical and Biophysical Research Communications*, **309**, 605-611.
- [29] Yan, J., Liang, S. H., Mao, Y. F., Li, L. W., Li, S. P. (2003) Construction of expression systems for flaA and flaB genes of Helicobacter pylori and determination of immunoreactivity and antigenicity of recombinant proteins. *World Journal of Gastroenterology*, **9**, 2240-2250.
- [30] Ebensen, T., Paukner, S., Link, C., Kudela, P., de Domenico, C., Lubitz, W. and Guzman, C. A. (2004) Bacterial ghosts are an efficient delivery system for DNA vaccines. *Journal of Immunology*, **172**, 6858-6865.
- [31] Piao, Y. F., Tang, T. Y., Niu, J. Q. and Wang, F. (2004) Construction of eukaryotic expression plasmids of hepatitis B surface antigen and helper T lymphocyte epitope. *Hepatobiliary & Pancreatic Diseases International Journal*, **3**, 219-222.
- [32] Schuck, S., Manninen, A., Honsho, M., Fullekrug, J. and Simons, K. (2004) Generation of single and double knock-downs in polarized epithelial cells by retrovirus-mediated RNA interference. *Proceedings of the National Academy of Science*, **101**, 4912-4917.
- [33] Belin, D., Guzman, L.M., Bost, S., Konakova, M., Silva, F. and Beckwith, J. (2004) Functional activity of eukaryotic signal sequences in Escherichia coli: The ovalbumin family of serine protease inhibitors. *Journal of Biological Chemistry*, **335**, 437-453.
- [34] Baldwin, S. L., Powell, T. D., Wonderling, R. S., Keiser, K. C., Morales, T., Hunter, S., McDermott, M., Radecki, S. V. and Milhausen, M. J. (2003) Transient and stable transfection of Chinese hamster ovary cells with the recombinant feline erythropoietin gene and expression, purification, and biological activity of feline erythropoietin protein. *American Journal of Veterinary Research*, **64**, 1465-1471.
- [35] Finch, P. W., Rubin, J. S., Miki, T., Ron, D. and Aaronson, S. A. (1989) Human KGF is FGF-related with properties of a paracrine effector of epithelial cell growth. *Science*, **245**, 752-755.
- [36] Fujio, Y. and Walsh, K. (1999) Akt mediates cytoprotection of endothelial cells by vascular endothelial growth factor in an anchorage-dependent manner. *Journal of Biological Chemistry*, **274**, 16349-16354.
- [37] Kauffmann-Zeh, A., Rodriguez-Viciano, P., Ulrich, E., Gilbert, C., Coffer, P., Downward, J. and Evan, G. (1997) Suppression of c-Myc-induced apoptosis by Ras signalling through PI(3)K and PKB. *Nature*, **385**, 544-548.
- [38] Lu, Y., Parkyn, L., Otterbein, L. E., Kureishi, Y., Walsh, K., Ray, A. and Ray, P. (2001) Activated Akt protects the lung from oxidant-induced injury and delays death of mice. *Journal of Experimental Medicine*, **193**, 545-549.

A validated, related substance, GC method for 1,4-cyclohexanedione mono-ethylene Ketal

B. Karthikeyan, V. Srinivasan*

Department of Chemistry; Annamalai university, Annamalainagar.608002, India; *Corresponding Author: vsynreddy@yahoo.com

Received 26 March 2010; revised 4 May 2010; accepted 10 May, 2010.

ABSTRACT

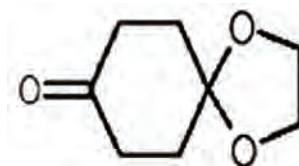
A simple, economic, and time-efficient related substance, GC method has been developed for the analysis of 1,4-Cyclohexanedione mono-ethylene ketal(will be specified as ketal) in the presence of a potential impurity 1,4-cyclohexanedione bis (ethylene ketal) [will be specified as diketal]. Successful chromatographic separation of the ketal from the impurity was achieved on a DBWAX ETR, 30 m x 0.32 mm x 1.0 μ FT column with nitrogen as carrier gas and FID detector. The method was validated for linearity, accuracy, precision, and specificity and can be used for quality control during manufacture of ketal. A validated GC method is reported for the ketal for the first time.

Keywords: Column Gas Chromatography; 1,4-Cyclohexanedione Mono-Ethylene Ketal; 1,4-Cyclohexanedione Bis (Ethylene Ketals); Validation

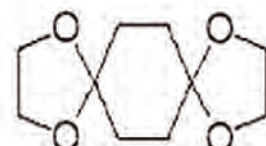
1. INTRODUCTION

Ketal chemically 1,4-Cyclohexanedione mono-ethylene ketal is a potential intermediate in organic synthesis [1-3]. Identification of the potential impurity diketal by GC is the main interest of this work. The reported synthesis of monoketal claim 50% of the presence of impurity diketal. This paper describes a simple GC method, which separates ketal from diketal. Ketal also have many importance and its hydrolysis rate has been studied experimentally [4-8]. On its synthesis diketal also formed and it can be detected with the help of gas chromatographic technique[6].GC method is a powerful analytical technique and used in widely in pharma and biochemical disciplines. GC combined with mass spectral technique activated the research in the field biophysical chemistry. The separation of dikeatl from ketal is an interesting as well as important procedure and no reports available on that. The structures of ketal, diketal are il-

lustrated in **Figure 1**.Organic impurities can arise during manufacture and storage of drugs and criteria for their acceptance up to certain limits are based on pharmaceutical studies or known safety data [9]. In accordance with regulatory guidelines, pharmaceutical studies using a sample of the isolated impurities can be used for the safety assessment. It is, therefore, essential to isolate and characterize unidentified impurities present in the drugs. Because a process for the synthesis of ketal has recently been developed in our laboratory, a GC method was developed for analysis of ketal and its diketal impurity in the synthetic product. The accuracy, precision, limit of detection (LOD), limit of quantification (LOQ), and linearity of the method were determined in accordance with ICH guidelines [10]. This paper reports, for the first time, a rapid, efficient, simple, and validated GC method for separation of potential impurity. To the best of our knowledge no validated method for the separation of ketal from its potential impurity was available by any of the instrumental technique and hence we have taken this study on the validation of ketal by GC method.



Ketal



Diketal

Figure 1. Chemical structures of Ketal and Diketal.

2. METHODS

2.1. Chemicals

Samples of ketal and its diketal impurity were synthesized in our laboratories and characterized by use of GC-MS, IR, and NMR. HPLC-grade methanol, HPLC-grade 1,4-dioxane were purchased from Merck and Spectrochem respectively. A stock solution of 1,4-Dioxane as internal standard (0.25 mg/mL) was prepared in methanol (ISTD solution). Working solution of 20 mg/mL was prepared by dissolving an appropriate amount of the ketal in ISTD solution and impurity solution of 0.2 mg/mL was also prepared in ISTD solution for related substances. Working solution of 10 mg/mL each of ketal and of 1,4-dioxane (Internal standard) was prepared in methanol for assay.

2.2. Chromatography

GC was performed with FID detector, an auto sampler, and an auto injector (Shimadzu GC model 2010; Shimadzu, Japan) connected to a FID detector, all were controlled by LC solution software (Shimadzu). Chromatographic separation was achieved for related substance method on a DBWAX ETR, 30 m × 0.32 mm × 1.0 μ Film Thickness column with nitrogen as carrier gas. The injection volume was 2.0 μ L, the carrier flow was 7.5 psi constant pressure, the detector temperature was 260°C, the injector temperature was 250°C and oven temperature was began at 45°C, held for 4 minutes and was then raised to 250°C at 60°C min⁻¹ and held for 28 minutes, and detection was with flame ionisation detector (FID). Chromatographic condition was achieved for assay method on a DBWAX ETR, 30 m × 0.32 mm × 1.0 μ Film Thickness column with nitrogen as carrier gas. The injection volume was 1.0 μ L, the carrier flow was 7.5 psi constant pressure, the detector temperature was 260°C, the injector temperature was 250°C and oven temperature was began at 45°C, held for 4 minutes and was then raised to 250°C at 60°C min⁻¹ and held for 28 minutes, and detection was with flame ionisation detector (FID). The test concentration for the related substance analysis was 20 mg/mL and for the assay was 10 mg/mL. Standard and test dilutions were prepared in methanol.

2.3. Validation of the Method

2.3.1. Specificity

A method is specific if it can be used to measure analyte response in the presence of potential impurities [9]. The specificity of this GC method for ketal was assessed in the presence of diketal impurity. Assay of ketal was performed after spiking with diketal impurity at the specification level (0.15%). Specificity of the method was further conformed by GC-MS, by comparing the spectral

match of the ketal peak at each data point verses the spectra of peak apex.

2.3.2. Precision

The precision of the method was assessed by performing six independent assays of ketal test sample in comparison with reference standard and calculating the RSD (%) of the assay. The precision of the related substance method was checked by injecting six individual preparations of ketal sample and RSD (%) was calculated for the content of impurity peak.

2.3.3. Limits of Detection and Quantification

The limits of detection (LOD) and limit of quantification (LOQ), defined as the amounts for which the signal-to-noise ratios were 3:1 and 10:1, respectively, were determined by S/N ratio method [10]. Precision and accuracy was also studied at the LOQ by injecting six separate solutions of the impurities and calculating the RSD (%) of the peak area.

2.3.4. Linearity

Solutions for testing the linearity of the assay method were prepared for five concentrations from 50 to 150% of the nominal assay concentration of the analyte (5, 7.5, 10, 12.5, and 15 mg/mL). Peak area and concentration data were treated by least squares linear regression analysis. Solutions for testing the linearity of the related substance method were prepared for six concentrations from the LOQ to 500% (1 mg/mL) of the specification level (LOQ, 0.25, 0.5, 1.0, 2.5, 5.0%). These tests were conducted and correlation coefficient was calculated between concentration verses area. The relative response factor was calculated from the slope of the impurity and ketal. Linearity calculations were performed with Microsoft Excel.

2.3.5. Accuracy

The accuracy of the assay method was evaluated in triplicate at three concentrations—1.0, 2.0, and 5.0 mg/mL (10, 20 and 50% of the nominal assay concentration of the analyte). Recovery (%) was calculated from the recovered area. Assessment of the accuracy of the method for analysis of the diketal impurity was performed in triplicate at 0.5, 1.0, 1.2% of the ketal analyte concentration (20 mg/mL). Recovery (%) of the impurity was calculated from the area of diketal in the recovery preparation.

2.3.6. Solution Stability

The solution stability of ketal in the assay method was carried out by leaving test solutions of sample and reference standard in methanol in tightly capped volumetric flasks at room temperature for 24 h. The sample solutions were assayed every 8 h up to 24 h. The solution stability of ketal and its impurity in the related substance method was determined by leaving sample and reference standard in methanol in tightly capped volumetric flask

at room temperature for 24 h. Area of the impurity in the sample solution and area of the ketal and diketal in the standard solution were determined every 4 h. Cumulative RSD was calculated.

3. RESULTS AND DISCUSSION

The main objective of the chromatographic method was to separate ketal from potential impurity diketal. In chemoselective reductive alkylation of ammonia with carbonyl compounds LC-MS method was used to identify the ketal [6]. In our study chromatographic separation was achieved for related substances and peak shape of ketal was symmetrical. Under the optimized conditions ketal and diketal were separated with resolution greater than 5; typical retention times of 1,4-Dioxane, ketal and diketal were approximately 6.65, 12.03, 13.46 respectively (**Figure 2**). System suitability data for the method are listed in the **Table 1**. The method was specific for ketal and diketal.

Chromatographic condition was achieved for assay and peak shape of ketal was symmetrical. Under the optimized conditions typical retention times of 1,4-dioxane and ketal were approximately 6.8, 12.3 respectively (**Figure 3**). System suitability data for the method are listed in the **Table 2**. The method was specific for ketal.

3.1. Validation of the Method

In the study of the precision of the assay method RSD of the peak area for assay of ketal was 0.21% or better. In

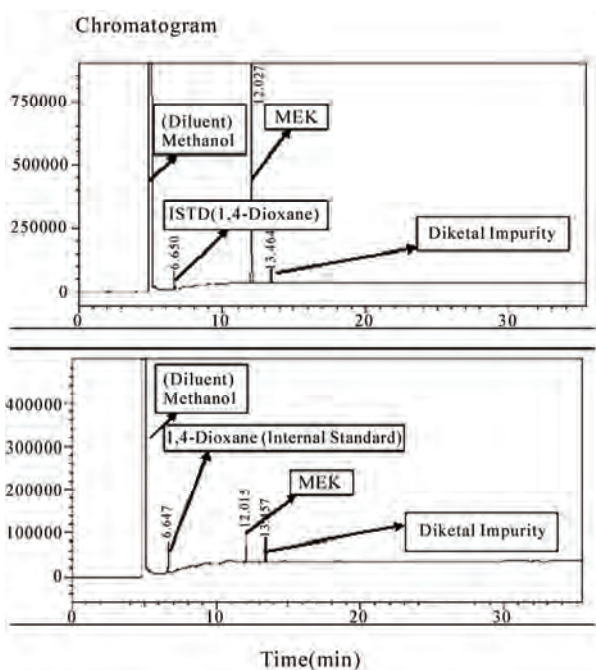


Figure 2. Typical chromatogram of system suitability and standard solution.

Table 1. System-suitability report for related substances.

| Compound | R _t | RRT | R _s |
|--------------------|----------------|------|----------------|
| Methanol (Diluent) | 5.00 | 0.42 | - |
| 1,4-Dioxane (ISTD) | 6.65 | 0.55 | - |
| Ketal | 12.03 | 1.00 | 83.6 |
| Diketal | 13.46 | 1.12 | 17.9 |

R_t retention time, RRT relative retention time, R_s USP resolution

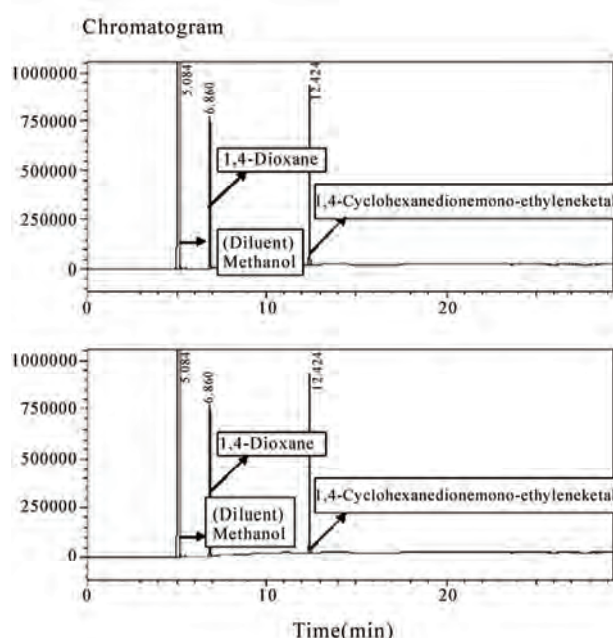


Figure 3. 1,4-cyclohexanedionemono-ethyleneketal standard chromatogram and 1,4-cyclohexanedionemono-ethyleneketal sample chromatogram.

Table 2. System-suitability report for assay.

| Compound | R _t | RRT | R _s |
|--------------------|----------------|------|----------------|
| Methanol (Diluent) | 5.0 | 0.41 | - |
| 1,4-Dioxane (ISTD) | 6.8 | 0.55 | - |
| Ketal | 12.3 | 1.00 | 87.2 |

R_t retention time, RRT relative retention time, R_s USP resolution

the study of the precision of the related substance method RSD of the peak area for assay of impurity was 1.10% or better. The limit of detection of the diketal impurity was 0.01% for 2 μ L injection volume having S/N ratio 3.2. The limit of quantification for the Diketal impurity was 0.05% for 2 μ L injection volume having S/N ratio 12.5 .Precision (as RSD) at the LOQ concen-

trations was 2.2% for the diketal impurity and recovery at LOQ level was 100%. In the assay method a linear relationship was obtained between response and concentration over the calibration range tested, i.e. 5.0-15 mg/mL; the correlation coefficient was > 0.99999. In the related substance method linear calibration plots were obtained for the diketal impurity over the calibration ranges tested. From the LOQ (0.05%) to 5.0% of the ketal concentration. The correlation coefficients obtained were > 0.999. The relative response factor was calculated as 1.1. These results show there was an excellent correlation between the peak areas and concentration of the impurity. Recovery of diketal from samples ranged from 88.0 to 105.0%. Recovery of ketal sample ranged from 100.7 to 108.6%. RSD for assay of ketal reference and sample during stability experiments was 0.04% and 0.04% respectively. There were no significant changes in the amount of the impurities during solution stability experiments performed using related substance method. The results from solution stability conformed that sample solution in methanol for assay and related substance analysis were stable for at least 24 h.

4. CONCLUSIONS

The GC method developed for quantitative assay of ketal and related substances is precise, accurate, rapid, and specific. Validation of the method furnished satisfactory results for all the method validation data tested. The method can be conveniently used by quality control departments for analysis of related substances, assay of ketal.

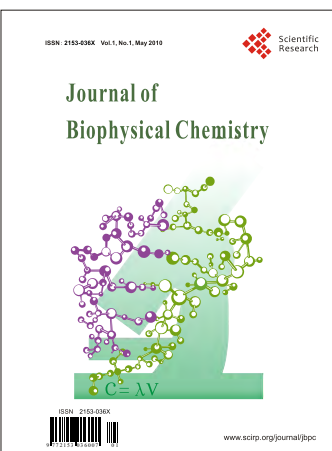
5. ACKNOWLEDGEMENTS

The authors would like to thank Prof K.Pandiyarajan HOD of Chemis-

try, Annamalai university for providing necessary facilities to carry out this work.

REFERENCES

- [1] Mussini, P., Orsini, F. and Pelizzoni, F. (1975) A preparation of the ethylene glycol monoketal of cyclohexane-1, 4-dione. *Synthetic Communications*, **5**(4), 283-286.
- [2] Huet, F., Pellet, M. and Conia, J. M. (1976) α -Diketone-monoketals and-monothioketals. *Tetrahedron Letters*, **17**(39), 3579- 3582.
- [3] Huet, F., Pellet, M. and Conia, J. M. (1976) α -cyclopropylidene-ketals-ketones and aldehydes. *Tetrahedron Letters*, **18**(29), 2521-2524.
- [4] Nangia, A. and Chandrakala, P. S. (1996) Experimental and computational studies on the hydrolysis rate of ethylene ketals in 1,3-cyclohexenediones. *Journal of the Chemical Society*, **108**(1), 51-56.
- [5] Volpe, T., Revial, G., Pfau, M. and dAnjelo, J. (1986) Synthesis of 2-methyl-1,3, cyclopentane dione mono-ethylene ketal. *Tetrahedron Letters*, **27**(25), 2853-2854.
- [6] Miriyala, B., Bhattacharyya, S. and Williamson, J. S. (2004) Chemoselective reductive alkylation of ammonia with carbonyl compounds: synthesis of primary and symmetrical secondary amines. *Tetrahedron*, **60**, 1463-1471.
- [7] Balko, T. W., Fields, S. C. and Webster, J. D. (1999) Total synthesis of (\pm)-8-trifluoromethyl abscisic acid. *Tetrahedron Letters*, **40**(35), 6347-6351.
- [8] Torbeck, L. (2002) Complying with ICH and FDA requirements for assay validation. Suffield press, Evanston.
- [9] (2006) International conferences on Harmonization. Draft revised guidance on impurities in new drug substances, Q3A(R2).
- [10] (1994) International Conferences on Harmonization. Validation of analytical procedures, Q2(R).



Call for Papers

Journal of Biophysical Chemistry

ISSN 2153-036X (Print) ISSN 2153-0378 (Online)

<http://www.scirp.org/journal/jbpc>

Journal of Biophysical Chemistry (JBPC) is an international journal dedicated to the latest advancement in related research fields. The goal of this journal is to provide a platform for scientists and academicians all over the world to promote, share, and discuss various new issues and developments in different aspects of biophysical chemistry.

Editor-in-Chief

Prof. Cornelis J. Van der Schyf Northeastern Ohio Universities Colleges of Medicine and Pharmacy, USA

Editorial Board (According to Alphabet)

Dr. Huizhong Chen

National Center for Toxicological Research, FDA, USA

Prof. I. Tuncer Degim

Gazi University, Turkey

Dr. Bouzid Menaa

Fluorotronics Inc., USA

Prof. Davood Nematollahi

Bu-Ali-Sina University, Iran

Prof. Kazuhisa Nishizawa

Teikyo University, Japan

Dr. Yoshiaki Ohashi

Human Metabolome Technologies, Inc., Japan

Dr. Marcella Pagano

Federal University of Ceará - UFC, Brazil

Prof. Ayyalusamy Ramamoorthy

University of Michigan, USA

Prof. Cornelis J. Van der Schyf

Ohio University, USA

Dr. Pasquale Stano

University of RomaTre, Italy

Dr. Andrei P. Surguchov

VA Medical Center and Kansas University Medical Center, USA

Prof. Armen Trchounian

Yerevan State University, Armenia

Dr. Izabela Tworowska

RadioMedix, Inc., USA

Prof. Suresh C. Tyagi

University of Louisville, USA

Dr. Qihui Wu

La Trobe University, Australia

Prof. Ling Yang

Dalian Institute of Chemical Physics, CAS, China

Prof. Anyun Zhang

Zhejiang University, China

Prof. Hailiang Zhu

Nanjing University, China

Prof. Erik R.P. Zuiderweg

University of Michigan, USA

Subject Coverage

This journal invites original research and review papers that address the following issues. Topics of interest include, but are not limited to:

Agronomy Agriculture
Bioenergetics
Biomechanics
Biomolecular and Drug Databases
Biomolecular Free Energy
Biomolecular Structure
Covering Dynamics
Dynamical Systems
Gene Regulation
Graph/Network Theory
Medicine and Neuroscience
Molecular Docking
Molecular Dynamics Simulation
Neural Networks

Nucleic Acid Structure
Patch Clamping
Pharmacology and Physiology
Phylogenetics
Population Modeling
Protein Structure Prediction
Quantum Biophysics
Quantum Chemistry
Sequence Alignment
Single Protein Dynamics
Stochastic Processes
Structural Alignment
Structural Biology
Structure-Activity Relationships

We are also interested in short papers (letters) that clearly address a specific problem, and short survey or position papers that sketch the results or problems on a specific topic. Authors of selected short papers would be invited to write a regular paper on the same topic for future issues of the *JBPC*.

Notes for Intending Authors

Submitted papers should not have been previously published nor be currently under consideration for publication elsewhere. Paper submission will be handled electronically through the website. All papers are refereed through a peer review process. For more details about the submissions, please access the website.

Website and E-Mail

<http://www.scirp.org/journal/jbpc>

E-mail: jbpc@scirp.org

TABLE OF CONTENTS

Volume 1 Number 1

May 2010

Water clusters in plants. Fast channel plant communications. Planet influence

Kristina Zubow, Anatolij Viktorovich Zubow, Viktor Anatolijevich Zubow..... 1

Patterns of synuclein expression throughout lens development

Irina Surgucheva, Belinda MacMahon, Andrei Surguchov..... 12

Molecular dynamics simulation analyses of viral fusion peptides in membranes prone to phase transition: effects on membrane curvature, phase behavior and lipid-water interface destabilization

Manami Nishizawa, Kazuhisa Nishizawa..... 19

Mode of pollen spread in clonal seed orchard of *Pinus koraiensis*

Fujuan Feng, Xin Sui, Minmin Chen, Dan Zhao, Shijie Han, Maihe Li..... 33

Correlations between delayed fluorescence of chlorophyll, metabolism and yield of plants. I. Influence of fertilizers on correlations

Armen B. Avagyan..... 40

Correlations between delayed fluorescence of chlorophyll, metabolism and yield of plants. II. Influence of moisture of leaf and temperature condition on delayed fluorescence of leaves

Armen B. Avagyan..... 52

Correlations between delayed fluorescence of chlorophyll, metabolism and yield of plants. III. Influence of viral infection on field plants and new technology of clone selection of virus-free planting potato

Armen B. Avagyan..... 58

A plasmid vector encoding functional human keratinocyte growth factor gene in vitro

Lin Qiu, Chunbao Guo..... 64

A validated, related substance, GC method for 1,4-cyclohexanedione mono-ethylene ketal

B. Karthikeyan, V. Srinivasan..... 72